

Optimization and Characterization of N-Acetamide Indoles as Antimalarials That Target PfATP4

Jon Kyle Awalt, Zi Kang Ooi, Trent D. Ashton, Mahta Mansouri, Petar P. S. Calic, Qingmiao Zhou, Santhya Vasanthan, Serena Lee, Katie Loi, Kate E. Jarman, Jocelyn S. Penington, Deyun Qiu, Xinxin Zhang, Adele M. Lehane, Emma Y. Mao, Maria R. Gancheva, Danny W. Wilson, Carlo Giannangelo, Christopher A. MacRaid, Darren J. Creek, Tomas Yeo, Tanaya Sheth, David A. Fidock, Alisje Churchyard, Jake Baum, Mufuliat T. Famodimu, Michael J. Delves, Mojca Kristan, Lindsay Stewart, Colin J. Sutherland, Rachael Coyle, Hannah Jagoe, Marcus C. S. Lee, Mrittika Chowdury, Tania F. de Koning-Ward, Delphine Baud, Stephen Brand, Paul F. Jackson, Alan F. Cowman, Madeline G. Dans,* and Brad E. Sleebs*



Cite This: *J. Med. Chem.* 2025, 68, 8933–8966



Read Online

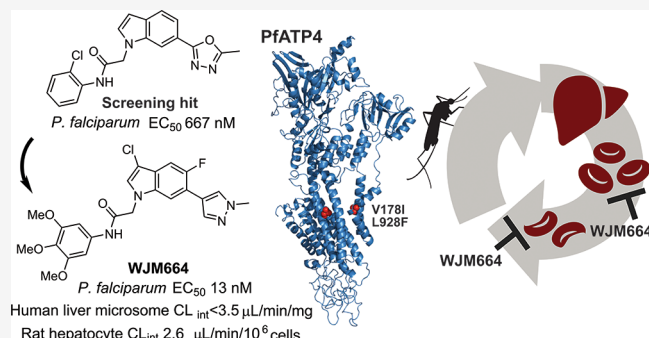
ACCESS |

Metrics & More

Article Recommendations

Supporting Information

ABSTRACT: To discover new antimalarials, a screen of the Janssen Jumpstarter library against *Plasmodium falciparum* uncovered the N-acetamide indole hit class. The structure–activity relationship of this chemotype was defined and culminated in the optimized frontrunner analog WJM664, which exhibited potent asexual stage activity and high metabolic stability. Resistant selection and whole-genome sequencing revealed mutations in PfATP4, which was validated as the target by showing that analogs exhibited reduced potency against parasites with resistance-conferring mutations in PfATP4, a metabolomic signature similar to that of the PfATP4 inhibitor KAE609, and inhibition of Na⁺-dependent ATPase activity consistent with on-target inhibition of PfATP4. WJM664 inhibited gamete development and blocked parasite transmission to mosquitoes but exhibited low efficacy in a *Plasmodium berghei* mouse model, which was attributed to ATP4 species differentiation and its moderate systemic exposure. Optimization of these attributes is required for N-acetamide indoles to be pursued for development as a curative and transmission-blocking therapy.



INTRODUCTION

Malaria is caused by unicellular protozoan parasites that belong to the genus *Plasmodium*. *Plasmodium* species are transmitted from human to human via the bite of an infected female *Anopheles* mosquito. Of the six species of *Plasmodium* that infect humans, *P. falciparum* and *P. vivax* pose the greatest threat to global health. *P. falciparum* malaria is the most virulent and fatal of the *Plasmodium* species. *P. falciparum* malaria commences with acute-like symptoms including vomiting, chills, headache, nausea, and myalgias, and can progress to a serious life-threatening disease if not managed. *P. falciparum* is most prevalent in the African continent presently, causing a significant number of cases, whereas *P. vivax* is often associated with indirect mortality and delayed morbidity which is often overlooked. *P. knowlesi* is simian of origin and many cases have been detected in South East Asia, although only a few known deaths have resulted. *P. ovale walkeri*, *P. ovale curtisi* and *P. malariae* cause mild symptoms, but deaths have rarely been reported.

Quinoline-containing antimalarial drugs such as mefloquine and chloroquine were once important chemotherapeutics in the treatment of malaria. However, the emergence of chloroquine and multidrug-resistant malaria parasites has resulted in the declining effectiveness of quinoline-containing antimalarials. Artemisinin-based combination therapies (ACTs) are now recommended as the frontline therapies to treat malaria, but concerning resistance has emerged in South East Asia¹ and more recently in Africa,² highlighting the increasing importance of discovering and developing new antimalarial chemotypes. This also resulted in the need to

Received: March 3, 2025

Revised: March 19, 2025

Accepted: March 25, 2025

Published: April 14, 2025



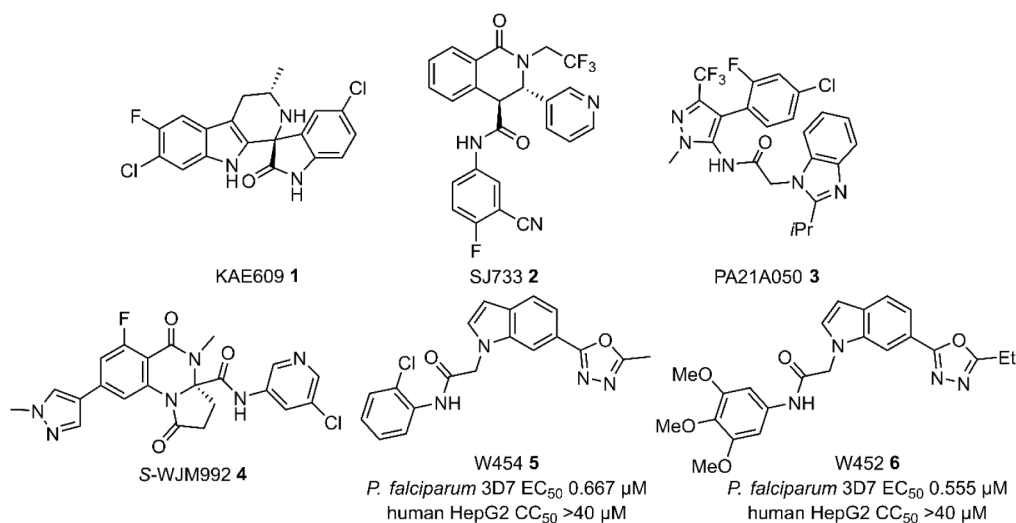


Figure 1. Structures of PfATP4 inhibitors and the biological activity of the N-acetamide indole hit compounds identified from a screen of the Jumpstarter Library against *P. falciparum* 3D7 parasites.

introduce strict resistance criteria and Target Candidate Profiles (TCPs) that antimalarials under development should abide by.³

At the turn of the century, there was a call by the world governing bodies for industry and academia to join forces to mass-screen compound libraries to uncover new starting points for the development of antimalarials. The screening efforts resulted in a plethora of unique hit scaffolds for optimization. Of these newly developed antimalarials, several have now advanced to human clinical trials.⁴ Two of these promising candidates, KAE609 and SJ733, are PfATP4 inhibitors.^{5,6}

PfATP4 is a P-type ATPase located on the parasite plasma membrane that is important in maintaining parasite cytosolic Na⁺ homeostasis and is essential for parasite development.^{6,7} It is one of the seven putative cation-transporting P-type ATPases found in *P. falciparum* and expressed throughout the erythrocytic stage and exports Na⁺ ions while importing H⁺ ions.^{7–9} Importantly, there are no close orthologs of PfATP4 found in mammals, making it an attractive antimalarial drug target.

Since the discovery of PfATP4, it has become an attractive molecular target in the development of next generation antimalarials. To date, several chemotypes have been found to inhibit PfATP4 in the *P. falciparum* asexual blood stage (Figure 1),^{5,6,10,11} with KAE609 (1) and SJ733 (2) advancing to human clinical trials.^{5,12,13} Although attractive rapid killing activity has been observed with both SJ733 and KAE609 in human challenge trials, resistant parasites with the PfATP4^{G358S} mutation were detected in participants treated with KAE609,¹⁴ underlining the concern with the rate at which resistance is acquired with PfATP4 inhibitors. This observation has emphasized the need for developing PfATP4 inhibitors with improved resistance profiles and certainly compounds that are not cross-resistant with existing drug candidates.

To discover new antimalarial chemotypes, we performed a high-throughput screen of the Janssen Jumpstarter 80,000 small molecule library against the *P. falciparum* asexual blood-stage parasite.¹⁵ The screen identified several hit classes,^{15–20} including a PfATP4 inhibitor class,^{11,21,22} with submicromolar antiparasmodial activity and no human HepG2 cell cytotoxicity. One of the other hit classes identified from the screen was the N-acetamide indole hit class (compounds W454 (5) and

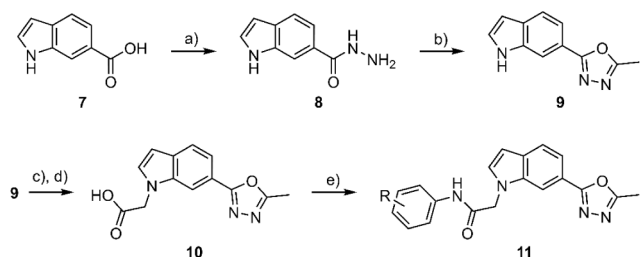
W452 (6) shown in Figure 1). To the best of our knowledge, the N-acetamide indole hit chemotype has not been investigated, highlighting its potential for optimization and characterization as a novel antimalarial scaffold.

Here we investigate the structure–activity relationship (SAR) of the N-acetamide indole chemotype against the *P. falciparum* parasite while monitoring physicochemical and ADME properties to develop compounds with potent activity and metabolic stability. Another goal was to investigate the mechanism of action and antiparasmodial properties of the N-acetamide indole class. To do this, we selected resistant parasites against two N-acetamide indole analogs and performed whole-genome sequencing of the resistant parasites which revealed mutations in PfATP4. To confirm PfATP4 was the molecular target, we profiled known PfATP4 inhibitors against the indole-resistant populations and evaluated N-acetamide indole compounds against known PfATP4 inhibitor-resistant strains. These data were complemented with further characterization of N-acetamide indole analogs in the asexual rate and stage of arrest, red blood cell lysis, and Na⁺-dependent membrane ATPase assays, which were all benchmarked against known PfATP4 inhibitors. Finally, we evaluate frontrunner N-acetamide indole analogs against transmission stage parasites, in a mosquito model and in an asexual *P. berghei* mouse model.

RESULTS AND DISCUSSION

Synthesis. Two general synthetic pathways were undertaken to access N-acetamide indole derivatives. The first pathway provided an avenue to synthesize analogs with the 1,3,4-oxadiazole moiety (11) in the 6-position of the indole framework (Scheme 1). This synthesis started by reacting the indole 6-carboxylic acid (7) with hydrazine using TCF and 1-methylimidazole to form hydrazide 8. The hydrazide 8 was then on-reacted with triethyl orthoformate at an elevated temperature to afford the 1,3,4-oxadiazole 9. The nitrogen on the indole was then alkylated with ethyl bromoacetate, and subsequently, the ester was deprotected under basic conditions to give carboxylic acid 10. The carboxylic acid was then reacted with a substituted aniline in the presence of either EDCI or T3P and base to give the N-acetamide indole analog scaffold

Scheme 1. General Synthetic Pathway to Access N-phenylacetamide Derivatives^a

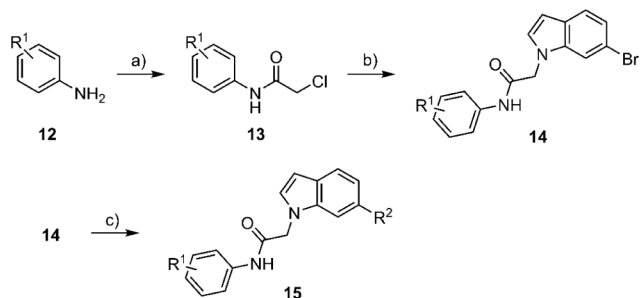


^aReagents and conditions: (a) TCFH, 1-methylimidazole, MeCN, 20 °C, 20 min, then hydrazine hydrate, 20 °C, 20 min, 61%; (b) triethyl orthoacetate, NH₄Cl, EtOH, reflux, 2 h, 82%; (c) NaH, 0 °C, 20 min, then ethyl bromoacetate, 0 °C, 20 °C, 16 h, 96%; (d) LiOH·H₂O, 1:1 THF/water, 96%; (e) substituted aniline, EDCI, Et₃N, MeCN, 20 °C, 16 h, or substituted aniline, T3P, pyridine, DMF, 20 °C, 16 h, 17–52%.

11. This pathway is geared toward generated analogs with a variety of substituents on the pendant aryl ring.

The second synthesis pathway enabled access to analogs with a (*N*-methyl)pyrazole in the 6-position of the indole core (Scheme 2). A substituted aniline 12 was reacted with

Scheme 2. General Synthetic Pathway to Access 6-Substituted Indole Derivatives^a



^aReagents and conditions: (a) chloro acetyl chloride, DIPEA, DCM, 20 °C, 16 h, 90–97%; (b) NaH, DMF, 0 °C, 1 h, then 6-bromoindole, DMF, 20 °C, 16 h, 80–84%; (c) R²-boronic acid or R²-BPin ester, Pd(dppf)Cl₂·CH₂Cl₂, K₂CO₃, 1,4-dioxane, H₂O, 110 °C, 3 h, 5–78%.

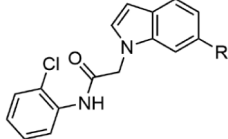
chloroacetyl chloride under basic conditions to afford the aryl carboxamide 13. The aryl carboxamide 13 was then used to alkylate the nitrogen of the indole using sodium hydride in DMF to yield the *N*-acetamide intermediate 14. The final step employed the Suzuki reaction in which the 6-bromo indole 14 was reacted with 4-Bpin (*N*-methyl)pyrazole using catalytic PdCl₂(PPh₃)₄ and K₂CO₃ in a mixture of dioxane and water to afford the *N*-acetamide indole product 15. The addition of the 6-bromo on the indole core enabled entry to a variety of heterocyclic iterations on the 6-position employing a Suzuki reaction. Moreover, both the synthetic pathways were generally amenable to the inclusion of substituents on a variety of positions on the indole framework, the aryl acetamide, or the 6-heterocyclic moieties to provide analogs for the SAR investigation.

Structure–Activity Relationships. The exploration of the SAR was performed iteratively against the asexual *P. falciparum* 3D7 parasite using LDH activity as the measure for

parasite growth. Human HepG2 cytotoxicity using Cell Titer Glo as a readout for cell growth was monitored through the optimization process, while in vitro metabolic stability and aqueous solubility were assessed for key compounds to determine their suitability for administration in a 4-day *P. berghei* mouse model.

The investigation of the SAR began with replacing the 5-methyl-1,3,4-oxadiazole on the 6-position of the indole core with suitable isosteric methyl substituted heterocyclic and aryl rings. It was found that the 5-methyl-1,2,4-oxadiazole variant (6) resulted in a 2-fold reduction in antiparasitic activity (EC₅₀ 0.955 μM) compared to W454 (5), while the 3-methyl-1,2,4-oxadiazole analog (7) ablated activity (EC₅₀ >10 μM) (Table 1). The difference in activities between the oxadiazole isomers

Table 1. Activity of 6-Heterocyclic and 6-Aryl Analogs^{abc}



compound	R	Pf LDH EC ₅₀ (SD) μM ^a	HepG2 CC ₅₀ (SD) μM ^b	PSA Å ² ^c	cLogP ^c
W454 (5)		0.667 (0.047)	>40	73	5.5
6		0.955 (0.285)	>40	73	5.2
7		>10	nd	73	5.2
8		>10	nd	52	5.0
9		0.593 (0.041)	>40	52	5.1
10		1.90 (0.60)	>40	47	6.1
11		>10	nd	34	6.5
12		>10	nd	34	6.7
13		1.11 (0.25)	>40	34	6.7
14		>10	nd	47	5.3
15		2.83 (0.85)	nd	47	5.3
16		3.65 (0.77)	nd	60	4.2

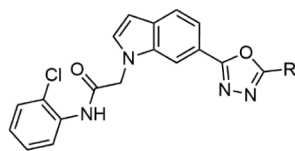
^aEC₅₀ data represents means and SDs for three or more independent experiments measuring *P. falciparum* 3D7 parasite growth at 72 h using an LDH assay. ^bCC₅₀ data represents means and SDs for three or more experiments measuring human HepG2 cell growth using a Cell TiterGlo assay. ^cCalculated using Dotmatics software. nd = no data.

may be explained by the variation in their intrinsic dipole moments which influence the physicochemical properties and the ability of each isomer to form hydrogen bond interactions.²³ The 4-(*N*-methyl-pyrazole) analog (9) exhibited equipotent activity (EC₅₀ 0.593 μM) relative to W454 (5), while the 3-(*N*-methyl-pyrazole) (8) was detrimental to activity (EC₅₀ >10 μM) suggesting that the

location of the endocyclic nitrogen in the heterocyclic ring was important for antimalarial activity. Supporting this notion, was the activity (EC_{50} 1.90 μ M) of the 2-methyl-thiazole analog which has an endocyclic nitrogen in the same relative position as the 4-(*N*-methyl-pyrazole) isomer (**9**). Moreover, the 2-methyl thiophene derivative (**11**) was inactive (EC_{50} > 10 μ M). Opposing the hypothesis that an endocyclic nitrogen was required for activity was the finding that the 3-methyl aryl analog (**13**) showed modest antiparasmodial activity (EC_{50} 1.11 μ M). The 4-methyl aryl and 3-(4-methylpyridine) analogs (**12** and **14**) were both inactive (EC_{50} > 10 μ M) implying that the methyl substituent vector is important for activity. Further evidence is that analogs **15** and **16**, whereby the methyl is maintained in the relative 3-position with a 4-endocyclic nitrogen exhibit modest activity (EC_{50} 2.83 and 3.65 μ M). Overall, the 4-(*N*-methyl-pyrazole) iteration (**9**) was the most suitable isosteric replacement for the 5-methyl-1,3,4-oxadiazole on the *N*-acetamide indole scaffold. Furthermore, the pyrazole modification did not induce cytotoxicity toward human HepG2 cells and was more amenable to synthesis and structural modification.

The importance of the methyl substitution in the 5-position of the 1,3,4-oxadiazole was then investigated. It was found that removal of the 5-methyl substitution (**17**) was deleterious to antiparasmodial activity (EC_{50} > 10 μ M) (Table 2), indicating

Table 2. Activity of Substituted Oxadiazole Analogs



compound	R	Pf LDH EC_{50} (SD) μ M ^a	HepG2 CC_{50} (SD) μ M ^b	PSA \AA^{2c}	cLogP ^c
W454 (5)	Me	0.667 (0.047)	>40	73	5.5
17	H	>10	nd	73	5.1
18	CF ₃	>10	nd	73	6.2
19	<i>i</i> -Pr	>10	nd	73	6.3

^a EC_{50} data represents means and SDs for three or more independent experiments measuring *P. falciparum* 3D7 parasite growth at 72 h using an LDH assay. ^b CC_{50} data represents means and SDs for three or more experiments measuring human HepG2 cell growth using a Cell TiterGlo assay. ^cCalculated using Dotmatics software. nd = no data.

the methyl group is required for activity. Replacing the methyl group with a trifluoromethyl (**18**) or an isopropyl substituent (**19**) also ablated activity (EC_{50} > 10 μ M). These data suggested that hydrophobic groups with larger steric volume than a methyl group were not tolerated, although a 5-ethyl substituent was found in the hit compound W452 (**6**) with a 3,4,5-trimethoxy aryl group on the acetamide functionality (Figure 1). We then examined whether the substitution with the same steric volume was tolerated on the orthologous *N*-1 position of the 4-pyrazole. It was found that a *N*-difluoromethyl group (**20**) was 3-fold less active (EC_{50} 1.5 μ M) than the *N*-methyl equivalent (**9**) (Table 3). Functionality with steric bulk larger than a *N*-difluoromethyl group, including trifluoromethyl, ethyl, isopropyl trifluoroethyl, and phenyl groups (**21**–**25**) ablated activity (EC_{50} > 10 μ M), consistent with the activity observed with 1,3,4-oxadiazole analogs **18** and **19**. These data demonstrated that the SAR was

largely transferrable between 4-pyrazole and 1,3,4-oxadiazole scaffolds.

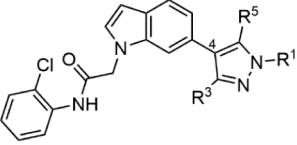
Methyl substitution at different positions on the 4-(*N*-methyl)pyrazole was next explored. It was revealed that methyl substitution either in the 5- and 3-position (**26** and **27**) both resulted in a 2-fold improvement in antiparasitic activity (EC_{50} 0.248 and 0.230 μ M) relative to the activity of analog **9** (Table 3). The 3,5-dimethyl substitution (**28**) gave an approximately 2-fold improvement in activity (EC_{50} 0.310 μ M), while the removal of the *N*-1 methyl group while retaining the 3-methyl group on the 4-pyrazole (**29**) resulted in a significant decrease in activity (EC_{50} 3.60 μ M). These data established that the 3-methyl substitution was driving antiparasitic potency. Strikingly, the 3-trifluoromethyl group (**30**) resulted in a 5-fold increase antiparasmodial potency (EC_{50} 0.046 μ M) to analog **27**. Notably, the improvement in antiparasmodial activity seen with analogs **26**, **27** and **30** was not accompanied by human HepG2 cell cytotoxicity.

The substitution on the aryl ring connected to the carboxamide was next explored. It was shown that the removal of the 2-chloro substituent (**31**) gave a 3-fold reduction in antiparasitic activity (EC_{50} 1.63 μ M) compared to the hit compound W454 (**5**) (Table 4). Halogen substitution in the 3-position (**32** and **35**) also exhibited similar activity (EC_{50} 0.898 and 1.45 μ M), while 4-halogen substitution (**33** and **36**) was 2-fold less active (EC_{50} 4.47 and 3.80 μ M). Methyl substitution in the 2-, 3- or 4- position (**37**–**39**) also resulted in a modest reduction in antiparasmodial activity (EC_{50} 1.18–5.35 μ M). Trifluoromethyl substitution in the 2- and the 4-positions (**40** and **42**) showed a modest increase in activity (EC_{50} 3.10 and 2.10 μ M) relative to the methyl orthologs, while the 3-trifluoromethyl substitution (**41**) appeared to be an outlier with activity (EC_{50} 0.615 μ M) equivalent to the hit compound W454 (**5**). Polar substituents, including methoxy and nitrile groups in the 2-, 3- and 4- positions (**43**–**48**) showed a wide range of antiparasitic activity (EC_{50} 1.0–>10 μ M). Overall, the different substituents applied to each position of the aryl ring only gave subtle variations in antiparasmodial activity, resulting in SAR that was difficult to interpret in this region of the *N*-acetamide indole framework.

We then postulated whether introducing di- or tri-substitution on the aryl ring would increase antiparasitic activity because the 3,4,5-trimethoxy substitution on the hit compound W452 (**6**) appears to have significantly contributed to the activity (Figure 1) whereby the ethyl substitution on the oxadiazole ablated antiparasmodial activity in earlier SAR (Tables 2 and 3). A cohort of analogs with both difluoro and dichloro substitution patterns (**49**–**56**) mostly exhibiting EC_{50} values of approximately 1 μ M (Table 5). 3,4- and 3,5-dimethoxy substitution (**57** and **58**) also gave similar activity (EC_{50} 1.55 and 1.18 μ M), but curiously, 3,4,5-trimethoxy substitution (**59**) was 5-fold more potent (EC_{50} 0.200 μ M) and was devoid of human HepG2 cell toxicity. The 3,4,5-trimethoxy aryl moiety, a catechol variant, from a drug standpoint is known to be susceptible to cytochrome P450 bioactivation potentially leading to toxic metabolites.²⁴ This moiety does increase the overall polarity of the *N*-acetamide indole scaffold and may oppose metabolism seen with lipophilic scaffolds.²⁵

We next explored the incorporation of an endocyclic nitrogen in the pendant aryl ring to determine if it was tolerated and would have a positive influence on the physicochemical parameters of the scaffold. It was shown

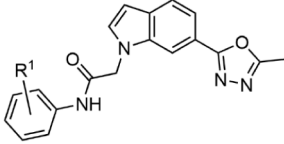
Table 3. Activity of Substituted Oxadiazole Analogs



compound	R ⁵	R ³	R ¹	Pf LDH EC ₅₀ (SD) μM ^a	HepG2 CC ₅₀ (SD) μM ^b	PSA Å ^{2c}	cLogP ^c
9	H	H	Me	0.593 (0.041)	>40	52	5.1
20	H	H	CF ₂ H	1.50	>40	52	5.8
21	H	H	CF ₃	>10	nd	52	6.5
22	H	H	Et	>10	>40	52	6.3
23	H	H	<i>i</i> -Pr	>10	nd	52	6.0
24	H	H	CH ₂ CF ₃	>10	nd	52	5.9
25	H	H	Ph	>10	nd	52	6.7
26	Me	H	Me	0.248 (0.054)	>40	52	5.3
27	H	Me	Me	0.230 (0.074)	>40	52	5.3
28	Me	Me	Me	0.310 (0.016)	>40	52	5.4
29	Me	Me	H	3.60 (1.06)	>40	63	6.1
30	H	CF ₃	Me	0.043 (0.003)	>40	52	6.0

^aEC₅₀ data represents means and SDs for three or more independent experiments measuring *P. falciparum* 3D7 parasite growth at 72 h using an LDH assay. ^bCC₅₀ data represents means and SDs for three or more experiments measuring human HepG2 cell growth using a Cell TiterGlo assay. ^cCalculated using Dotmatics software. nd = no data.

Table 4. Activity of Substituted Aryl Carboxamide Analogs

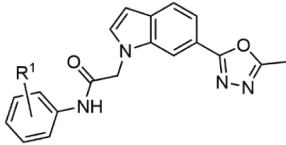


compound	R ¹	Pf LDH EC ₅₀ (SD) μM ^a	HepG2 CC ₅₀ (SD) μM ^b	PSA Å ^{2c}	cLogP ^c
W454 (5)	2-Cl	0.667 (0.047)	>40	73	5.5
31	H	1.63 (0.43)	>40	73	4.9
32	3-Cl	0.898 (0.205)	>40	73	5.5
33	4-Cl	4.47 (1.72)	>40	73	5.5
34	2-F	2.10 (0.39)	>40	73	5.3
35	3-F	1.45 (0.30)	>40	73	5.3
36	4-F	3.80 (0.60)	>40	73	5.3
37	2-Me	1.18 (0.24)	nd	73	5.1
38	3-Me	2.80 (0.32)	>40	73	5.1
39	4-Me	5.35 (1.68)	>40	73	5.1
40	2-CF ₃	3.10 (0.26)	>40	73	5.9
41	3-CF ₃	0.615 (0.006)	>40	73	5.9
42	4-CF ₃	2.10 (0.22)	>40	73	5.9
43	2-MeO	>10	nd	83	4.8
44	3-MeO	3.60 (1.27)	>40	83	4.8
45	4-MeO	7.80 (1.64)	>40	83	4.8
46	2-CN	3.48 (1.35)	>40	97	4.6
47	3-CN	0.99 (0.16)	>40	97	4.6
48	4-CN	>10	nd	97	4.6

^aEC₅₀ data represents means and SDs for three or more independent experiments measuring *P. falciparum* 3D7 parasite growth at 72 h using an LDH assay. ^bCC₅₀ data represents means and SDs for three or more experiments measuring human HepG2 cell growth using a Cell TiterGlo assay. ^cCalculated using Dotmatics software. nd = no data.

that the inclusion of an endocyclic nitrogen into the 2-, 3- or 4-positions of the unsubstituted aryl ring (**60** and **61**) led to a 3-fold reduction in antiparasitic activity (EC₅₀ 4.25–4.78 μM) compared to the carbocycle ortholog **31** (Table 6).

Table 5. Activity of Di- and Tri-Substituted Aryl Carboxamide Analogs



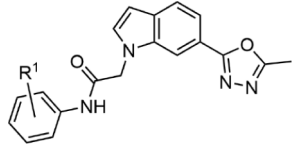
compound	R ¹	Pf LDH EC ₅₀ (SD) μM ^a	HepG2 CC ₅₀ (SD) μM ^b	PSA Å ^{2c}	cLogP ^c
W454 (5)	2-Cl	0.667 (0.047)	>40	73	5.5
49	2,4-diF	4.25 (0.06)	>40	73	5.8
50	2,5-diF	1.25 (0.13)	>40	73	5.1
51	2,6-diF	1.65 (0.25)	>40	73	5.1
52	3,5-diF	1.18 (0.05)	>40	73	5.1
53	3,5-diCl	3.88 (0.54)	>40	73	5.1
54	2,3-diCl	1.33 (0.22)	>40	73	5.1
55	2-Cl, 3-F	1.33 (0.22)	>40	73	6.1
56	2-Cl, 5-F	0.683 (0.169)	>40	73	6.1
57	3,4-diMeO	1.55 (0.26)	>40	73	5.6
58	3,5-diMeO	1.18 (0.13)	>40	92	4.8
59	3,4,5-triMeO	0.200 (0.024)	>40	92	4.8

^aEC₅₀ data represents means and SDs for three or more independent experiments measuring *P. falciparum* 3D7 parasite growth at 72 h using an LDH assay. ^bCC₅₀ data represents means and SDs for three or more experiments measuring human HepG2 cell growth using a Cell TiterGlo assay. ^cCalculated using Dotmatics software.

Incorporation of a 2-chloro in combination with an endocyclic nitrogen in different positions showed the 2-chloro 3-pyridyl variant (**63**) was the most potent (EC₅₀ 1.17 μM) while the 2-chloro 3-pyridyl iteration (**64**) was 7-fold less active (EC₅₀ 7.13 μM). These data suggest that an endocyclic nitrogen could be incorporated into more advanced analogs at a later stage to assist in improving physicochemical properties without significant loss in antiparasitic activity.

We next explored substitution on the carboxamide and the alpha-carbon adjacent to the carboxamide. It was found that *N*-

Table 6. Activity of Heteroaryl Carboxamide Analogs

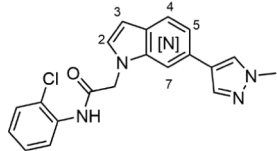


compound	R ¹	PfLDH EC ₅₀ (SD) μM ^a	HepG2 CC ₅₀ (SD) μM ^b	PSA Å ^{2c}	cLogP ^c
31	H	1.63 (0.43)	>40	73	4.9
60	2-[N]	4.78 (0.30)	>40	86	4.0
61	3-[N]	4.25 (0.4)	>40	86	3.6
62	4-[N]	4.68 (0.21)	>40	86	3.6
W454 (5)	2-Cl	0.667 (0.047)	>40	73	5.5
63	3-[N]-2-Cl	1.17 (0.14)	>40	86	4.6
64	4-[N]-2-Cl	7.13 (2.44)	>40	86	4.2

^aEC₅₀ data represents means and SDs for three or more independent experiments measuring *P. falciparum* 3D7 parasite growth at 72 h using an LDH assay. ^bCC₅₀ data represents means and SDs for three or more experiments measuring human HepG2 cell growth using a Cell TiterGlo assay. ^cCalculated using Dotmatics software.

methylation of the carboxamide nitrogen (**65**) was not tolerated (EC₅₀ >10 μM), while monomethylation of the alpha-carbon (**66**) was slightly less active (EC₅₀ 1.12 μM) than the unsubstituted counterpart **9** (Table 7). In literature, it is well established that the 2- and 3- positions on the indole are metabolic soft spots,²⁶ and therefore blocking these positions with a substituent or an endocyclic nitrogen would be important for moving into a mouse efficacy model. It was shown that analogs **67** and **68** with a methyl group in either the 2- or 3- position exhibited similar potency (EC₅₀ 0.603 and 0.868 μM) to the unsubstituted precursor **9**. Further exploration of the 3-position with different substitutions, revealed that halogen substituents (**69–71**) and a nitrile group (**72**) were between 3- and 4-fold more potent (EC₅₀ 0.138–0.330 μM) than analog **9**, while an endocyclic nitrogen in either the 2- or 3- position of the indole were detrimental to antiparasitic activity (EC₅₀ >10 μM) (Table 8). These data implied that a small halogen or a nitrile in the 3-position may

Table 8. Activity of Endocyclic Nitrogen Analogs



compound	[N]	Pf LDH EC ₅₀ (SD) μM ^a	HepG2 CC ₅₀ (SD) μM ^b	PSA Å ^{2c}	cLogP ^c
9	-	0.593 (0.041)	>40	52	5.1
73	2	>10	nd	65	4.0
74	3	>10	nd	65	4.6
75	4	>10	nd	65	3.9
76	5	8.45 (0.72)	>40	65	3.7
77	7	1.53 (0.10)	>40	65	3.8

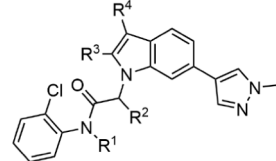
^aEC₅₀ data represents means and SDs for three or more independent experiments measuring *P. falciparum* 3D7 parasite growth at 72 h using an LDH assay. ^bCC₅₀ data represents means and SDs for three or more experiments measuring human HepG2 cell growth using a Cell TiterGlo assay. ^cCalculated using Dotmatics software. nd = no data.

mitigate metabolism, although it was noted that synthetic difficulties were encountered with further manipulations with the 3-nitrile substituted indole scaffold and consequently the 3-nitrile substituent was deprioritized in preference for a 3-chloro substituent.

We also explored the incorporation of an endocyclic nitrogen in the indole core as a possible avenue to improve physiochemical properties. It was shown that an endocyclic nitrogen in the 2-, 3-, 4- or 5-positions (**73–76**) was not tolerated (EC₅₀ 8.45–>10 μM), while the 7-position (**77**) showed 3-fold less activity (EC₅₀ 1.53 μM) than the corresponding unsubstituted analog **9** (Table 8). Incorporation of an endocyclic nitrogen at the 7-position on a more potent advanced compound may be beneficial for improving solubility or metabolic stability.

With the SAR established, we then iteratively introduced the modifications into the N-acetamide indole scaffold that were shown to give significant improvements in antiparasitic

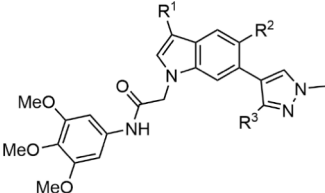
Table 7. Activity of Substituted Analogs



compound	R ¹	R ²	R ³	R ⁴	PfLDH EC ₅₀ (SD) μM ^a	HepG2 CC ₅₀ (SD) μM ^b	PSA Å ^{2c}	cLogP ^c
9	H	H	H	H	0.593 (0.041)	>40	52	5.1
65 ^d	Me	H	H	H	>10	nd	65	5.4
66	H	Me	H	H	1.12 (0.16)	>40	52	5.6
67	H	H	Me	H	0.603 (0.017)	>40	52	5.3
68	H	H	H	Me	0.868 (0.471)	>40	52	5.3
69	H	H	H	F	0.330 (0.023)	>40	52	5.2
70	H	H	H	Cl	0.138 (0.015)	>40	52	5.7
71	H	H	H	Br	0.165 (0.010)	>40	52	5.8
72	H	H	H	CN	0.240 (0.020)	>40	76	4.8

^aEC₅₀ data represents means and SDs for three or more independent experiments measuring *P. falciparum* 3D7 parasite growth at 72 h using an LDH assay. ^bCC₅₀ data represents means and SDs for three or more experiments measuring human HepG2 cell growth using a Cell TiterGlo assay. ^cCalculated using Dotmatics software. ^dAnalog with 2-methyl-1,3,4-oxadiazole in place of 4-(N-methyl-pyrazole). nd = no data.

Table 9. Activity of Analogs with a Combination of Substituents



compound	R ¹	R ²	R ³	Pf LDH EC ₅₀ (SD) μM ^a	HepG2 CC ₅₀ (SD) μM ^b	PSA Å ^{2c}	cLogP ^c
78	H	H	H	0.385 (0.093)	>40	80	4.3
79	Cl	H	H	0.049 (0.010)	>40	80	4.9
80	H	F	H	0.007 (0.001)	>40	80	4.4
81	H	H	Me	0.100 (0.008)	>40	80	4.5
WJM664 (82)	Cl	F	H	0.013 (0.003)	>40	80	5.0
83	Cl	H	Me	0.022 (0.006)	nd	80	5.1
84	Cl	F	Me	0.108 (0.011)	>40	80	5.2

^aEC₅₀ data represents means and SDs for three or more independent experiments measuring *P. falciparum* 3D7 parasite growth at 72 h using an LDH assay. ^bCC₅₀ data represents means and SDs for three or more experiments measuring human HepG2 cell growth using a Cell TiterGlo assay. ^cCalculated using Dotmatics software. nd = no data.

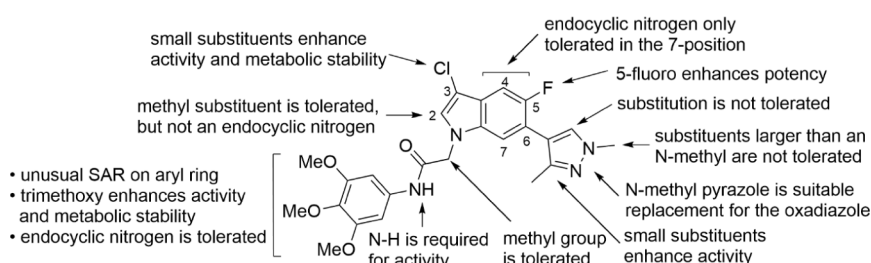


Figure 2. Summary of the SAR.

Table 10. Aqueous Solubility, In Vitro Metabolism, and eLogD Values for Selected Compounds

compound	aqueous solubility; pH 7.4 (μM) ^a	human liver microsomes; CL _{int} (μL/min/mg)	mouse liver microsomes; CL _{int} (μL/min/mg)	rat hepatocytes; CL _{int} (μL/min/10 ⁶ cells)	eLogD ^b
W454 (5)	10.9	>462	410	>92	3.1
9	4.1	>462	nd	91	3.6
30	2.5	488	nd	92	4.7
59	5.1	42	69	8.9	2.7
63	73	57	nd	27	2.1
70	<2.5	65	177	29	4.6
72	4.9	62	nd	59	3.0
77	2.5	458	nd	92	3.3
78	4.6	95	nd	4.6	3.5
79	2.5	15	53	<1	4.2
80	2.7	69	90	1.9	3.2
81	8.6	105	207	11	3.2
WJM664 (82)	<2.5	<3.5	6.8	2.6	4.8
84	2.5	64	73	5.7	4.8

^aKinetic in PBS. ^bShake-flask method. nd = no data.

potency. Starting with the progenitor analog **78** with a 3,4,5-trimethoxy aryl group on the carboxamide and a 4-(N-methyl pyrazole) in the 6-position (EC₅₀ 0.385 μM) (Table 9), the addition of either a 3-chloro substituent (**79**) or a methyl group on the 3-position of the pyrazole (**81**) gave a 6- and 3-fold enhancement in activity (EC₅₀ 0.049 and 0.100 μM), while a 5-fluoro substituent (**80**) gave a 50-fold increase in antiparasitic potency (EC₅₀ 0.007 μM). A combination of the 3-chloro and 5-fluoro substituents (WJM664 (**82**)) gave a 20-fold improvement in potency (EC₅₀ 0.013 μM) relative to **78**. The additional methyl group on the 3-position of the pyrazole

with a combination of 3-chloro and 5-fluoro substituents resulted in the analog **84** which did not have improved antiparasitic activity (EC₅₀ 0.108 μM). It was reasoned that the 3-methyl group on the pyrazole and the 5-fluoro substituent were sterically repulsive resulting in an unfavorable orientation of the pyrazole moiety for binding to the molecular target.

Overall, the exploration of the SAR on the N-acetamide indole scaffold (Figure 2) found that subtle changes in functionality and positioning refined the antiparasitic potency and engendered the frontrunner compound

Table 11. Activity of Compounds against W454-Resistant Populations

compound	Pf 3D7 EC ₅₀ (SD) μM^a	3D7 W454-resistant populations EC ₅₀ (SD) $\mu\text{M}^{a,b}$		
		#1	#2	#3
W454 (5)	0.569 (0.042)	>10	>10	>10
W452 (6)	0.123 (0.034)	1.94 (0.31)	1.99 (0.29)	1.80 (0.05)
80	0.004 (<0.001)	0.047 (0.008)	0.044 (0.009)	0.044 (0.009)
KAE609 (1)	0.0007 (0.0002)	0.002 (<0.001)	0.002 (<0.001)	0.002 (<0.001)
SJ733 (2)	0.061 (0.009)	0.579 (0.104)	0.537 (0.060)	0.533 (0.058)

^aEC₅₀ values represent averages and SDs of 3 biological replicates against 3D7 *P. falciparum* using a 72 h Pf LDH assay. ^b*P. falciparum* 3D7 W454-resistant populations all have a L928F mutation in PfATP4. Dose–response curves are shown in Figure S2.

WJM664 (82). The information gleaned from the SAR study could also aid in the future modulation of physicochemical properties to enhance aqueous solubility and metabolic stability.

In Vitro ADME Profiling. The in vitro metabolic stability and aqueous solubility of the N-acetamide indole series were assessed on selected analogs over the optimization process to determine which functionality on the scaffold was contributing favorable parameters that would be suitable for efficacy studies in a mouse model. The aqueous solubility at physiological pH 7.4 of the hit compound W454 (5) and closely related analogs 9, 59 and 72 was modest (4.1–10.9 μM) (Table 10). The addition of a lipophilic halogen to the scaffold (30, 70, 79 and 80) was typically accompanied by an increase in eLogD and a decrease in the aqueous solubility (<2.7 μM). The inclusion of an endocyclic nitrogen into the indole scaffold (77) did not improve aqueous solubility whereas an endocyclic nitrogen in the exocyclic (63) gave a marked increase in solubility (73 μM), however, this change resulted in lower antiparasitic activity (EC₅₀ 1.17 μM). Overall, the aqueous solubility of the N-acetamide indole class was limited which may have implications on absorption and systemic exposure in vivo. The introduction of polarity into the scaffold largely resulted in decreased antiparasitic activity. Improving the solubility will be a challenge in the future optimization of this scaffold.

It was found that the metabolic stability of the hit compound W454 (5) in both human liver microsomes and rat hepatocytes was low (CL_{int} >462 $\mu\text{L}/\text{min}/\text{mg}$; CL_{int} >92 $\mu\text{L}/\text{min}/10^6$ cells) (Table 10). Replacing the oxadiazole on the hit compound W454 (5) with a 4-(N-methyl)pyrazole (9) did not improve metabolic stability (CL_{int} >462 $\mu\text{L}/\text{min}/\text{mg}$; CL_{int} 91 $\mu\text{L}/\text{min}/10^6$ cells). Unexpectedly, replacing the 2-Cl aryl with a 3,4,5-trimethoxy aryl group (59 and 78) markedly improved the metabolic stability in both human liver microsomes and rat hepatocytes (CL_{int} 95 and 62 $\mu\text{L}/\text{min}/\text{mg}$; CL_{int} 8.9 and 4.6 $\mu\text{L}/\text{min}/10^6$ cells). It was reasoned that the increase in polarity of the methoxy groups was important in enhancing metabolic stability, even though there was only a subtle change in eLogD values from analogs W454 (5) and 9 to analogs 59 and 78. It was shown that the substitution of the 3-position of the indole (with the 2-chloro aryl moiety present) (72 and 70) also led to an improvement in metabolic stability (CL_{int} 62 and 65 $\mu\text{L}/\text{min}/\text{mg}$; CL_{int} 59 and 29 $\mu\text{L}/\text{min}/10^6$ cells) compared to the hit compound W454 (5). It was established that the addition of the 5-fluoro substituent (80) did not impact metabolic stability (CL_{int} 431 and 69 $\mu\text{L}/\text{min}/\text{mg}$; CL_{int} >92 and 1.9 $\mu\text{L}/\text{min}/10^6$ cells) relative to their nonfluorinated counterparts (5 and 59). It was also established that the inclusion of an endocyclic nitrogen in the 2-chloro aryl group (63) had modest metabolic stability (CL_{int} 57 $\mu\text{L}/\text{min}/\text{mg}$; CL_{int} 27 $\mu\text{L}/\text{min}/10^6$ cells), whereas endocyclic nitrogen

in the 7-position of the indole framework (77) did not improve metabolic stability (CL_{int} 458 $\mu\text{L}/\text{min}/\text{mg}$; CL_{int} 92 $\mu\text{L}/\text{min}/10^6$ cells). The combination of a 3,4,5-trimethoxy aryl group and 3-chloro substituent on the indole core (79 and WJM664 (82)) gave a significant improvement in metabolic stability (CL_{int} 15 and <3.5 $\mu\text{L}/\text{min}/\text{mg}$; CL_{int} <1 and 2.6 $\mu\text{L}/\text{min}/10^6$ cells), while the inclusion of a 3-methyl substituent on the pyrazole (81) reduced metabolic stability (CL_{int} 105 $\mu\text{L}/\text{min}/\text{mg}$; CL_{int} 11 $\mu\text{L}/\text{min}/10^6$ cells). The stability of analogs in the presence of mouse liver microsomes was generally slightly lower than the stability in human liver microsomes. For example, WJM664 (82) in human liver microsomes CL_{int} < 3.5 $\mu\text{L}/\text{min}/\text{mg}$ versus mouse liver microsomes CL_{int} 6.8 $\mu\text{L}/\text{min}/\text{mg}$. Collectively, these data established that the combination of the 3,4,5-trimethoxy aryl group and 3-chloro substituent led to analogs, for example, derivatives 79, WJM664 (82), and 84 with suitable antiparasitic potency and metabolic stability for assessment in a malaria mouse model. WJM664 (82) was found to have low apical to basolateral permeability (0.8×10^{-6} cm/sec) and a moderate basolateral to apical translocation (1.5×10^{-6} cm/sec) (Table S1) which may indicate low systemic absorption in vivo.

Target Identification Using Forward Genetics. To uncover the mechanism of action of the N-acetamide indole class, we used W454 (5) to select resistance in *P. falciparum* 3D7 parasites. Three independent 3D7 parasite populations were treated with increasing concentrations of W454 (5), starting at $2 \times \text{EC}_{50}$ and incrementally increasing to $6 \times \text{EC}_{50}$. Each incremental increase was accompanied by the removal of W454 (5) from the culture media until parasite levels had recovered before applying the next incremental treatment of W454 (5). At the end of the selection, the lactate dehydrogenase (LDH) assay was used to confirm the development of resistance. All three populations showed decreased activity against W454 (5) (EC₅₀ >10 μM) compared to the parental 3D7 parasites (Table 11 and Figure S2).

To detect genetic determinants responsible for W454-resistance, genomic DNA was prepared from each W454-resistant parasite population and the 3D7 parental strain for whole genome sequencing. Whole genome sequencing of all three W454-resistant populations revealed a nonsynonymous single nucleotide variant (SNV) encoding for L928F in PfATP4 (Table S2). The allele frequencies of L928F SNV were >98% in all 3 populations and 0% in the 3D7 parental strain (Table S3). There were no differences in copy numbers between the W454-resistant and the 3D7 parental strain (Figure S3). Four insertion-deletion mutations (indels) were detected, however, none of them are in the coding regions (Table S4).

The L928F mutation was mapped to a homology model of PfATP4 constructed from the X-ray structure of rabbit

sarcoendoplasmic reticulum calcium ATPase (SERCA) pump (PDB 2C88),²⁷ which shows the L928F mutation located in the transmembrane region of PfATP4 and in close proximity to other mutations (PfATP4^{I398F,P990R,D1247Y} and PfATP4^{G358S}) found in other PfATP4 drug-resistant parasites (Figure 3).

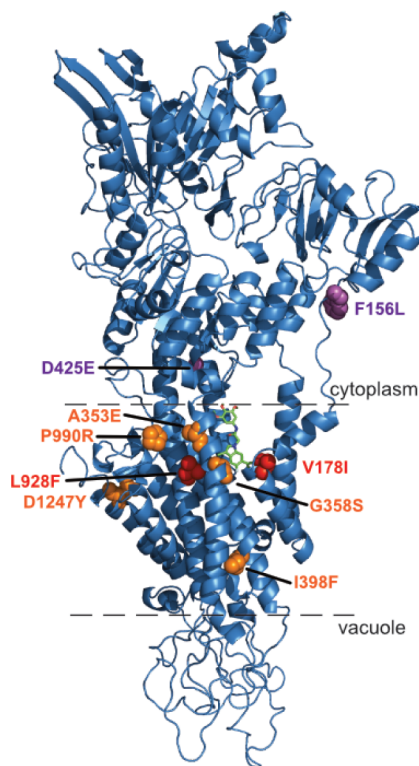


Figure 3. PfATP4 homology model showing mutations observed in W454- and analog **80**-resistant populations (red), PfATP4 drug-resistant (SJ733 and KAE609) strains (orange) and compound “49” resistant (purple) strains used in this study. The PfATP4 homology model was constructed from the rabbit sarcoendoplasmic reticulum calcium ATPase (SERCA) crystal structure (PDB 2C88).²⁷ WJM664 (**82**) (green) was docked to the intramembrane groove of PfATP4 showing the possible binding site of the compound relative to the resistant mutations. The predicted transmembrane region is shown by the dashed line.

This observation suggests the N-acetamide indoles may have a similar transmembrane binding site to other PfATP4 inhibitors, such as KAE609 (**1**), SJ733 (**2**) and WJM921.^{5,6,11} Moreover, the L928F mutation has been previously detected in SJ733-resistant parasites.⁵ WJM664 (**82**) was docked into the PfATP4 homology model and was predicted to fit in the intermembrane binding region (Figures 3 and S23). The predicted binding orientation indole moiety of WJM664 (**82**) was similar to the indole portion of CAD204520 in complex with SERCA,²⁸ whereas the trimethoxy aryl motif was directed toward a large cavity which may explain the unusual and flat SAR around this aryl ring (Table 4). Importantly, WJM664 (**82**) was predicted to bind adjacent to the L928F mutation and near other PfATP4 drug-resistant mutations. The binding orientation of the N-acetamide indoles to the transmembrane region of PfATP4 illustrated by docking will need to be confirmed by X-ray structural analysis. Overall, the forward genetic study provided evidence that the N-acetamide indole class kills the malaria parasite by targeting PfATP4.

Minimum Inoculum of Resistance. To give further evidence that the N-indole acetamide series target PfATP4, analog **80** was assessed in a minimum inoculum of resistance (MIR) assay. The MIR assay determines the rate of onset of resistance by treating parasites at a range of inocula with compound for 40 days and monitoring for parasite recrudescence. The recrudescence parasites are subsequently phenotyped and genotyped. The mean IC₅₀ of compound **80** was initially determined to be 17.3 nM and the mean IC₉₀ was determined to be 29.7 nM in the *P. falciparum* Dd2-B2 clone. One single-step selection was set up using 3.3×10^6 Dd2-B2 parasites in each well of a 24-well plate and compound **80** at $3 \times \text{IC}_{90}$ (89 nM). We observed parasite clearance over the first 5 days. This selection had a consistent drug pressure of $3 \times \text{IC}_{90}$ over 42 days, and cultures were screened three times weekly by flow cytometry and smearing. Wells are considered positive for recrudescence when the overall parasitemia reaches 0.3% and parasites are seen on a blood smear. No recrudescence was observed over the course of this selection.

Two higher inoculum selections were set up to determine the MIR. This included two single-step selections, the first using 8×10^7 Dd2-B2 parasites in three flasks at 3% hematocrit each for a total of 2.4×10^8 parasites and compound **80** at $3 \times \text{IC}_{90}$ (89 nM). The second selection consisted of three flasks each containing 3.3×10^8 D2-B2 parasites with 5% hematocrit, for a total of 9.9×10^8 parasites. We observed parasite clearance over the first 5 days. Both these selections had a consistent drug pressure of $3 \times \text{IC}_{90}$ over 40 days, and cultures were screened three times weekly by flow cytometry and smearing. For the lower inoculum (8×10^7) flask selection, recrudescence parasites were not observed in any of the flasks. For the higher inoculum selection (3.3×10^8), recrudescence parasites were observed in flask F1 on day 13 and in flask F2 on day 15 (Table S5). An approximately 100-fold shift in IC₅₀ values and IC₉₀ values for compound **80** was observed (Figure S4 and Table S6). Taken together the calculated Log10 MIR was 8.7 (Table S5) signifying that the N-acetamide indole class has a moderate-to-low risk of resistance onset in further development.

Parasites from flasks F1 and F2 were then analyzed by whole-genome sequencing. Sequencing of both samples revealed SNPs with missense mutations in PF3D7_0932500 (D111N) that encode a putative palmitoyltransferase, DHHC6 and PF3D7_1211900 (V178I) that encodes PfATP4 (Tables S7 – S9). Based on piggyBac transposon insertional mutagenesis study, DHHC6 is not essential for parasite survival,²⁹ and therefore we suspect that the DHHC6 mutation is a bystander and does not contribute to resistance. The V178I mutation was previously detected in parasites resistant to pyrazoleamide compounds (**3** in Figure 1).³⁰ The V178I mutation is in close proximity to the L928F mutation in PfATP4 (Figures 3 and S23) from the forward genetic study on W454 (**5**) in the previous section and located in the predicted binding site of WJM664 (**82**) (Figure 3). These findings from the two forward genetic studies implicate PfATP4 as the target.

Antimalarial Resistance Barcoding Analysis. To provide further evidence that the N-acetamide indole class targets PfATP4 and potentially uncover other molecular targets of this compound class, W452 (**6**) was profiled in a pooled-screening approach using 47 barcoded parasites lines each with mutations conferring resistance to antimalarials in the field or under development. This platform, called the

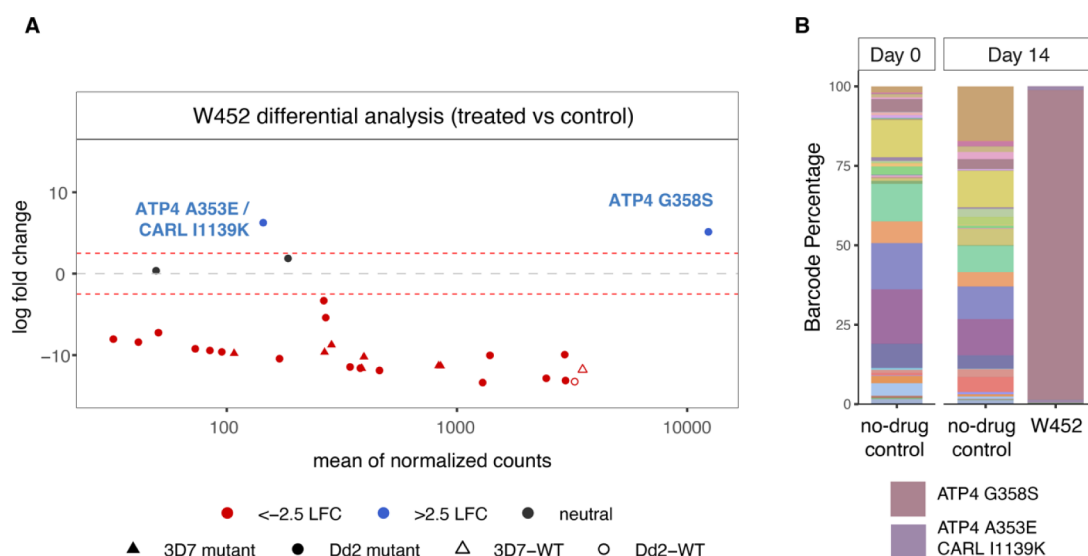


Figure 4. Differential analysis of Antimalarial Resistome Barcode Sequencing (AREBar) profiling of compound W452 (6) reveals enrichment of ATP4 mutant lines. (A) Plot showing barcode counts (x -axis) and log fold change (LFC) of individual barcoded lines (y -axis) after treatment with W452, relative to the untreated control on day 14. Two mutant lines, ATP4^{G358S} and ATP4^{A353E}/CARL^{I1139K}, were found with a significant response to compound (LFC > 2.5 and $p < 0.001$). Symbols indicate strain background, and colors indicate LFC relative to the no-drug control. Data shown in Table S10. (B) Barcode proportions of W452-treated (day 14) and untreated control samples (day 0 and 14), showing the expansion of the ATP4^{G358S} line to 97.4% of the population.

Table 12. Evaluation of N-Acetamide Indole Analogs against *P. falciparum* Strains with Resistance-Confering Mutations in PfATP4

compound	Dd2 EC ₅₀ (SD) μM^a	Dd2 PfATP4 drug-resistant EC ₅₀ (SD) $\mu\text{M}^{a,b}$		Dd2 PfATP4 49-resistant EC ₅₀ (SD) $\mu\text{M}^{a,c}$		
		I398F, P990R, D1247Y	G358S	F156L	D425E	2.8 \times CNV
W454 (5)	0.563 (0.149)	2.54 (0.32)	1.28 (0.13)	1.16 (0.14)	0.786 (0.095)	0.901 (0.057)
W452 (6)	0.194 (0.035)	0.238 (0.065)	1.37 (0.29)	0.382 (0.069)	0.241 (0.013)	0.290 (0.335)
9	0.409 (0.241)	2.51 (0.21)	1.65 (0.11)	0.803 (0.087)	0.892 (0.031)	1.16 (0.11)
80	0.004 (0.002)	0.010 (<0.001)	0.042 (0.006)	0.040 (0.001)	0.019 (0.003)	0.023 (0.002)
"49"	0.016 ^d	0.142 ^d	0.028 ^d	0.025 ^d	0.030 ^d	0.030 ^d
KAE609 (1)	0.0007 (0.0002)	0.004 (<0.001)	>0.10	0.003 ^d	0.002 ^d	0.004 ^d
SJ733 (2)	0.061 (0.009)	0.095 (0.007)	>10	0.112 ^d	0.079 ^d	0.136 ^d

^aEC₅₀ values are an average of 3 independent experiments against PfATP4 drug-resistant *P. falciparum* Dd2 strains in a LDH 72 h assay format. Dose response curves are shown in Figures S7 and S8. ^bDd2 PfATP4^{I398F, P990R, D1247Y} and PfATP4^{G358S} resistant strains. ^cCompound "49" resistant strains. ^dCompound "49" reference data taken from Ashton, Dans et al.¹¹

Antimalarial Resistance Barcoding (AREBar) assay, comprises drug-resistant parasite lines that were genome editing edited to introduce a 101 bp barcode cassette into a nonessential locus.³¹ The pooled barcoded lines were treated with W452 (6) ($3 \times \text{EC}_{50}$ against the Dd2 strain (0.55 μM)) for 14 days and the outgrowth of parasites was monitored by flow cytometry using SYBR green staining. At the end of the selection period, the parasite pool was subjected to PCR to enable library preparation for sequencing of the barcode amplicons. Analysis of the barcode reads determines the proportion change of each line after compound pressure, and in turn the genetic determinants responsible for the survival of one or more parasite lines in the pool.

Differential analysis of the barcode count revealed that compared to the untreated control there was a >2.5-fold increase in the proportion of one line that has a PfATP4^{G358S} mutation and another line with a double PfATP4^{A353E}/CARL^{I1139K} mutation (Figure 4 and Table S10). The barcode count analysis showed that the PfATP4^{G358S} parasite line had the highest proportion of counts (97%). To validate this result, W452 (6) was evaluated against the PfATP4^{G358S} parasite line

(in a later section) and showed an approximately 20-fold increase in the EC₅₀ value versus the parental line (Table 12). The barcoding analysis demonstrated that the N-acetamide indole class was active against 45 drug-resistant parasite lines and reassessed PfATP4 as the molecular target.

PfATP4 Drug Resistant Parasite Profiling. To support the N-acetamide class targeting PfATP4, we next investigated whether the known PfATP4 clinical candidates, KAE609 (1) and SJ733 (2) have reduced sensitivity against the W454-resistant populations. We observed that both KAE609 (1) and SJ733 (2) had 3- and 8-fold reduced activity (EC₅₀ 2.2–2.2 nM; EC₅₀ 533–579 nM) against the three W454-resistant populations in comparison to 3D7 parasites (EC₅₀ 0.7 nM and 61 nM) (Table 11 and Figure S6). This result provided evidence that the N-acetamide indoles target PfATP4 as W454-resistant parasites are cross-resistant to KAE609 (1) and SJ733 (2).

We then evaluated whether N-acetamide indoles had reduced activity against *P. falciparum* strains resistant to other PfATP4 inhibitors. In this study, we used *P. falciparum* Dd2 lines harboring PfATP4^{I398F, P990R, D1247Y} and PfATP4^{G358S}.

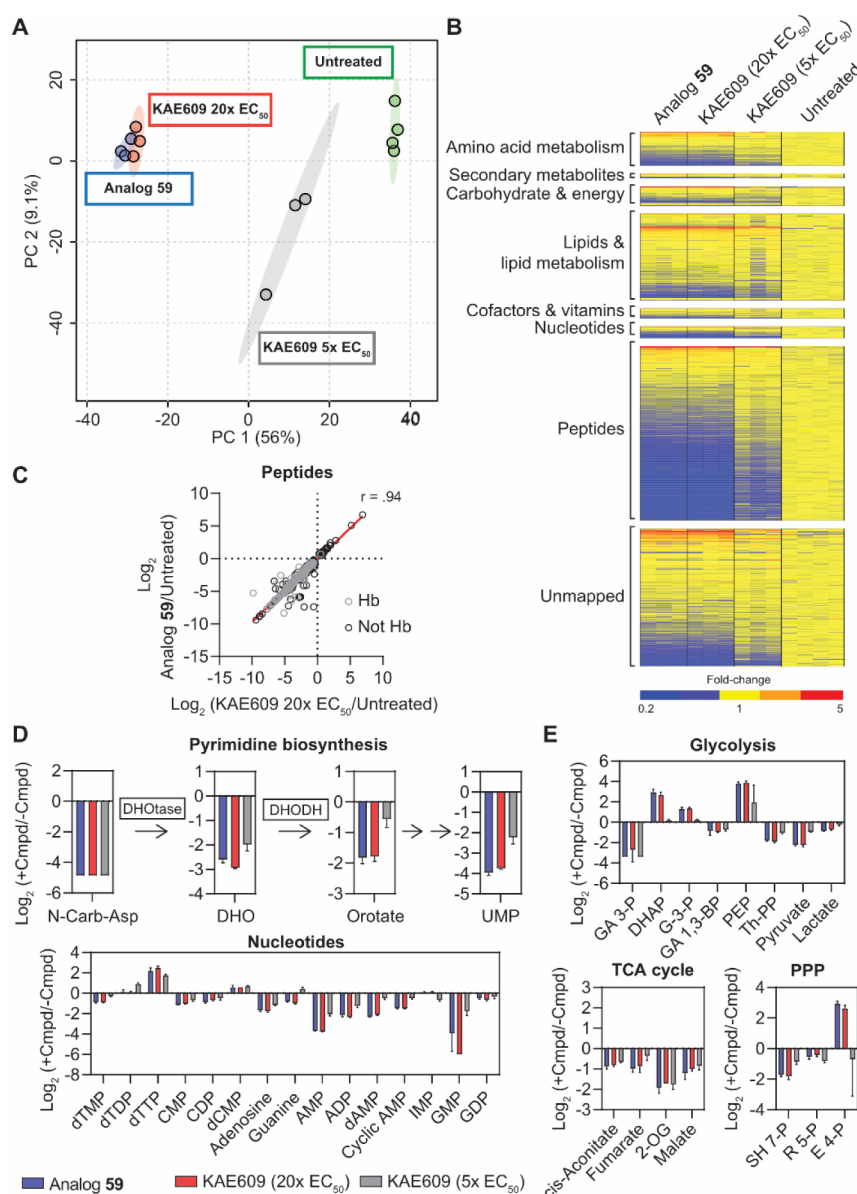


Figure 5. Metabolomic fingerprint of analog **59** matches KAE609. **A.** Principal component analysis of the global metabolite profiles showing overlap of analog **59** with KAE609 (**1**). **B.** Heatmap analysis of the relative abundance of all metabolites revealed that both **59** and KAE609 induce widespread metabolic disruption. **C.** Pearson correlation of the average log₂ fold-change for all peptides significantly perturbed by analog **59** and KAE609 (**1**) ($p < 0.05$ and fold-change ≥ 1.5 or ≤ 0.67). Approximately 40% of perturbed peptides were mapped to the sequence of hemoglobin. **D.** Significant perturbations to pyrimidine biosynthesis and nucleotide metabolites ($p < 0.05$ and fold-change ≥ 1.5 or ≤ 0.67). **E.** Significant perturbations to central carbon metabolites ($p < 0.05$ and fold-change ≥ 1.5 or ≤ 0.67). For D–E data represents the log₂ fold-change of treated samples expressed relative to the average of the untreated control ($n = 3–4$).

The PfATP4^{I398F,P990R,D1247Y} Dd2 line was a lab generated line selected for resistance to KAE609,⁶ and the PfATP4^{G358S} Dd2 line was selected for resistance to SJ733.⁵ The G358S mutation was also detected in patients treated with KAE609 in a clinical trial.¹⁴ It was found that N-acetamide indole derivatives W454 (**5**) and **9** have a 5-fold decrease in activity against the PfATP4^{I398F,P990R,D1247Y} line in comparison to the parental Dd2 strain, while analogs W452 (**6**) and **80** are equipotent (Table 12 and Figure S7). Notably, W452 (**6**) and **80** have a 3,4,5-trimethoxy aryl group as the major point of difference in comparison to W454 (**5**) and **9**, hinting that the 3,4,5-trimethoxy aryl group reduces the susceptibility of the N-acetamide indole chemotype to PfATP4^{I398F,P990R,D1247Y} mediated resistance. Conversely, analogs W454 (**5**) and **9** exhibited

a 3-fold decrease, while W452 (**6**) and **80** showed a 10-fold decrease in activity against the PfATP4^{G358S} line relative to the parental Dd2 strain, suggesting the 2-chloroaryl group reduces the susceptibility of the N-acetamide indole chemotype to PfATP4^{G358S} mediated resistance. Moreover, these data provide further evidence that the indole acetamides target PfATP4.

We recently optimized the dihydroquinazolinone scaffold to have potent antiplasmodial activity (Figure 1).^{11,21,22} Whole genome sequencing of three dihydroquinazolinone analog “49” resistant parasite populations revealed either a PfATP4^{F156L}, PfATP4^{D425E}, or a 2.8 × CNV in PfATP4 in each population.¹¹ To determine if the activity of the N-acetamide indole class was affected by these changes to PfATP4, we tested N-

acetamide indole analogs against the three compound “49”-resistant populations. It was found that analogs W454 (5), W452 (6) and 9 had approximately 2-fold decreased activity against PfATP4^{F156L} line (EC_{50} 0.382 – 1.16 μ M) and the PfATP4^{2.8 \times CNV} line (EC_{50} 0.290–1.16 μ M) compared to the parental Dd2 parasite strain (Table 12 and Figure S8), whereas 80 was 10-fold and 5-fold less potent against the PfATP4^{F156L} and PfATP4^{2.8 \times CNV} lines (EC_{50} 0.040 and 0.023 μ M). In contrast, analogs W454 (5) and W452 (6) exhibited similar activity (EC_{50} 0.786 and 0.241 μ M) against the PfATP4^{D425E} strain relative to the parental Dd2 strain, while analogs 9 and 80 were 2- and 4-fold less active (EC_{50} 0.892 and 0.019 μ M) suggesting that the structural differences in these compounds may modulate a binding interaction with D425 in PfATP4.

We next investigated whether W454-resistant lines were cross-resistant to selected N-acetamide indole analogs to determine if the molecular target was altered during the optimization process. It was observed that the analogs W452 (6) and 80 exhibited a 10-fold decrease in activity against the three W454-resistant populations (EC_{50} 1.80–1.99 and 0.050–0.050 μ M) in comparison to the 3D7 strain (EC_{50} 0.123 and 0.004 μ M) (Table 11 and Figure S6). These data are consistent with the approximate 10-fold EC_{50} shift of compound W454 (5) against W454-resistant parasite populations and implies that during the medicinal chemistry optimization of the N-acetamide indole class, the molecular target was not altered.

Metabolomic Analysis. To confirm that this series targets PfATP4, we profiled the cellular metabolomic response to analog 59 compared to the known PfATP4 inhibitor, KAE609 (1). Purified *P. falciparum* 3D7 infected red blood cells were incubated for 5 h with 1.1 μ M of analog 59 ($5 \times EC_{50}$), 5 nM ($5 \times EC_{50}$) or 20 nM ($20 \times EC_{50}$) of KAE609 (1), or vehicle (DMSO), followed by metabolite extraction and untargeted LC-MS analysis. The PfATP4 protein maintains the Na⁺ gradient across the parasite plasma membrane.⁷ Functional inhibition of PfATP4 results in loss of this ionic gradient and metabolic collapse, which produces a pleiotropic metabolomics fingerprint, as we, and others, have shown previously.^{11,32–35} Principal component and heatmap analyses of the global metabolite profiles demonstrated that the metabolic response to analog 59 overlaps with KAE609 (1) (Figure 5A), and that both compounds cause widespread metabolic disruption (Figures 5B and Supplementary File S1). These data indicate that analog 59 and KAE609 (1) share a common mode of action, consistent with the inhibition of PfATP4. Peptide metabolism was the most significantly perturbed metabolic pathway after analog 59 and KAE609 (1) treatment (Figure S9A), and of the top 50 significantly perturbed metabolites, all except four were depleted putative peptides (Figure S9B). Analog 59 treatment significantly perturbed 70% of detected putative peptides (<0.05 and fold-change ≥ 1.5 or ≤ 0.67), and the majority of these (94%) were decreased in abundance compared to the untreated control (Figures 5B–C and Supplementary File S1). KAE609 (1) treatment induced the same profile of perturbed putative peptides ($r = 0.945$, $p < 0.0001$). Among the overall 419 peptides significantly perturbed in this study, 92% were dysregulated by both analog 59 and KAE609 (1) (Figures 5B–C, S9 and Supplementary File S1). These significantly perturbed peptides consist of a subset (~40%) that can be mapped to the sequences of hemoglobin (α , β and δ chains), while the majority likely

originate from altered turnover of other host or parasite proteins (Figure 5C).

The other major metabolic impact in parasites treated with analog 59 or KAE609 (1) was nucleotide metabolism (Figure S9A). This response included depletion of pyrimidine biosynthesis pathway metabolites and decreased general nucleotide levels, except for the pyrimidine deoxyribonucleotides, deoxythymidine triphosphate, deoxythymidine diphosphate and deoxycytidine monophosphate, which were increased (Figure 5D). The pleiotropic metabolic response to analog 59 and KAE609 (1) also included significant perturbations in central carbon metabolites (Figure 5E), cofactors and vitamins, amino acid derivatives, and lipids (Figures 5B and S10–S12). This general insult on parasite metabolism is consistent with the known metabolomic signature of PfATP4 inhibition, and distinct from the signature observed for other compounds with different known targets.^{11,32–35}

Evaluation of Asexual Stage and Rate of Arrest. The asexual stage of arrest assay and parasite reduction ratio assay (PRR) aid in determining the alignment of a compound series with Target Candidate Profiles (TCPs) and inclusion as a partner agent in the Target Product Profile (TPP).³ These assays can also be used to determine if the stage specificity and rate of kill are consistent with that of other PfATP4 inhibitors.

To assess the rate of kill, synchronized ring-staged *P. falciparum* 3D7 parasites were treated with hit compound W452 (6) at $10 \times EC_{50}$ and incubated for 120 h. Samples were collected every 24 h for 120 h, and the compound was removed from each sample with new media and RBCs added. The samples were incubated for another 16 days, at which time, parasitemia was evaluated using an LDH assay. It was observed that W452 (6) reduced parasitemia to below detectable levels at 72 h. This aligned with the fast-to-moderate killing rate of chloroquine and pyrimethamine (Figure 6A). The fast-to-moderate killing rate is the same as that observed with other PfATP4 inhibitors.

To determine the point of the asexual stage cycle at which N-acetamide indoles arrest parasites, *P. falciparum* 3D7 parasites were treated with selected N-acetamide indoles analogs and the known PfATP4 inhibitor, SJ733 (2) at $10 \times EC_{50}$ for 48 h. Parasite samples were collected from the culture at 0, 12, 24, 36, and 48 h and microscopy was performed on Giemsa-stained thin blood-smear samples. Samples were also stained with SYBR Green for flow cytometry quantification. It was revealed that N-acetamide indole analogs W454 (5), W452 (6) and 9 arrested asexual parasites at the trophozoite stage (Figures 6B and S13). Quantification of the asexual parasite growth revealed that the percentage of parasitemia plateaus and declines after 24 h (Figure 6C). Microscopy unveiled that N-acetamide indole treated parasites presented with a vacuolated-like phenotype (Figures 6B and S13)—a characteristic common to PfATP4 inhibitors.^{5,11,36,37} The stage of arrest and morphologies observed was consistent with those parasites treated with the PfATP4 inhibitor, SJ733 (2). Overall, asexual phenotyping supports the N-acetamide indole class targeting PfATP4.

Evaluation of Red Blood Cell Lysis. In addition to the vacuolization of asexual stage parasites, it is established that PfATP4 inhibitors lead to the lysis of the infected RBCs, which is believed to cause an increase in the osmotic fragility of infected RBCs, which can lead to lysis.^{8,36,37} To investigate whether N-acetamide indole analogs caused lysis of *P.*

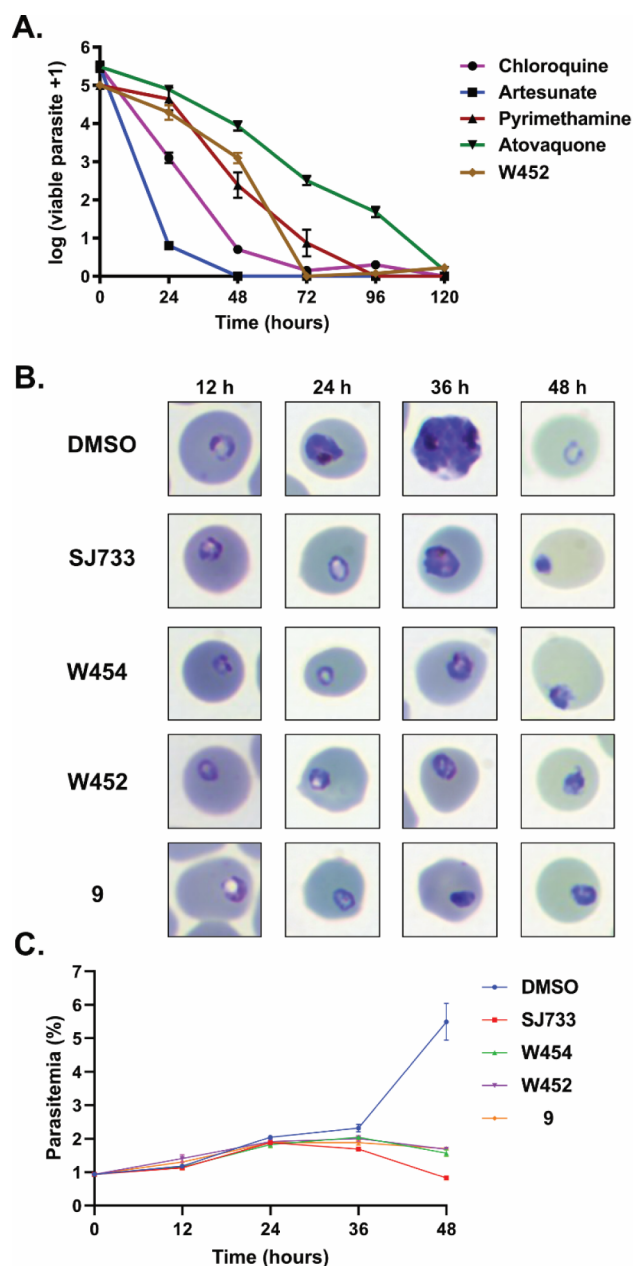


Figure 6. Parasite reduction ratio and stage of asexual arrest analysis on selected N-acetamide indole analogs. **A.** Activity in a parasite reduction ratio assay in comparison to antimalarial drugs. Data represent the means and SDs for three replicate experiments using *P. falciparum* 3D7 parasites in an LDH assay. **B.** Microscopy images are representative of *P. falciparum* 3D7 parasite morphology determined by Giemsa-stained blood smears at $10 \times EC_{50}$ of each compound after treatment of ring-stage parasites. More representative microscopy images are shown in Figure S13. Compounds cause vacuolated parasites consistent with the morphology observed with the PfATP4 inhibitor SJ733. **C.** Quantification of asexual parasite growth over 48 h. Data represent the means and SDs for three experiments.

falciparum infected RBCs, we treated *P. falciparum* 3D7 expressing the Hyp-1 nano luciferase (NLuc) fusion protein³⁷ with selected N-acetamide indole analogs, PfATP4 inhibitors, KAE609 (**1**) and SJ733 (**2**), and chloroquine (RBC lysis negative control) at $10 \times EC_{50}$ for 8 h. Cultures were incubated and samples were collected at 0, 2, 4, 6, and 8 h. NanoGlo substrate was added, and luminescence was

measured which is proportional to RBC lysis. Additionally, microscopic images were taken from Giemsa-stained thin blood smears at 0 and 8 h to quantify the percentage of extracellular parasites and intracellular parasites in each treatment.

It was shown that N-acetamide indole analogs W454 (**5**) and **80** caused greater RBC lysis than DMSO and chloroquine over 8 h (Figures 7A and S14). W454 (**5**) caused 2-fold more lysis than DMSO and 1.6-fold more lysis than chloroquine at 8 h, while a 5-fold increase in lysis was caused by analog **80**. This result was similar to that observed for the PfATP4 inhibitors KAE609 (**1**) and SJ733 (**2**) which gave rise to an approximately 5-fold increase in RBC lysis compared to

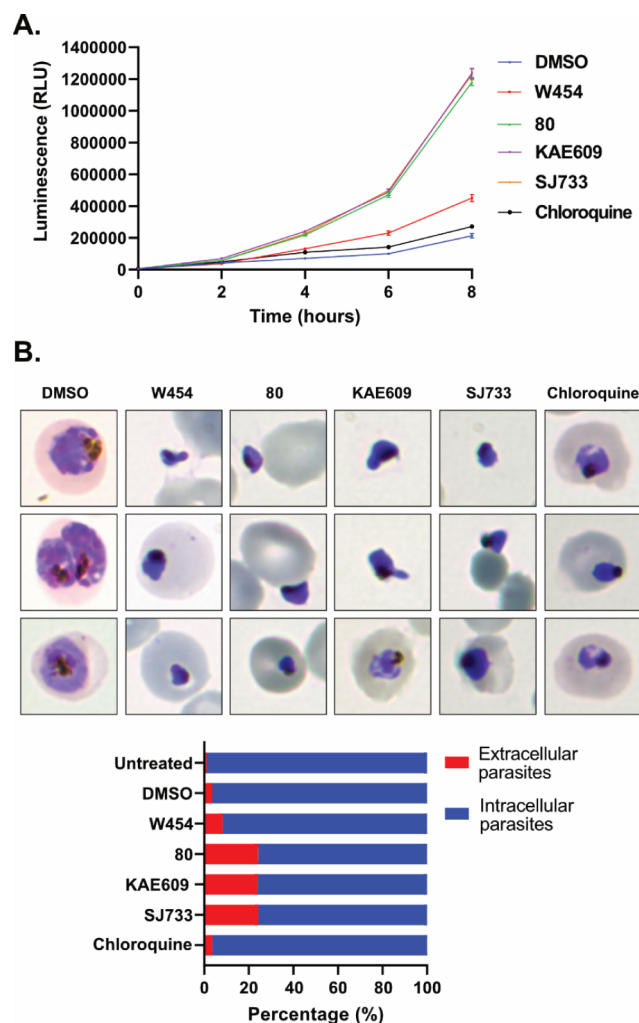


Figure 7. N-Acetamide indole analogs induce the lysis of red blood cells infected with *P. falciparum* 3D7 expressing the Hyp-1 NLuc fusion protein. Parasitized red blood cells were treated with the selected compounds, W454 (**5**) ($5.7 \mu M$) and **80** ($0.03 \mu M$) and PfATP4 inhibitors, KAE609 (**1**) ($6.7 nM$) and SJ733 (**2**) ($0.7 \mu M$), and chloroquine ($0.15 \mu M$) at a concentration of $10 \times EC_{50}$ for 8 h. The luminescence measured was proportional to the amount of red blood cell lysis. **A.** Red blood cell lysis over time. $n = 1$ data represent means and SD of 3 technical replicates. $n = 2$ and 3 are shown in Figure S14. **B.** Microscopic images from Giemsa-stained thin blood smears at 8 h. Quantification of the percentage of extracellular and intracellular parasites with each treatment at 8 h versus untreated parasites at 0 h. Replicates for cell lysis assay can be found in Figure S14.

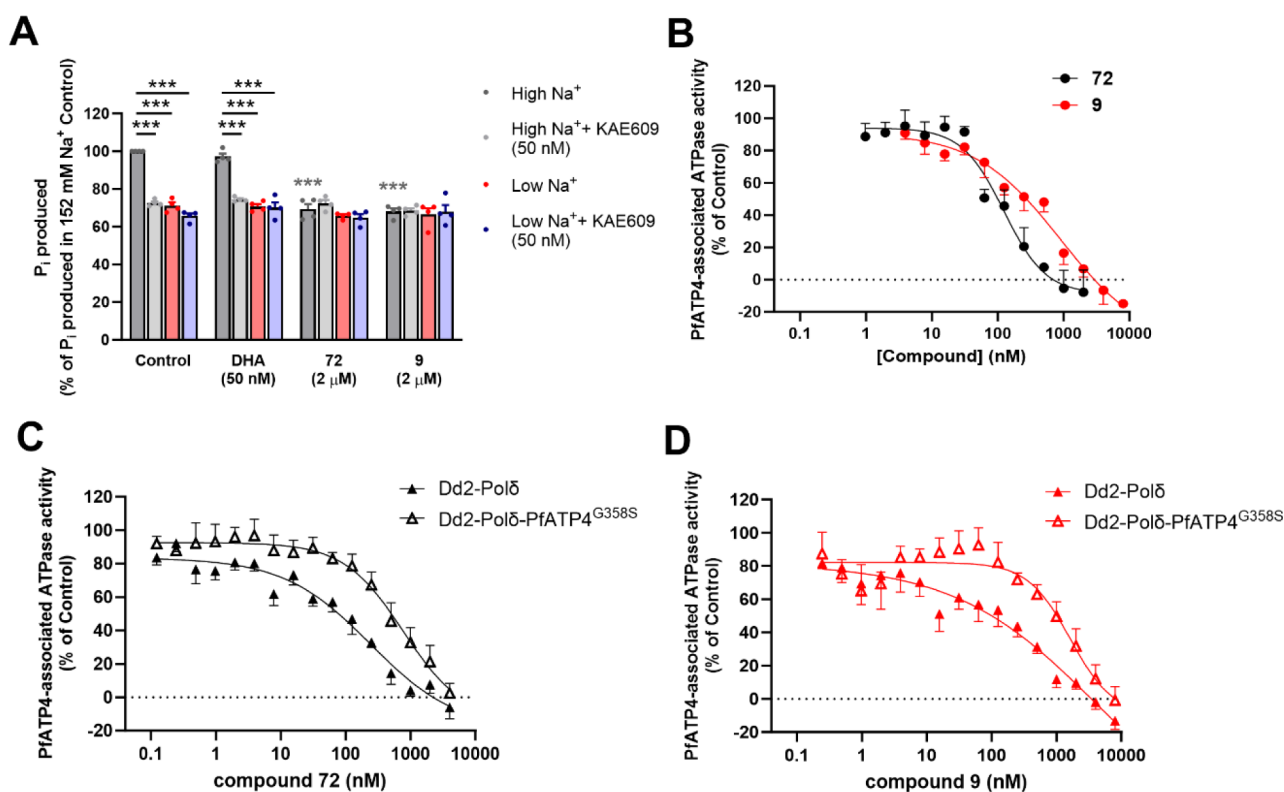


Figure 8. N-Acetamide indole analogs inhibit Na^+ -ATPase activity in parasite membrane preparations, consistent with them targeting PfATP4. **A.** The effects of 0.2% v/v DMSO (solvent-only control), dihydroartemisinin (DHA; 50 nM; negative control), analog 9 (2 μ M) and analog 72 (2 μ M) on membrane ATPase activity under high- $[Na^+]$ conditions (152 mM Na^+) and low- $[Na^+]$ conditions (2 mM Na^+); stemming from the addition of 1 mM Na_2ATP in the presence and absence of KAE609 (1) (50 nM). The data are from four independent experiments, each performed with different membrane preparations. The symbols show the data from individual experiments and the bars show the mean (+SEM). The P_i produced is expressed as a percentage of that measured in the 152 mM Na^+ Control. In individual experiments, the P_i produced in the 152 mM Na^+ control varied from 67 to 103 nmol per mg (total) protein per min. The prenormalized data for different compounds and conditions were compared using a repeated measures ANOVA with a *post hoc* Tukey test. For comparisons between different conditions for the same test compound (or for the control), significant differences are shown with black asterisks. For comparisons between the control and a compound under the same test condition, significant differences are shown with colored asterisks (in this case, gray asterisks, as the only significant differences were between the control and the N-acetamide indole compounds in the 152 mM Na^+ condition). *** $p < 0.001$. **B.** The effects of a range of different concentrations of 9 (red circles) and 72 (black circles) on PfATP4-associated ATPase activity. The data were obtained from four independent experiments performed with different membrane preparations, with the exception of the two highest concentrations of analog 9, for which data are from three independent experiments. In A and B, the membranes were prepared from isolated trophozoite-stage 3D7 parasites. **(C, D)** The effects of a range of different concentrations of 72 (black; C) and 9 (red; D) on PfATP4-associated ATPase activity in membranes prepared from Dd2-Pol δ -PfATP4^{G358S} parasites (open triangles) and their Dd2-Pol δ parents (closed triangles). In C, the data are from four (Dd2-Pol δ) or five (Dd2-Pol δ -PfATP4^{G358S}) independent experiments (except for the four lowest concentrations, for which data are $n = 2-3$). In D, the data are from five independent experiments (except for the lowest four concentrations, for which data are $n = 2-3$). In B-D, the P_i production measured in the low- $[Na^+]$ (2 mM) condition was subtracted from that measured in the high- $[Na^+]$ (152 mM) condition in the presence of each of the different concentrations of analogs 9 and 72 to calculate the PfATP4-associated ATPase activity. The PfATP4-associated ATPase activity is expressed as a percentage of that obtained for the high- $[Na^+]$ (152 mM) Control, and shown as mean \pm SEM.

vehicle control at 8 h. Quantification of the Giemsa-stained smears revealed that 8% of parasites were extracellular in cultures treated with W454 (5) compared to 3.5% with the vehicle control or chloroquine (Figures 7B and S14). Approximately 24% of parasites were extracellular in cultures treated with analog 80 and PfATP4 inhibitors KAE609 (1) and SJ733 (2). Although most parasite-infected RBCs treated with N-acetamide indoles and PfATP4 inhibitors remain intracellular, they do not mature into late-stage trophozoites which is consistent with the findings from the stage of arrest assay (Figure 6B). Similarly, parasites treated with chloroquine remain intracellular as the mechanism of action is not related to RBC lysis. Collectively the RBC lysis data indicates that the N-acetamide indoles increased the lysis of the parasite-infected RBCs which is consistent with the phenotype observed with

the PfATP4 inhibitors, KAE609 (1) and SJ733 (2), providing additional evidence the N-acetamide indole class targets PfATP4.

Evaluation of PfATP4 Inhibition. Inhibitors of the PfATP4 pump, which is believed to import H^+ while exporting Na^+ , can be detected in pH-based assays.^{7,38} In the assays used here to test the N-acetamide indoles, trophozoites (3D7 strain) isolated from RBCs were loaded with the pH-sensitive dye, 2,7-bis(2-carboxyethyl)-5(6)-carboxyfluorescein (BCECF) and depleted of ATP (through incubation in a glucose-free saline). The parasites were then suspended in a saline solution containing glucose, concanamycin A (100 nM; an inhibitor of the parasite's primary pH regulator, the V-type H^+ ATPase),^{39,40} and then treated with the hit compounds W454 (5), W452 (6) (5 μ M), KAE609 (50 nM) or DMSO

Table 13. Evaluation of Selected Compounds against *P. knowlesi* Parasites and *P. falciparum* Multidrug Resistant Strains^a

compound	wildtype parasites EC ₅₀ (SD) μ M		<i>P. falciparum</i> multidrug-resistant parasites EC ₅₀ (SD) μ M			
	<i>P. falciparum</i> 3D7	<i>P. knowlesi</i> YH1	Dd2	W2 ^{mef}	7G8	Cam3.1
W452 (5)	0.249 (0.028)	0.431 (0.288)	0.320 (0.063)	0.272 (0.005)	0.578 (0.153)	0.381 (0.041)
9	0.236 (0.038)	0.661 (0.184)	0.385 (0.122)	0.279 (0.042)	0.526 (0.153)	0.476 (0.172)
59	0.073 (0.033)	0.195 (0.149)	0.099 (0.011)	0.077 (0.019)	0.165 (0.037)	0.124 (0.027)
SJ733 (2)	0.043 (0.027)	0.227 (0.022)	nd	nd	nd	nd
MFQ	0.023 (0.006)	nd	0.035 (0.001)	0.064 (0.019)	nd	0.009 (0.003)

^aEC₅₀ values are an average of 3 independent experiments against *P. falciparum* asexual parasites for 48 h and *P. knowlesi* asexual parasites for 30 h quantified by flow cytometry using a SYBR-green stain. MFQ = mefloquine. Dose response plots are shown in Figures S17 and S18. nd = no data.

(0.1% v/v; solvent control). The fluorescence ratio (obtained through excitation of the fluorophore at two different wavelengths) was monitored over 30 min. It was found that W454 (5), W452 (6) and KAE609 (1) gave rise to an increase in fluorescence ratio (which signifies an increase in parasite cytosolic pH) relative to the DMSO control (Figure S15). This is consistent with W454 (5) and W452 (6) being PfATP4 inhibitors.

PfATP4 inhibitors give rise to an increase in the Na⁺ concentration in the parasite cytosol ([Na⁺]_{cyt}).⁷ To investigate the impact of the N-acetamide indole class on [Na⁺]_{cyt} trophozoites isolated from RBCs were loaded with the Na⁺ sensitive dye, benzofuran isophthalate (SBFI) and treated with N-acetamide indole analogs. Fluorescence was then measured over 60 min. The N-acetamide indole analogs W454 (5) and W452 (6) gave rise to an increase in [Na⁺]_{cyt} in both a time-dependent and concentration-dependent manner (Figure S16), consistent with them being PfATP4 inhibitors. Both compounds gave rise to half-maximal effects in this assay at a concentration of approximately 0.4 μ M.

We next investigated whether optimized analogs 9 and 72 inhibit ATPase activity in membranes prepared from isolated trophozoite-stage parasites. The Na⁺-dependent fraction of membrane ATPase activity has previously been attributed to PfATP4 activity.^{7,41,56} We first tested the compounds for their effects on ATPase activity in membranes prepared from 3D7 parasites under high-[Na⁺] (152 mM) and low-[Na⁺] (2 mM) conditions, in the presence and absence of a supramaximal concentration of the PfATP4 inhibitor KAE609 (1) (50 nM). Consistent with previous results,^{21,22} the antimalarial dihydroartemisinin (DHA; 50 nM) did not affect membrane ATPase activity under any of the conditions tested (Figure 8A). Analogs 9 and 72 significantly inhibited ATPase activity in the high-[Na⁺], no-KAE609 condition, reducing it to levels similar to those observed in low-[Na⁺] conditions or in the presence of KAE609 (1) (Figure 8A). This is consistent with both compounds giving rise to complete inhibition of PfATP4 at the concentration tested (2 μ M). Analogs 9 and 72 did not affect ATPase activity under low-[Na⁺] conditions or in the presence of KAE609 (1) (Figure 8A), suggesting that they do not inhibit other membrane ATPases that were active in the experiments. We then tested a range of concentrations of analogs 9 and 72 to investigate the potency by which they inhibit PfATP4. Analogs 9 and 72 inhibited PfATP4(3D7)-associated ATPase activity with IC₅₀s of 0.79 \pm 0.40 μ M and 0.15 \pm 0.06 μ M, respectively (mean \pm SEM; *n* = 4; Figure 8B).

We also investigated the potencies by which analogs 9 and 72 inhibit the PfATP4 isoforms from Dd2-Pol δ -PfATP4^{G358S} parasites (generated previously⁴¹ and Dd2-Pol δ parental parasites⁴²). In addition to the G358S mutation in the former, both isoforms have a G1128R mutation that is found in Dd2

parasites but not 3D7 parasites. Analog 72 inhibited Na⁺-dependent ATPase activity with IC₅₀s of 0.23 \pm 0.04 μ M (mean \pm SEM; *n* = 4) and 1.1 \pm 0.4 μ M (mean \pm SEM; *n* = 5) in membranes prepared from Dd2-Pol δ and Dd2-Pol δ -PfATP4^{G358S} parasites, respectively (*p* = 0.1, unpaired *t*-test; Figure 8C). For analog 9, the respective IC₅₀s were 0.59 \pm 0.19 μ M and 1.6 \pm 0.4 μ M (mean \pm SEM; *n* = 5; *p* = 0.04, unpaired *t*-test; Figure 8D). Thus, the G358S mutation reduces the potency by which analogs 9 and 72 inhibit PfATP4, although for 72 the difference was not statistically significant.

Evaluation of Activity against Multidrug-Resistant Parasites. To ensure the N-acetamide indole class was not susceptible to common antimalarial drug-resistance mechanisms, we profiled a cohort of analogs against a panel of multidrug-resistant parasite strains. These strains included Dd2 and W2^{mef}, which both have an amplification in the P-glycoprotein homologue (Pgh-1) encoding *pfmdr1* gene which confers resistance to pyrimethamine, chloroquine, mefloquine, and quinine,⁴³ Dd2, W2^{mef} and 7G8 with multiple mutations in PfCRT,⁴⁴ which results in resistance to chloroquine and pyrimethamine and Cam3.1, an artemisinin resistant strain with a mutation in Kelch13.⁴⁵ It was shown that analogs W452 (6), 9, and 59 exhibited comparable activity against the Dd2, W2^{mef}, and Cam3.1 parasite strains relative to the 3D7 parasite strain (Table 13 and Figure S17). The analogs, however, showed a 2-fold decrease in activity against the 7G8 strain compared to the 3D7 strain. This suggests that the N-acetamide analogs maybe slightly vulnerable to the 7G8 allele that antimalarial drugs chloroquine and pyrimethamine are also susceptible to. These data suggest that resistance mechanisms investigated will not pose major risks for the future development of the N-acetamide indole class.

Evaluation of *P. knowlesi* Activity. PfATP4 inhibitors typically have decreased activity against other *Plasmodium* species compared to *P. falciparum*,⁴⁶ presumably due to the differences in amino acids located in the putative ATP4 transmembrane binding region of each species. To assess whether the N-acetamide indoles will have varying activity against different *Plasmodium* species other than *P. falciparum*, we elected to test representative analogs against *P. knowlesi* YH1 in a 30-h parasite growth assay. It was revealed that analogs W452 (6), 9, and 59 were 2- to 3-fold less active (EC₅₀ 0.20–0.66 μ M) against *P. knowlesi* parasites contrasted with the activity against *P. falciparum* (EC₅₀ 0.07–0.25 μ M) (Table 13 and Figure S18). In comparison, the PfATP4 inhibitor SJ733 was 5-fold less active (EC₅₀ 0.23 μ M) against *P. knowlesi* parasites than *P. falciparum* (EC₅₀ 0.04 μ M). These data are consistent with previous findings for PfATP4 inhibitors against *P. knowlesi* and may have implications in assessing the efficacy

of N-acetamide indole analogs in a mouse model using a non-*P. falciparum* species.

Evaluation of Activity against Transmission Stages.

PfATP4 inhibitors have been shown to block the transmission of sexual stage parasites to the mosquito.⁴⁷ To assess the effectiveness of N-acetamide indole compounds at inhibiting the functionality of mature stage V gametocytes and blocking parasite transmission to mosquitoes we performed a dual gamete formation assay⁴⁸ and a standard membrane feeding assay.⁴⁹

In the dual gamete formation assay, *P. falciparum* NF54 stage V gametocytes were treated with selected N-acetamide indole analogs for 48 h and then xanthurenic acid was added and the temperature decreased from 37 °C to 20 °C to simulate the mosquito gut environment and induce male and female gamete formation. After a 30 min incubation period, male gamete viability was determined by brightfield microscopy measuring exflagellation, and after a subsequent 24 h incubation period, female viability was analyzed by fluorescence microscopy using a Cy3-labeled Pfs25 antibody.⁵⁰ It was shown that hit compounds W454 (**5**) and W452 (**6**), and analog **59** showed modest inhibition of male and female gamete formation (EC₅₀ 1.5–7.4 μM) (Table 14 and Figure

Table 14. *P. falciparum* NF54 Gamete Activity of Selected Compounds^a

compound	male gamete EC ₅₀ μM	female gamete EC ₅₀ μM
W454 (5)	3.6	5.0
W452 (6)	7.4	7.2
59	1.5	3.4
80	0.19	0.18
WJM664 (82)	0.21	0.25

^aEC₅₀ data represents the averages of four replicate experiments following exposure of stage V *P. falciparum* gametocytes to compounds for 48 h prior to inducing gametogenesis. Thereafter, male gametogenesis was quantified 30 min later and female gametogenesis quantified after 24 h. The viability of male gametes was quantified by automated brightfield microscopy measuring exflagellation and for female gametes viability was measured by fluorescence microscopy to detect Pfs25-positive cells. Error is shown in dose response plots in Figure S19.

S19). The frontrunner compounds **80** and WJM664 (**82**) were substantially more potent against both male and female gametes (EC₅₀ 0.19 and 0.21 and 0.18 and 0.25 μM). The trends in gamete activity between compounds W454 (**5**), W452 (**6**) and **59** and the frontrunner compounds **80** and WJM664 (**82**) are aligned with their activity against asexual blood stage parasites (Figure 1, Tables 5 and 9). This activity observed with N-acetamide indole analogs against male and female gametes is consistent with data on PfATP4 inhibitors from literature.^{5,11,21,22,47}

On establishing that the frontrunner compound WJM664 (**82**) inhibits gamete development, we next assessed whether the inhibition of gametogenesis would block transmission to the mosquito using a standard membrane feeding assay. In this assay, blood infected with *P. falciparum* NF54 stage V gametocytes were treated with compound WJM664 (**82**) (100 and 500 nM) and fed to *Anopheles stephensi* mosquitoes. After the blood meal, mosquitoes were incubated for 7 days before they were harvested, and their midguts were dissected to count the oocyst numbers in the hemolymph by microscopy. It was shown that at 100 nM of WJM664 (**82**)

the average oocyst count was reduced by 59%, and at 500 nM of WJM664 (**82**) the average oocyst count was decreased by 83% relative to the vehicle control group (Figure 9). These

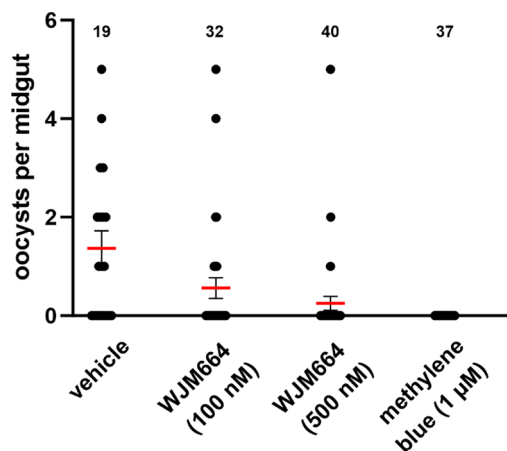


Figure 9. Activity of WJM664 (**82**) in a standard membrane feeding assay. Oocyst counts from midguts dissected from *Anopheles stephensi* mosquitoes 7 days post a blood meal infected with *P. falciparum* NF54 stage V gametocytes treated with compound at the indicated concentration. Numbers indicate the total number of mosquito midguts dissected per treatment group. Red bars indicate average oocyst intensity and error bars represent SEM. WJM664 (**82**) at 100 and 500 nM versus the vehicle *t* test *p* = 0.04 and 0.001 respectively. The repeat experiment is shown in Figure S20.

data were supported by the trends observed in the repeat experiment (Figure S20). These data are consistent with those obtained for other PfATP4 inhibitors,^{5,21,47} and demonstrate the transmission-blocking potential of the N-acetamide indole class.

Efficacy in an Asexual *P. berghei* Mouse Model. The frontrunner N-acetamide compound WJM664 (**82**) was found to have suitable antiparasitic potency and metabolic stability for efficacy assessment in an asexual *P. berghei* mouse model. In this mouse model, mice were infected with the mouse-specific *P. berghei* ANKA strain. Two hours after the mice were infected, compounds WJM664 (**82**), at 50 mg/kg dihydroartemisinin (DHA) at 30 mg/kg and vehicle control were administered b.i.d. by oral gavage. The compounds were then delivered again at the same dose 24, 48, and 72 h after the infection. 24 h after the last dose, blood samples were taken. Giemsa blood stains were prepared and the level of parasitemia was then analyzed by microscopy. It was shown that compound WJM664 (**82**) did not significantly reduce parasite levels compared to the vehicle control (Table 15 and Figure S21). DHA, the positive control, showed a complete reduction in parasitemia.

A plasma exposure study in mice showed that WJM664 (**82**) was characterized by a moderate rate and level of absorption (*T*_{max} 5.33 h; *C*_{max} 0.70 μg/mL), moderate systemic exposure (AUC_{0–last} 8.19 h*μg/mL), a short terminal half-life (2.16 h) and moderate clearance (42.02 mL/min/kg) (Figure S22 and Table S11). The moderate absorption and systemic exposure of WJM664 (**82**) in mice may be attributed to the low aqueous solubility (Table 10) and low Caco-2 permeability (Table S1). The plasma concentration of WJM664 (**82**) in mice remains well above the *in vitro* *P. falciparum* 3D7 EC₅₀ of 0.013 μM for over 20 h (Figure S22) and is consistent with the *in vitro* metabolic stability (Table 10). This implies that the structural

Table 15. Evaluation of Compounds in a *P. berghei* 4-Day Mouse Model^a

compound	p.o. dose (mg/kg)	% parasitemia ^b	% reduction in parasitemia ^c
WJM664 (82)	50	15.3	55.0
artemisinin	30	2.6	92.4

^aCompounds were administered by oral gavage at the indicated dose at 2, 24, 48, and 72 h after infection with *P. berghei* ANKA parasites. Parasitemia was quantified by measuring microscopy. ^bAverage % parasitemia for 5 mice on day 5. ^cAverage % reduction in parasitemia versus the vehicle control (34% parasitemia) for 4 mice on day 5. Figure S21 shows plotted data and error.

differences in the N-acetamide indole binding site between *P. falciparum* and *P. berghei* ATP4 are the major contributing factors to the low efficacy observed in the *P. berghei* model. For this reason, it is typical practice for PfATP4 inhibitors to be evaluated in a *P. falciparum* humanized mouse model.^{5,21} At the time of this study, we did not have access to the *P. falciparum* humanized mouse model, and therefore, in the future advancement of the N-acetamide indole series efficacy studies in a *P. falciparum* humanized mouse model are recommended.

CONCLUSIONS

The N-acetamide indole chemical class was one of several hit series identified from a screen of the Janssen Jumpstarter library against the *P. falciparum* asexual blood stage parasite. Structure–activity analysis revealed that the inclusion of a small substituent at the 3-position and a fluoro at the 6-position of the indole architecture led to significant increases in antiparasitic potency and improved metabolic stability in liver microsomes and hepatocytes. It was found that the 7-(4-methyl)oxadiazole could be replaced with the isosteric 4-(N-methyl)pyrazole without loss of activity thus benefiting from a chemical synthesis with reduced complexity and notionally improved physical attributes. Manipulations to the pendant aryl group resulted in little variation in antiplasmodial activity suggesting this moiety may be orientated toward solvent space rather than substantial binding to its molecular target. Confoundingly, analogs with the pendant 2-choro aryl and the 3,4,5-trimeythyloxy aryl groups exhibited the greatest potency, although it was revealed that the 3,4,5-trimeythyloxy aryl group consistently gave enhanced metabolic stability. These modifications led to the frontrunner N-acetamide indole WJM664 (82) that exhibited potent asexual stage activity (EC₅₀ 0.013 μ M) with no human HepG2 cell cytotoxicity and high metabolic stability in human and mouse liver microsomes and rat hepatocytes (CL_{int} <3.5 and 6.8 μ L/min/mg and CL_{int} 2.6 μ L/min/10⁶ cells). Improving the aqueous solubility and Caco-2 absorption will be key to the future optimization of the N-acetamide indole class.

A forward genetic approach was undertaken to elucidate the molecular target of the N-acetamide indole class. Resistance selection with the hit compound W454 (5) resulted in three resistant parasite populations with a 10-fold shift in the EC₅₀ value versus the parental 3D7 strain. Whole genome sequencing of these three resistant populations revealed a L928F mutation in PfATP4, suggesting PfATP4 was the molecular target of the N-acetamide indole class. These data were supported by genome sequencing of recrudescence parasites from the MIR study conducted with analog 80,

which resulted in a previously identified V178I mutation³⁰ in PfATP4 which was located close to the L928F mutation. PfATP4 was further verified as the target by showing that the clinical candidates KAE609 (1) and SJ733 (2) were rendered less active by the L928F mutation and that the L928F mutation was previously detected in SJ733-resistant parasites.⁵ The N-indole acetamide class showed decreased activity against parasites with PfATP4^{L398F,P990R,D1247Y} and PfATP4^{G358S} in cross-resistance profiling, and the AReBar platform further supported this chemical class targeting PfATP4. Phenotypic characterization of asexual parasites showed the N-acetamide indole class gave rise to a similar rate and stage of parasite arrest and similar vacuolar and red blood cell lysis phenotypes observed with PfATP4 inhibitors KAE609 (1) and SJ733 (2). It was also shown that N-acetamide indole analogs increased parasite cytosolic Na⁺ and pH levels and inhibited Na⁺-dependent ATPase activity in parasite membrane preparations—characteristic traits of PfATP4 inhibitors. Collectively, these data support PfATP4 as the molecular target of the N-acetamide indole class.

The N-acetamide indole class was shown to kill both female and male gametes in vitro and in turn prevent infection of the mosquito in a standard membrane feeding assay. Akin to other PfATP4 inhibitors, the asexual and sexual stage killing capacity aligns the N-acetamide indole class with the TCPs 1 and 5 and the possibility for inclusion in a curative or mass-administered population control antimalarial therapy.³ A common observation with PfATP4 inhibitors is the relatively quick rate by which parasites acquire resistance, which was concerning observed when parasites were detected with the PfATP4^{G358S} mutation from patients treated with KAE609 in a clinical trial.¹² Resistance selection in a minimum inoculum of resistance platform suggested a moderate-to-low risk of resistance for N-acetamide indoles, underscoring the suitability of this chemotype for further development. Oral administration of WJM664 (82) at 50 mg/kg did not significantly reduce parasitemia in an asexual stage *P. berghei* mouse model. It was reasoned that differences in the putative binding site in ATP4 between *P. berghei* and *P. falciparum* orthologs resulted in the lack of efficacy observed in a *P. berghei* mouse model. This hypothesis was supported by the finding that N-acetamide indoles had different potencies against *P. falciparum* and *P. knowlesi* (Table 13). It is also possible that the limited aqueous solubility and low absorption contributed to the moderate systemic exposure (Figure S22 and Table S11) and low efficacy observed with WJM664 (82) in a *P. berghei* mouse model. Optimization of these physical parameters and assessment in a *P. falciparum* humanized mouse model will be important for the N-acetamide indole chemotype joining the compendium of antimalarials under development to treat and eliminate malaria.

EXPERIMENTAL SECTION

General Chemistry Methods. NMR spectra were recorded on a Bruker Ascend 300. Chemical shifts are reported in ppm on the δ scale and referenced to the appropriate solvent peak. MeOD, DMSO-*d*₆, D₂O, and CDCl₃ contain H₂O. Chromatography was performed with silica gel 60 (particle size 0.040–0.063 μ m) using an automated CombiFlash Rf Purification System. LCMS were recorded on an Agilent LCMS system comprised of an Agilent G6120B Mass Detector, 1260 Infinity G1312B Binary pump, 1260 Infinity G1367E HiPALS autosampler and 1260 Infinity G4212B Diode Array Detector. Conditions for LCMS were as follows, column: Luna Omega 3 μ m PS C18 100 Å, LC Column 50 \times 2.1 mm at 20 $^{\circ}$ C, injection volume 2 μ L, gradient: 5–100% B over 3 min (solvent A:

H₂O 0.1% formic acid; solvent B: ACN 0.1% formic acid), flow rate: 1.5 mL/min, detection: 254 nm, acquisition time: 4.3 min. Unless otherwise noted, all compounds were found to be >95% pure by this method. HRMS were acquired through the Bio21 Mass Spectrometry and Proteomics Facility using a Thermo Scientific nano-LC Q Exactive Plus Mass spectrometer. Compounds **31**, **32**, **35**, **36**, **38**, **43**, **44**, **45**, **47**, **49**, and **60** were purchased commercially. The integrity and purity of these compounds was confirmed by LCMS to be >95%.

Chemistry Procedures. *N*-(2-Chlorophenyl)-2-(6-(5-methyl-1,3,4-oxadiazol-2-yl)-1H-indol-1-yl)acetamide (**5**). General Procedure A: A stirring mixture of **85** (106 mg, 0.412 mmol) and EDCI-HCl (104 mg, 0.543 mmol) in MeCN (4 mL) at 20 °C was treated with 2-chloroaniline (60 μ L, 0.57 mmol) and the mixture was stirred for 3 h. The mixture was then diluted with H₂O (~3 mL) and the solid was collected using vacuum filtration to afford **5** as an off-white powder requiring no further purification (53 mg, 35%). ¹H NMR (300 MHz, DMSO-*d*₆) δ 9.95 (s, 1H), 8.13 (d, *J* = 1.3 Hz, 1H), 7.75 (d, *J* = 8.3 Hz, 2H), 7.67 (dd, *J* = 8.3, 1.4 Hz, 1H), 7.62 (d, *J* = 3.1 Hz, 1H), 7.52 (dd, *J* = 7.9, 1.5 Hz, 1H), 7.37–7.27 (m, 1H), 7.20 (td, *J* = 7.7, 1.7 Hz, 1H), 6.61 (d, *J* = 3.1 Hz, 1H), 5.30 (s, 2H), 2.58 (s, 3H). ¹³C NMR (75 MHz, DMSO-*d*₆) δ 166.7, 165.2, 163.2, 136.0, 134.3, 133.1, 130.7, 129.5, 127.5, 126.5, 126.2, 125.7, 121.3, 117.4, 116.4, 108.6, 101.7, 49.0, 10.6. LCMS *m/z* 367.2 [M + H]. HRMS *m/z*: [M + H] Calcd for C₁₉H₁₅ClN₄O₂ 367.0956; Found 367.0955.

N-(2-Chlorophenyl)-2-(6-(5-methyl-1,2,4-oxadiazol-3-yl)-1H-indol-1-yl)acetamide (**6**). A mixture of **88** (78 mg, 0.23 mmol), DCC (55 mg, 0.27 mmol) and AcOH (16 μ L, 0.28 mmol) in 1,4-dioxane (2 mL) was heated at 90 °C for 3 h before being cooled to 20 °C and treated with AcOH (50.0 μ L, 0.874 mmol), DIPEA (160 μ L, 0.919 mmol) and 50% T3P in DMF (330 μ L, 0.565 mmol) before heating again at 90 °C for 1 h. The mixture was then diluted with EtOAc (10 mL), washed with 1 M aq. HCl (10 mL), H₂O (10 mL), and brine (10 mL), filtered and dried over MgSO₄. Volatiles were removed under reduced pressure to afford an orange oil which was purified by reverse phase preparative HPLC eluting with a gradient of 5–75% MeCN/H₂O (including 0.1% formic acid) to afford **6** as a white powder (19 mg, 23%). ¹H NMR (300 MHz, DMSO-*d*₆) δ 9.94 (s, 1H), 8.16 (d, *J* = 1.1 Hz, 1H), 7.75 (dd, *J* = 8.1, 1.6 Hz, 1H), 7.71 (t, *J* = 0.9 Hz, 2H), 7.58 (d, *J* = 3.1 Hz, 1H), 7.51 (dd, *J* = 8.0, 1.5 Hz, 1H), 7.32 (td, *J* = 7.7, 1.6 Hz, 1H), 7.20 (td, *J* = 7.7, 1.7 Hz, 1H), 6.58 (dd, *J* = 3.1, 0.9 Hz, 1H), 5.29 (s, 2H), 2.65 (s, 3H). ¹³C NMR (75 MHz, DMSO-*d*₆) δ 176.9, 168.6, 166.8, 136.1, 134.4, 132.7, 130.5, 129.6, 127.5, 126.6, 126.3, 125.7, 121.1, 119.2, 117.9, 109.3, 101.5, 49.0, 12.0. LCMS *m/z* 367.2 [M + H]. HRMS *m/z*: [M + H] Calcd for C₁₉H₁₅ClN₄O₂ 367.0956; Found 367.0960.

N-(2-Chlorophenyl)-2-(6-(3-methyl-1,2,4-oxadiazol-5-yl)-1H-indol-1-yl)acetamide (**7**). A stirring mixture containing **91** (69 mg, 0.21 mmol), *N*-hydroxyacetamide (32 mg, 0.43 mmol), DIPEA (150 μ L, 0.86 mmol) and 50% T3P in DMF (300 μ L, 0.51 mmol) in 1,4-dioxane (2 mL) was heated at 100 °C for 16 h. Additional portions of DIPEA (150 μ L, 0.86 mmol) and 50% T3P in DMF (300 μ L, 0.51 mmol) were added and the stirred an additional 24 h at 100 °C before being diluted with EtOAc (20 mL) and washed with 1 M aq. HCl (20 mL) and brine (20 mL), dried over MgSO₄ and concentrated under reduced pressure. The crude product was purified by reverse phase preparative HPLC eluting with a gradient of 5–75% MeCN/H₂O (including 0.1% formic acid) to afford **7** as a tan powder (11 mg, 14%). ¹H NMR (300 MHz, DMSO-*d*₆) δ 9.98 (s, 1H), 8.32 (s, 1H), 7.81–7.71 (m, 3H), 7.68 (d, *J* = 3.1 Hz, 1H), 7.52 (dd, *J* = 8.0, 1.5 Hz, 1H), 7.32 (td, *J* = 7.8, 1.6 Hz, 1H), 7.20 (td, *J* = 7.7, 1.7 Hz, 1H), 6.64 (dd, *J* = 3.1, 0.9 Hz, 1H), 5.33 (s, 2H), 2.41 (s, 3H). ¹³C NMR (75 MHz, DMSO-*d*₆) δ 176.0, 167.4, 166.6, 135.9, 134.3, 134.0, 131.7, 129.5, 127.5, 126.5, 126.2, 125.7, 121.3, 118.4, 116.1, 110.4, 101.8, 49.0, 11.2. LCMS *m/z* 367.2 [M + H]. HRMS *m/z*: [M + H] Calcd for C₁₉H₁₅ClN₄O₂ 367.0956; Found 367.0958.

N-(2-Chlorophenyl)-2-(6-(1-methyl-1H-pyrazol-3-yl)-1H-indol-1-yl)acetamide (**8**). A 10 mL microwave vial equipped with stir bar was charged with **92** (75 mg, 0.21 mmol), K₂CO₃ (68 mg, 0.49 mmol), 1,4-dioxane (1.8 mL) and H₂O (0.2 mL). The mixture was purged with N₂ for 25 min before the addition of Pd(dppf)Cl₂·CH₂Cl₂ (31

mg, 0.038 mmol) and 1-methyl-3-(4,4,5,5-tetramethyl-1,3,2-dioxaborolan-2-yl)pyrazole (78 mg, 0.37 mmol). The resultant mixture was heated at 120 °C for 30 min using microwave irradiation. The mixture was filtered over a pad of Celite and washed using EtOAc. The filtrate was concentrated and purified by column chromatography, eluting with 20–100% EtOAc/heptane, followed by reverse phase preparative HPLC eluting with a gradient of 5–75% MeCN/H₂O (including 0.1% formic acid) to afford **8** as a white powder (9.0 mg, 12%). ¹H NMR (300 MHz, CDCl₃) δ 8.31 (dd, *J* = 8.2, 1.5 Hz, 1H), 7.86 (d, *J* = 1.4 Hz, 1H), 7.70 (dd, *J* = 8.3, 0.7 Hz, 1H), 7.66–7.55 (m, 2H), 7.38 (d, *J* = 2.3 Hz, 1H), 7.25–7.14 (m, 3H), 7.03–6.92 (m, 1H), 6.69 (dd, *J* = 3.2, 0.9 Hz, 1H), 6.58 (d, *J* = 2.3 Hz, 1H), 5.03 (s, 2H), 3.96 (s, 3H). ¹³C NMR (75 MHz, CDCl₃) δ 166.6, 152.0, 136.7, 133.7, 131.9, 129.1, 129.0, 128.9, 127.8, 127.7, 125.4, 123.5, 121.8, 121.7, 119.3, 106.4, 104.4, 103.1, 50.7, 39.1. LCMS *m/z* 365.2 [M + H]. HRMS *m/z*: [M + H] Calcd for C₂₀H₁₇ClN₄O 365.1164; Found 365.1167.

N-(2-Chlorophenyl)-2-(6-(1-methyl-1H-pyrazol-4-yl)-1H-indol-1-yl)acetamide (**9**). A flask equipped with stir bar was charged with **92** (740 mg, 2.0 mmol), 1-methyl-4-(4,4,5,5-tetramethyl-1,3,2-dioxaborolan-2-yl)pyrazole (560 mg, 2.7 mmol), K₂CO₃ (560 mg, 4.1 mmol), 1,4-dioxane (18 mL) and H₂O (2 mL). The flask was purged with N₂ for 10 min and then treated with G3-Pd-Xphos (37 mg, 0.044 mmol) and heated at 100 °C for 16 h. An additional portion of G3-Pd-Xphos (37 mg, 0.044 mmol) was added and the mixture heated at 100 °C for a further 24 h. The mixture was then allowed to cool to 20 °C, diluted with EtOAc (25 mL) and H₂O (50 mL), filtered through a pad of Celite into a separatory funnel. The Celite was washed with additional portions of EtOAc and the organics were separated and further washed with brine before being dried over MgSO₄, filtered and concentrated under reduced pressure. The crude residue was purified by column chromatography eluting with 20–100% EtOAc/heptane to afford **9** as a white powder (160 mg, 21%). ¹H NMR (300 MHz, DMSO-*d*₆) δ 9.73 (s, 1H), 8.07 (s, 1H), 7.91–7.77 (m, 2H), 7.70 (s, 1H), 7.60–7.47 (m, 2H), 7.42–7.25 (m, 3H), 7.20 (td, *J* = 7.7, 1.6 Hz, 1H), 6.47 (d, *J* = 3.1 Hz, 1H), 5.19 (s, 2H), 3.88 (s, 3H). ¹³C NMR (75 MHz, DMSO-*d*₆) δ 167.0, 137.0, 135.8, 134.4, 129.8, 129.5, 127.5, 127.2, 126.7, 126.4, 126.1, 125.8, 125.4, 123.2, 120.7, 117.5, 105.9, 101.3, 48.9, 38.6. LCMS *m/z* 365.2 [M + H]. HRMS *m/z*: [M + H] Calcd for C₂₀H₁₇ClN₄O 365.1164; Found 365.1166.

N-(2-Chlorophenyl)-2-(6-(2-methylthiazol-5-yl)-1H-indol-1-yl)acetamide (**10**). General Procedure B: A mixture of **92** (50 mg, 0.14 mmol), 2-methyl-5-(4,4,5,5-tetramethyl-1,3,2-dioxaborolan-2-yl)-thiazole (46 mg, 0.21 mmol) and K₂CO₃ (58 mg, 0.41 mmol) in 1,4-dioxane (1.8 mL) and H₂O (0.2 mL) was purged with a stream of N₂ for 10 min before Pd(dppf)Cl₂·CH₂Cl₂ (6 mg, 0.007 mmol) was then added and the mixture was stirred at 110 °C for 16 h. The mixture was then cooled to 20 °C and diluted with EtOAc (10 mL), filtered through Celite and the filtrate washed with H₂O (5 mL) and brine (5 mL). The organic fraction was concentrated under reduced pressure and the crude residue purified by column chromatography eluting with 20–100% EtOAc/heptane to afford **10** as a white powder (10 mg, 19% yield). ¹H NMR (300 MHz, CDCl₃) δ 8.39–8.22 (m, 1H), 7.80 (s, 1H), 7.69 (d, *J* = 8.2 Hz, 1H), 7.56 (s, 1H), 7.46 (s, 1H), 7.38 (d, *J* = 8.2 Hz, 1H), 7.27–7.14 (m, 3H), 7.11–6.92 (m, 1H), 6.70 (d, *J* = 3.1 Hz, 1H), 5.00 (s, 2H), 2.73 (s, 3H). ¹³C NMR (75 MHz, CDCl₃) δ 166.3, 165.0, 140.0, 137.3, 136.6, 133.5, 129.2, 129.0, 127.8, 126.7, 125.6, 123.3, 122.2, 121.7, 120.3, 107.4, 104.7, 50.8, 19.5. LCMS *m/z* 382.2 [M + H]. HRMS *m/z*: [M + H] Calcd for C₂₀H₁₆ClN₃OS 382.0775; Found 382.0775.

N-(2-Chlorophenyl)-2-(6-(5-methylthiophen-2-yl)-1H-indol-1-yl)acetamide (**11**). General Procedure B was followed using 4,4,5,5-tetramethyl-2-(5-methyl-2-thienyl)-1,3,2-dioxaborolane (37 mg, 0.16 mmol). Column chromatography eluting with 0–40% EtOAc/heptane afforded **11** as a beige solid (22 mg, 53%). ¹H NMR (300 MHz, DMSO-*d*₆) δ 9.82 (s, 1H), 7.78–7.71 (m, 1H), 7.66 (s, 1H), 7.61–7.46 (m, 2H), 7.42 (d, *J* = 3.1 Hz, 1H), 7.38–7.26 (m, 2H), 7.26–7.13 (m, 2H), 6.86–6.74 (m, 1H), 6.49 (dd, *J* = 8.8, 3.1 Hz, 1H), 5.18 (d, *J* = 6.8 Hz, 2H), 2.46 (s, 3H). ¹³C NMR (75 MHz, DMSO-*d*₆) δ 166.9, 142.7, 137.7, 136.7, 134.4, 130.9, 129.5, 127.7,

127.6, 127.6, 126.6, 126.5, 125.7, 122.3, 122.1, 120.9, 117.5, 106.3, 101.3, 48.9, 15.1. LCMS m/z 381.0 [M + H]. HRMS m/z : [M + H] Calcd for $C_{21}H_{17}ClN_4O$ 381.0823; Found 381.0823.

N-(2-Chlorophenyl)-2-(6-(*p*-tolyl)-1*H*-indol-1-yl)acetamide (12). A mixture containing **92** (76 mg, 0.21 mmol), K_2CO_3 (92 mg, 0.67 mmol) and *p*-tolylboronic acid (48 mg, 0.35 mmol) in 1,4-dioxane (1.8 mL) and H_2O (0.2 mL) was purged using N_2 for 15 min. The mixture was charged with $Pd(dppf)Cl_2 \cdot CH_2Cl_2$ (24 mg, 0.029 mmol) and then stirred and heated at 120 °C for 30 min using microwave irradiation. The mixture was diluted with EtOAc and filtered over Celite before being purified by column chromatography, eluting with 10–40% EtOAc/heptane followed by reverse phase preparative HPLC eluting with a gradient of 5–75% MeCN/ H_2O (including 0.1% formic acid) to afford **12** as a white solid (4 mg, 5%). 1H NMR (300 MHz, DMSO- d_6) δ 8.30 (dd, J = 8.2, 1.6 Hz, 1H), 7.73 (dd, J = 8.3, 0.7 Hz, 1H), 7.59 (s, 1H), 7.56–7.49 (m, 3H), 7.45 (dd, J = 8.2, 1.5 Hz, 1H), 7.26–7.16 (m, 5H), 6.99 (td, J = 7.7, 1.6 Hz, 1H), 6.72 (dd, J = 3.2, 0.9 Hz, 1H), 5.02 (s, 2H), 2.39 (s, 3H). LCMS m/z 375.2 [M + H]. HRMS m/z : [M + H] Calcd for $C_{23}H_{19}ClN_2O$ 375.1259; Found 375.1260.

N-(2-Chlorophenyl)-2-(6-(*M*-tolyl)-1*H*-indol-1-yl)acetamide (13). General Procedure B was followed using *m*-tolylboronic acid (22 mg, 0.16 mmol). Column chromatography eluting with 0–40% EtOAc/heptane afforded **13** as a beige solid (32 mg, 78%). 1H NMR (300 MHz, DMSO- d_6) δ 9.82 (s, 1H), 7.79–7.72 (m, 2H), 7.63 (d, J = 8.2 Hz, 1H), 7.55–7.42 (m, 4H), 7.39–7.28 (m, 3H), 7.23–7.10 (m, 2H), 6.50 (d, J = 3.1 Hz, 1H), 5.24 (s, 2H), 2.38 (s, 3H). ^{13}C NMR (75 MHz, DMSO- d_6) δ 167.0, 141.4, 137.8, 136.9, 134.4, 133.8, 130.7, 129.5, 128.7, 127.6, 127.5, 127.4, 127.3, 126.5, 125.7, 123.9, 122.1, 120.7, 118.6, 107.9, 101.0, 48.9, 21.2. LCMS m/z 375.0 [M + H]. HRMS m/z : [M + H] Calcd for $C_{23}H_{19}ClN_2O$ 375.1259; Found 375.1258.

N-(2-Chlorophenyl)-2-(6-(6-methylpyridin-3-yl)-1*H*-indol-1-yl)acetamide (14). General Procedure B was followed using (6-methylpyridin-3-yl)boronic acid (17 mg, 0.12 mmol). Column chromatography eluting with 0–3% MeOH/DCM afforded **14** as a beige solid (16 mg, 52%). 1H NMR (300 MHz, $CDCl_3$) δ 8.80 (d, J = 2.4 Hz, 1H), 8.34 (dd, J = 8.2, 1.5 Hz, 1H), 7.91–7.77 (m, 2H), 7.63 (s, 1H), 7.55 (s, 1H), 7.45 (dd, J = 8.2, 1.5 Hz, 1H), 7.29 (dd, J = 8.1, 1.4 Hz, 2H), 7.27–7.21 (m, 2H), 7.04 (td, J = 7.7, 1.6 Hz, 1H), 6.78 (d, J = 3.2 Hz, 1H), 5.08 (s, 2H), 2.64 (s, 3H). LCMS m/z 376.2 [M + H]. HRMS m/z : [M + H] Calcd for $C_{22}H_{18}ClN_3O$ 376.1211; Found 376.1214.

N-(2-Chlorophenyl)-2-(6-(2-methylpyridin-4-yl)-1*H*-indol-1-yl)acetamide (15). General Procedure B was followed using 2-methyl-4-(4,4,5,5-tetramethyl-1,3,2-dioxaborolan-2-yl)pyridine (42 mg, 0.19 mmol). Column chromatography eluting with 0–40% EtOAc/DCM afforded **15** as a pale yellow solid (31 mg, 65%). 1H NMR (300 MHz, DMSO- d_6) δ 9.83 (s, 1H), 8.47 (d, J = 5.3 Hz, 1H), 7.96 (s, 1H), 7.77 (dd, J = 8.1, 1.6 Hz, 1H), 7.68 (d, J = 8.3 Hz, 1H), 7.62 (d, J = 1.8 Hz, 1H), 7.58 – 7.45 (m, 4H), 7.32 (td, J = 7.7, 1.5 Hz, 1H), 7.19 (td, J = 7.7, 1.6 Hz, 1H), 6.54 (d, J = 3.1 Hz, 1H), 5.27 (s, 2H), 2.53 (s, 3H). ^{13}C NMR (75 MHz, DMSO- d_6) δ 166.9, 158.3, 149.3, 148.5, 136.9, 134.4, 131.6, 130.5, 129.5, 128.9, 127.5, 126.5, 126.0, 125.6, 121.0, 120.3, 118.4, 118.2, 108.4, 101.2, 48.9, 24.2. LCMS m/z 376.0 [M + H]. HRMS m/z : [M + H] Calcd for $C_{22}H_{18}ClN_3O$ 376.1211; Found 376.1213.

N-(2-Chlorophenyl)-2-(6-(6-methylpyridazin-4-yl)-1*H*-indol-1-yl)acetamide (16). General Procedure B was followed using 3-methyl-5-(4,4,5,5-tetramethyl-1,3,2-dioxaborolan-2-yl)pyridazine (12 mg, 0.054 mmol). Column chromatography eluting with 0–40% EtOAc/DCM afforded **16** as a brown solid (6 mg, 27%). 1H NMR (300 MHz, DMSO- d_6) δ 9.87 (s, 1H), 9.59 (d, J = 2.3 Hz, 1H), 8.22 (s, 1H), 8.03 (d, J = 2.2 Hz, 1H), 7.76 (dd, J = 9.5, 7.5 Hz, 2H), 7.64 (dd, J = 8.3, 1.5 Hz, 1H), 7.58 (d, J = 3.1 Hz, 1H), 7.50 (dd, J = 7.9, 1.4 Hz, 1H), 7.31 (td, J = 7.8, 1.5 Hz, 1H), 7.19 (dt, J = 7.9, 3.9 Hz, 1H), 6.58 (d, J = 3.1 Hz, 1H), 5.31 (s, 2H), 2.70 (s, 3H). ^{13}C NMR (75 MHz, DMSO- d_6) δ 166.8, 159.4, 147.5, 139.2, 137.0, 134.4, 132.5, 129.8, 129.5, 127.5, 126.4, 126.3, 126.0, 125.6, 123.4, 121.4, 118.2, 109.3,

101.5, 48.9, 21.4. LCMS m/z 378.0 [M + H]. HRMS m/z : [M + H] Calcd for $C_{21}H_{17}ClN_4O$ 377.1164; Found 377.1162.

2-(6-(1,3,4-Oxadiazol-2-yl)-1*H*-indol-1-yl)-N-(2-chlorophenyl)acetamide (17). A stirring mixture of **93** (418 mg, 1.54 mmol) in THF (6 mL) and H_2O (6 mL) at 20 °C was treated with lithium hydroxide monohydrate (327 mg, 7.79 mmol) for 1 h. The mixture was then diluted with H_2O (20 mL) and 1 M aq. HCl (10 mL). The aqueous mixture was extracted using EtOAc (3 \times 25 mL) and the isolated organic phase was washed using H_2O (25 mL) and brine (25 mL), dried over $MgSO_4$, filtered and concentrated to afford a pale yellow powder which was used directly in the next step. General Procedure A was then followed using the crude acid (46 mg, 0.19 mmol) and 2-chloroaniline (26 μ L, 0.25 mmol) to afford **17** as a white powder (45 mg, 67%). 1H NMR (300 MHz, DMSO- d_6) δ 9.96 (s, 1H), 9.30 (s, 1H), 8.21 (s, 1H), 7.82 – 7.68 (m, 3H), 7.64 (d, J = 3.1 Hz, 1H), 7.51 (dd, J = 8.0, 1.5 Hz, 1H), 7.32 (td, J = 7.7, 1.6 Hz, 1H), 7.20 (td, J = 7.7, 1.7 Hz, 1H), 6.62 (dd, J = 3.1, 0.8 Hz, 1H), 5.31 (s, 2H). ^{13}C NMR (75 MHz, DMSO- d_6) δ 166.7, 164.9, 154.0, 136.0, 134.4, 133.4, 131.0, 129.5, 127.5, 126.6, 126.3, 125.7, 121.4, 117.7, 116.0, 109.1, 101.7, 49.0. LCMS m/z 353.2 [M + H]. HRMS m/z : [M + H] Calcd for $C_{18}H_{13}ClN_4O_2$ 353.08; Found 353.0804.

N-(2-Chlorophenyl)-2-(6-(5-(trifluoromethyl)-1,3,4-oxadiazol-2-yl)-1*H*-indol-1-yl)acetamide (18). To a stirring mixture of **94** (51 mg, 0.15 mmol) and DBU (56 μ L, 0.38 mmol) in THF (1.5 mL) at 60 °C was added TFAA (53 μ L, 0.38 mmol). The mixture was stirred at 60 °C for 1 h. LCMS shows full conversion to the intermediate with only a trace amount of the desired cyclized product. No further progress was observed after 16 h. The mixture was cooled to 20 °C and volatiles removed under a stream of N_2 . The resulting orange oil was redissolved in THF (1.5 mL) and treated with DIPEA (40 μ L, 0.23 mmol) and methoxycarbonyl-(triethylammonio)sulfonyl-azanide (53 mg, 0.22 mmol). The mixture was heated to 60 °C and stirred for 16 h before being allowed to cool to 20 °C, diluted with EtOAc (20 mL) and washed with 10% aq. citric acid (20 mL), H_2O (20 mL), and brine (20 mL), dried over $MgSO_4$, filtered and concentrated under reduced pressure. Column chromatography eluting with 10–40% EtOAc/heptane afforded **18** as a white solid (13 mg, 21%). 1H NMR (300 MHz, $CDCl_3$) δ 8.33 (dd, J = 8.2, 1.5 Hz, 1H), 8.16 (d, J = 1.3 Hz, 1H), 7.94 (dd, J = 8.3, 1.4 Hz, 1H), 7.85 (dd, J = 8.4, 0.7 Hz, 1H), 7.50 (s, 1H), 7.40 (d, J = 3.2 Hz, 1H), 7.20–7.20 (m, 2H), 7.02 (ddd, J = 8.9, 7.4, 1.5 Hz, 1H), 6.81 (dd, J = 3.2, 0.9 Hz, 1H), 5.09 (s, 2H). ^{13}C NMR (75 MHz, DMSO- d_6) δ 167.4, 166.6, 153.5 (d, J = 43.3 Hz), 152.6, 135.9, 134.3, 134.2, 131.8, 129.5, 127.5, 126.5 (d, J = 19.4 Hz), 125.8, 121.5, 118.0, 116.4 (d, J = 270.7 Hz), 114.3, 109.9, 101.9, 49.0. LCMS m/z 421.2 [M + H]. HRMS m/z : [M + H] Calcd for $C_{19}H_{12}ClF_3N_4O_2$ 421.0674; Found 421.0674.

N-(2-Chlorophenyl)-2-(6-(5-isopropyl-1,3,4-oxadiazol-2-yl)-1*H*-indol-1-yl)acetamide (19). General Procedure C: An oven-dried 20 mL vial fitted with stir bar was cooled under vacuum and backfilled using N_2 . The flask was charged with **95** (57 mg, 0.25 mmol) and anhydrous DMF (2.5 mL) then cooled to 0 °C on an ice bath. Sodium hydride (19 mg, 0.48 mmol) was added and the mixture stirred for 30 min before a solution of **90** (71 mg, 0.35 mmol) in DMF (1 mL) was added dropwise. The mixture was allowed to gradually warm to 20 °C and stirred an additional 17 h. The mixture was diluted with EtOAc (20 mL), washed with saturated NH_4Cl and H_2O (1:1, 20 mL), H_2O (20 mL), brine (20 mL), dried over $MgSO_4$, filtered and reduced in vacuo onto Celite. Purification using column chromatography, eluting with 0–4% MeOH/DCM (w/1% aq. NH_3) gives a tan solid which was further purified by reverse phase preparative HPLC eluting with a gradient of 5–75% MeCN/ H_2O (including 0.1% formic acid) to afford **19** as a white powder (14 mg, 14%). 1H NMR (300 MHz, DMSO- d_6) δ 9.98 (s, 1H), 8.13 (s, 1H), 7.81–7.65 (m, 3H), 7.62 (d, J = 3.1 Hz, 1H), 7.52 (dd, J = 7.9, 1.5 Hz, 1H), 7.37–7.28 (m, 1H), 7.21 (td, J = 7.7, 1.7 Hz, 1H), 6.61 (d, J = 3.1 Hz, 1H), 5.30 (s, 2H), 3.33 – 3.23 (m, 3H), 1.38 (d, J = 6.9 Hz, 6H). ^{13}C NMR (75 MHz, DMSO- d_6) δ 170.0, 166.7, 165.0, 136.0, 134.3, 133.2, 130.8, 129.5, 127.5, 126.7, 126.5, 125.9, 121.3, 117.5, 116.4, 108.6, 101.7, 49.0, 25.7, 19.8. LCMS m/z 395.2 [M + H].

HRMS m/z : [M + H] Calcd for $C_{21}H_{19}ClN_4O_2$ 395.1269; Found 395.1269.

N-(2-Chlorophenyl)-2-(6-(1-(difluoromethyl)-1H-pyrazol-4-yl)-1H-indol-1-yl)acetamide (20). General Procedure B was followed using 1-(difluoromethyl)-4-(4,4,5,5-tetramethyl-1,3,2-dioxaborolan-2-yl)pyrazole (54.9 mg, 0.225 mmol). Column chromatography eluting with 0–5% MeOH/DCM afforded **20** as a white powder (14 mg, 23%). 1H NMR (300 MHz, DMSO- d_6) δ 9.71 (s, 1H), 8.63 (s, 1H), 8.26 (s, 1H), 7.86 (s, 1H), 7.83 (t, J = 59.4 Hz, 1H), 7.80 (dd, J = 8.1, 1.6 Hz, 1H), 7.59 (d, J = 8.2 Hz, 1H), 7.50 (dd, J = 8.0, 1.5 Hz, 1H), 7.44–7.28 (m, 3H), 7.18 (td, J = 7.7, 1.6 Hz, 1H), 6.49 (d, J = 3.1 Hz, 1H), 5.19 (s, 2H). ^{13}C NMR (75 MHz, DMSO- d_6) δ 166.9, 139.9, 136.9, 134.4, 130.4, 129.5, 127.5, 127.4, 126.4, 125.8, 125.8, 125.4, 124.3, 124.1, 120.8, 117.7, 110.6 (t, J = 247.8 Hz), 107.0, 101.4, 48.9. LCMS m/z 401.2 [M + H]. HRMS m/z : [M + H] Calcd for $C_{20}H_{15}ClF_2N_4O$ 401.0975; Found 401.0974.

N-(2-Chlorophenyl)-2-(6-(1-(trifluoromethyl)-1H-pyrazol-4-yl)-1H-indol-1-yl)acetamide (21). General Procedure B was followed using 4,4,5,5-tetramethyl-2-(5-methylthiophen-2-yl)-1,3,2-dioxaborolane (40 mg, 0.17 mmol). Column chromatography eluting with 0–40% EtOAc/DCM afforded **21** as a white powder (20 mg, 53%). 1H NMR (300 MHz, DMSO- d_6) δ 9.69 (s, 1H), 8.88 (s, 1H), 8.45 (s, 1H), 7.92 (s, 1H), 7.82 (dd, J = 8.1, 1.6 Hz, 1H), 7.61 (d, J = 8.2 Hz, 1H), 7.47 (ddd, J = 15.9, 7.0, 2.0 Hz, 3H), 7.32 (td, J = 7.7, 1.5 Hz, 1H), 7.18 (td, J = 7.7, 1.6 Hz, 1H), 6.50 (d, J = 3.2 Hz, 1H), 5.20 (s, 2H). ^{13}C NMR (75 MHz, DMSO- d_6) δ 166.9, 142.2, 136.9, 134.4, 130.6, 129.5, 127.7, 127.6, 126.5, 126.4, 125.7, 125.4, 125.3, 123.2, 120.9, 118.0 (d, J = 261.6 Hz), 117.9, 107.3, 101.5, 48.9. LCMS m/z 381.0 [M + H]. HRMS m/z : [M + H] Calcd for $C_{20}H_{14}ClF_3N_4O$ 419.0881; Found 419.0881.

N-(2-Chlorophenyl)-2-(6-(1-ethyl-1H-pyrazol-4-yl)-1H-indol-1-yl)acetamide (22). General Procedure B was followed using 1-ethyl-4-(4,4,5,5-tetramethyl-1,3,2-dioxaborolan-2-yl)pyrazole (33 mg, 0.15 mmol). Column chromatography eluting with 0–5% MeOH/DCM followed by reverse phase preparative HPLC eluting with a gradient of 5–75% MeCN/H₂O (including 0.1% formic acid) afforded **22** as a white powder (16 mg, 42%). 1H NMR (300 MHz, DMSO- d_6) δ 9.71 (s, 1H), 8.11 (s, 1H), 7.87–7.75 (m, 2H), 7.68 (s, 1H), 7.58–7.45 (m, 2H), 7.39–7.24 (m, 3H), 7.23–7.14 (m, 1H), 6.45 (d, J = 3.2 Hz, 1H), 5.17 (s, 2H), 4.15 (q, J = 7.3 Hz, 2H), 1.41 (t, J = 7.3 Hz, 3H). ^{13}C NMR (75 MHz, DMSO- d_6) δ 167.1, 137.1, 135.7, 134.4, 129.9, 129.6, 127.6, 126.7, 126.5, 126.2, 125.9, 125.8, 125.5, 123.0, 120.7, 117.6, 105.9, 101.3, 48.9, 46.4, 15.5. LCMS m/z 379.2 [M + H]. HRMS m/z : [M + H] Calcd for $C_{21}H_{19}ClN_4O$ 379.132; Found 379.1319.

N-(2-Chlorophenyl)-2-(6-(1-isopropyl-1H-pyrazol-4-yl)-1H-indol-1-yl)acetamide (23). General Procedure B was followed using 1-isopropyl-4-(4,4,5,5-tetramethyl-1,3,2-dioxaborolan-2-yl)pyrazole (53 mg, 0.23 mmol). Column chromatography eluting with 0–40% EtOAc/DCM afforded **23** as a white solid (25 mg, 42%). 1H NMR (300 MHz, DMSO- d_6) δ 9.72 (s, 1H), 8.15 (s, 1H), 7.90–7.77 (m, 2H), 7.70 (s, 1H), 7.59–7.46 (m, 2H), 7.42–7.26 (m, 3H), 7.20 (td, J = 7.7, 1.6 Hz, 1H), 6.46 (d, J = 3.1 Hz, 1H), 5.18 (s, 2H), 4.51 (hept, J = 6.7 Hz, 1H), 1.46 (d, J = 6.6 Hz, 6H). ^{13}C NMR (75 MHz, DMSO- d_6) δ 167.0, 137.0, 135.3, 134.4, 129.8, 129.5, 127.6, 126.6, 126.4, 126.3, 125.8, 125.4, 124.0, 122.7, 120.7, 117.6, 105.9, 101.3, 53.0, 48.9, 22.7. LCMS m/z 393.2 [M + H]. HRMS m/z : [M + H] Calcd for $C_{22}H_{21}ClN_4O$ 393.1477; Found 393.1476.

N-(2-Chlorophenyl)-2-(6-(1-(2,2,2-trifluoroethyl)-1H-pyrazol-4-yl)-1H-indol-1-yl)acetamide (24). General Procedure B was followed using 4-(4,4,5,5-tetramethyl-1,3,2-dioxaborolan-2-yl)-1-(2,2,2-trifluoroethyl)-1H-pyrazole (40 mg, 0.13 mmol). Column chromatography eluting with 0–40% EtOAc/DCM afforded **24** as a white solid (20 mg, 65%). 1H NMR (300 MHz, DMSO- d_6) δ 9.71 (s, 1H), 8.21 (s, 1H), 8.02 (s, 1H), 7.80 (dd, J = 8.1, 1.6 Hz, 1H), 7.74 (s, 1H), 7.56 (d, J = 8.2 Hz, 1H), 7.50 (dd, J = 8.0, 1.5 Hz, 1H), 7.39 (d, J = 3.2 Hz, 1H), 7.32 (td, J = 7.9, 1.5 Hz, 2H), 7.19 (td, J = 7.7, 1.6 Hz, 1H), 6.47 (d, J = 3.2 Hz, 1H), 5.34–5.01 (m, 4H). ^{13}C NMR (75 MHz, DMSO- d_6) δ 167.0, 137.8, 137.0, 134.4, 130.1, 129.5, 128.2, 127.5, 127.0, 126.4, 125.8, 125.4, 125.1, 124.3, 123.7 (q, J = 279.8 Hz), 120.8,

117.6, 106.4, 101.3, 51.6 (q, J = 33.4 Hz), 48.9. LCMS m/z 433.0 [M + H]. HRMS m/z : [M + H] Calcd for $C_{21}H_{16}ClF_3N_4O$ 433.1037; Found 433.1036.

N-(2-Chlorophenyl)-2-(6-(1-phenyl-1H-pyrazol-4-yl)-1H-indol-1-yl)acetamide (25). General Procedure B was followed using 1-phenyl-4-(4,4,5,5-tetramethyl-1,3,2-dioxaborolan-2-yl)pyrazole (61 mg, 0.23 mmol). Column chromatography eluting with 0–40% EtOAc/DCM afforded **25** as a white solid (10 mg, 16%). 1H NMR (300 MHz, DMSO- d_6) δ 9.72 (s, 1H), 8.93 (s, 1H), 8.20 (s, 1H), 7.94–7.76 (m, 4H), 7.62–7.39 (m, 6H), 7.36–7.28 (m, 2H), 7.19 (td, J = 7.7, 1.6 Hz, 1H), 6.49 (d, J = 3.1 Hz, 1H), 5.20 (s, 2H). ^{13}C NMR (75 MHz, DMSO- d_6) δ 166.9, 139.6, 138.9, 138.5, 137.0, 134.4, 130.1, 129.6, 129.5, 129.5, 127.5, 127.1, 126.4, 126.1, 125.8, 125.5, 125.3, 125.2, 123.9, 123.8, 120.8, 118.1, 117.7, 106.4, 101.4, 48.9. LCMS m/z 427.2 [M + H]. HRMS m/z : [M + H] Calcd for $C_{25}H_{19}ClN_4O$ 427.132; Found 427.1319.

N-(2-Chlorophenyl)-2-(6-(1,5-dimethyl-1H-pyrazol-4-yl)-1H-indol-1-yl)acetamide (26). General Procedure B was followed using 1,5-dimethyl-4-(4,4,5,5-tetramethyl-1,3,2-dioxaborolan-2-yl)pyrazole (33 mg, 0.15 mmol). Column chromatography eluting with 0–5% MeOH/DCM afforded **26** as a white solid (21 mg, 56%). 1H NMR (300 MHz, DMSO- d_6) δ 9.81 (s, 1H), 7.75 (dd, J = 8.1, 1.6 Hz, 1H), 7.62–7.47 (m, 3H), 7.45–7.37 (m, 2H), 7.32 (td, J = 7.7, 1.5 Hz, 1H), 7.19 (td, J = 7.7, 1.6 Hz, 1H), 7.09 (dd, J = 8.1, 1.4 Hz, 1H), 6.47 (dd, J = 3.2, 0.9 Hz, 1H), 5.18 (s, 2H), 3.78 (s, 3H), 2.37 (s, 3H). ^{13}C NMR (75 MHz, DMSO- d_6) δ 167.1, 136.8, 136.4, 134.5, 134.4, 130.1, 129.6, 127.6, 127.1, 126.5, 126.1, 125.6, 120.8, 120.6, 119.6, 108.3, 101.0, 49.0, 36.3, 10.1. LCMS m/z 379.2 [M + H]. HRMS m/z : [M + H] Calcd for $C_{21}H_{19}ClN_4O$ 379.132; Found 379.1319.

N-(2-Chlorophenyl)-2-(6-(1,3-dimethyl-1H-pyrazol-4-yl)-1H-indol-1-yl)acetamide (27). General Procedure B was followed using 1,3-dimethyl-4-(4,4,5,5-tetramethyl-1,3,2-dioxaborolan-2-yl)pyrazole (33 mg, 0.15 mmol). Column chromatography eluting with 0–5% MeOH/DCM afforded **27** as a white solid (23 mg, 61%). 1H NMR (300 MHz, DMSO- d_6) δ 9.79 (s, 1H), 7.87–7.69 (m, 2H), 7.59–7.41 (m, 3H), 7.38 (d, J = 3.2 Hz, 1H), 7.31 (td, J = 7.7, 1.5 Hz, 1H), 7.18 (td, J = 7.7, 1.6 Hz, 1H), 7.11 (dd, J = 8.1, 1.4 Hz, 1H), 6.46 (d, J = 3.1 Hz, 1H), 5.17 (s, 2H), 3.78 (s, 3H), 2.29 (s, 3H). ^{13}C NMR (75 MHz, DMSO- d_6) δ 167.1, 143.9, 136.8, 134.4, 130.1, 129.6, 129.3, 127.6, 126.9, 126.5, 126.5, 126.0, 125.5, 120.9, 120.6, 119.4, 108.0, 101.0, 49.0, 38.2, 13.2. LCMS m/z 379.2 [M + H]. HRMS m/z : [M + H] Calcd for $C_{21}H_{19}ClN_4O$ 379.132; Found 379.1320.

N-(2-Chlorophenyl)-2-(6-(1,3,5-trimethyl-1H-pyrazol-4-yl)-1H-indol-1-yl)acetamide (28). General Procedure B was followed using (1,3,5-trimethyl-1H-pyrazol-4-yl)boronic acid hydrochloride (39 mg, 0.21 mmol). Column chromatography eluting with 0–5% MeOH/DCM afforded **28** as a white solid (28 mg, 52%). 1H NMR (300 MHz, CDCl₃) δ 8.38 (dd, J = 8.2, 1.5 Hz, 1H), 7.78 (d, J = 8.1 Hz, 1H), 7.65 (s, 1H), 7.36–7.23 (m, 4H), 7.17 (dd, J = 8.1, 1.4 Hz, 1H), 7.07 (ddd, J = 8.5, 7.4, 1.6 Hz, 1H), 6.78 (dd, J = 3.2, 0.9 Hz, 1H), 5.05 (s, 2H), 3.85 (s, 3H), 2.28 (d, J = 4.9 Hz, 6H). LCMS m/z 393.2 [M + H]. HRMS m/z : [M + H] Calcd for $C_{22}H_{21}ClN_4O$ 393.1477; Found 393.1478.

N-(2-Chlorophenyl)-2-(6-(3,5-dimethyl-1H-pyrazol-4-yl)-1H-indol-1-yl)acetamide (29). General Procedure B was followed using 3,5-dimethyl-4-(4,4,5,5-tetramethyl-1,3,2-dioxaborolan-2-yl)-1H-pyrazole (29 mg, 0.12 mmol). Column chromatography eluting with 0–5% MeOH/DCM followed by reverse phase preparative HPLC eluting with a gradient of 5–75% MeCN/H₂O (including 0.1% formic acid) afforded **29** as a white solid (8 mg, 26%). 1H NMR (300 MHz, MeOD) δ 7.92 (dd, J = 8.1, 1.6 Hz, 1H), 7.63 (d, J = 8.1 Hz, 1H), 7.40–7.22 (m, 4H), 7.12 (td, J = 7.7, 1.6 Hz, 1H), 7.02 (dd, J = 8.2, 1.4 Hz, 1H), 6.58 (d, J = 3.2 Hz, 1H), 5.12 (s, 2H), 2.21 (s, 6H). LCMS m/z 379.2 [M + H]. HRMS m/z : [M + H] Calcd for $C_{21}H_{19}ClN_4O$ 379.132; Found 379.1326.

N-(2-Chlorophenyl)-2-(6-(1-methyl-3-(trifluoromethyl)-1H-pyrazol-4-yl)-1H-indol-1-yl)acetamide (30). General Procedure B was followed using (1-methyl-3-(trifluoromethyl)pyrazol-4-yl)boronic acid (40.0 mg, 0.206 mmol). Column chromatography eluting with

0–40% EtOAc/DCM followed by reverse phase preparative HPLC eluting with a gradient of 5–75% MeCN/H₂O (including 0.1% formic acid) afforded **30** as a white solid (44 mg, 73%). ¹H NMR (300 MHz, CDCl₃) δ 8.29 (d, *J* = 8.2 Hz, 1H), 7.70 (d, *J* = 8.1 Hz, 1H), 7.55 (s, 1H), 7.49 (s, 1H), 7.37 (s, 1H), 7.24–7.19 (m, 3H), 7.00 (t, *J* = 7.8 Hz, 1H), 6.71 (d, *J* = 3.2 Hz, 1H), 4.98 (s, 2H), 3.97 (s, 3H). ¹³C NMR (75 MHz, CDCl₃) δ 166.3, 138.9, 138.4, 136.3, 133.6, 132.2, 131.1, 129.1, 128.8, 128.5, 127.7, 125.5, 125.5, 123.5, 123.3, 123.2, 122.0, 121.6, 121.6, 120.0, 109.4 (d, *J* = 1.6 Hz), 104.3, 50.7, 39.6. LCMS *m/z* 433.0 [M + H]. HRMS *m/z*: [M + H] Calcd for C₂₁H₁₆ClF₃N₄O 433.1037; Found 433.1037.

N-(4-Chlorophenyl)-2-(6-(5-methyl-1,3,4-oxadiazol-2-yl)-1*H*-indol-1-yl)acetamide (**33**). General Procedure D: To a stirred solution of **86** (51 mg, 0.20 mmol) in MeCN (2 mL) was added 3,5-dichloroaniline (36 mg, 0.22 mmol) followed by TCFH (67 mg, 0.24 mmol) and 1-methylimidazole (48 μL, 0.60 mmol) and the reaction vessel was sealed. The mixture was stirred at 20 °C for 16 h followed by dilution with EtOAc (10 mL). The organics were washed with H₂O (3 × 5 mL) and brine (1 × 5 mL), dried over MgSO₄, filtered and concentrated. Column chromatography, eluting with 0–5% MeOH/DCM afforded **33** as a white solid (30 mg, 41%). ¹H NMR (300 MHz, DMSO-*d*₆) δ 10.56 (s, 1H), 8.09 (dt, *J* = 1.6, 0.8 Hz, 1H), 7.78–7.58 (m, 5H), 7.44–7.29 (m, 2H), 6.60 (dd, *J* = 3.1, 0.9 Hz, 1H), 5.22 (s, 2H), 2.57 (s, 3H). ¹³C NMR (75 MHz, DMSO-*d*₆) δ 166.3, 165.2, 163.3, 137.7, 136.2, 133.2, 130.6, 128.8, 127.1, 121.3, 120.7, 117.3, 116.3, 108.7, 101.6, 49.1, 10.7. LCMS *m/z* 367.2 [M + H]. HRMS *m/z*: [M + H] Calcd for C₁₉H₁₅ClN₄O₂ 367.0956; Found 367.0957.

N-(2-Fluorophenyl)-2-(6-(5-methyl-1,3,4-oxadiazol-2-yl)-1*H*-indol-1-yl)acetamide (**34**). To a stirred solution of **85** (51 mg, 0.20 mmol) in DMF (2 mL) was added 2-fluoroaniline (22 mg, 0.20 mmol) followed by TCFH (84 mg, 0.30 mmol) and DIPEA (70 μL, 0.60 mmol) and the reaction vessel was sealed. The mixture was stirred at 20 °C for 16 h and then poured into ice-cold H₂O (20 mL). An off-white precipitate was collected by vacuum filtration and was further washed with H₂O (3 × 5 mL) and dried. Column chromatography, eluting with 0–5% MeOH/DCM afforded **34** as a white solid (31 mg, 44%). ¹H NMR (300 MHz, DMSO-*d*₆) δ 10.25 (s, 1H), 8.11 (s, 1H), 7.99–7.87 (m, 1H), 7.79–7.57 (m, 3H), 7.38–7.23 (m, 1H), 7.23–7.07 (m, 2H), 6.67–6.55 (m, 1H), 5.29 (s, 2H), 2.57 (s, 3H). ¹³C NMR (75 MHz, DMSO-*d*₆) δ 166.7, 165.2, 163.3, 153.4 (d, *J* = 245.2 Hz), 136.1, 133.2, 130.7, 125.8 (d, *J* = 11.5 Hz), 125.5 (d, *J* = 7.6 Hz), 124.5 (d, *J* = 3.5 Hz), 123.6, 121.3, 117.4, 116.3, 115.6 (d, *J* = 19.3 Hz), 108.6, 101.7, 49.0, 10.7. LCMS *m/z* 351.2 [M + H]. HRMS *m/z*: [M + H] Calcd for C₁₉H₁₅FN₄O₂ 351.1252; Found 351.1249.

2-(6-(5-Methyl-1,3,4-oxadiazol-2-yl)-1*H*-indol-1-yl)-*N*-(*O*-tolyl)acetamide (**37**). A solution of **86** (40 mg, 0.20 mmol) in anhydrous DMF (4 mL) was degassed, filled with N₂, and cooled to 0 °C. Sodium hydride (60% in mineral oil) (20 mg, 0.50 mmol) was added portion-wise, and the mixture was stirred at 0 °C. After 30 min, a solution of 2-chloro-*N*-(*O*-tolyl)acetamide (40 mg, 0.23 mmol) in DMF (2 mL) was added dropwise and left to react at 20 °C. After 16 h, minimal product was observed with majority of the starting materials present, so the mixture was heated to 70 °C. After 3 h of heating, the mixture was cooled and diluted slowly with H₂O (15 mL). The aqueous layer was extracted with EtOAc (2 × 10 mL), and the combined organic layers were washed with brine, dried over MgSO₄, and concentrated under reduced pressure to give the crude material which was then purified using reverse phase preparative HPLC eluting with a gradient of 5–75% MeCN/H₂O (including 0.1% formic acid) to give **37** as a white solid (20 mg, 24%). ¹H NMR (300 MHz, DMSO-*d*₆) δ 9.75 (s, 1H), 8.12 (s, 1H), 7.75 (d, *J* = 8.3 Hz, 1H), 7.67 (dd, *J* = 8.3, 1.4 Hz, 1H), 7.62 (d, *J* = 3.1 Hz, 1H), 7.43 (d, *J* = 7.8 Hz, 1H), 7.22 (d, *J* = 7.1 Hz, 1H), 7.12 (dq, *J* = 14.3, 7.4 Hz, 2H), 6.60 (d, *J* = 3.1 Hz, 1H), 5.24 (s, 2H), 2.58 (s, 3H), 2.25 (s, 3H). ¹³C NMR (75 MHz, DMSO-*d*₆) δ 166.2, 165.2, 163.2, 136.0, 135.7, 133.2, 131.6, 130.7, 130.4, 126.0, 125.4, 124.7, 121.3, 117.3, 116.3, 108.5, 101.5, 49.0, 17.8, 10.7. LCMS *m/z* 347.0 [M + H].

HRMS *m/z*: [M + H] Calcd for C₂₀H₁₈N₄O₂ 347.1502; Found 347.1501.

2-(6-(5-Methyl-1,3,4-oxadiazol-2-yl)-1*H*-indol-1-yl)-*N*-(*P*-tolyl)acetamide (**39**). General Procedure D was followed using 4-methylaniline (25 mg, 0.23 mmol). When the reaction was deemed to be complete, the mixture was diluted with H₂O (~2 mL) and the solid was collected using vacuum filtration. Washing with H₂O (3 × 5 mL) afforded **39** as an off-white powder (36 mg, 69%). ¹H NMR (300 MHz, DMSO-*d*₆) δ 10.34 (s, 1H), 8.08 (s, 1H), 7.74 (d, *J* = 8.3 Hz, 1H), 7.66 (dd, *J* = 8.3, 1.4 Hz, 1H), 7.60 (d, *J* = 3.1 Hz, 1H), 7.48 (d, *J* = 8.4 Hz, 2H), 7.12 (d, *J* = 8.2 Hz, 2H), 6.59 (d, *J* = 3.1 Hz, 1H), 5.18 (s, 2H), 2.57 (s, 3H), 2.24 (s, 3H). ¹³C NMR (75 MHz, DMSO-*d*₆) δ 165.8, 165.2, 163.2, 136.2, 133.2, 132.5, 130.6, 129.2, 121.2, 119.1, 117.3, 116.3, 108.6, 101.5, 49.1, 20.4, 10.7. LCMS *m/z* 347.4 [M + H]. HRMS *m/z*: [M + H] Calcd for C₂₀H₁₈N₄O₂ 347.1502; Found 347.1503.

2-(6-(5-Methyl-1,3,4-oxadiazol-2-yl)-1*H*-indol-1-yl)-*N*-(2-(trifluoromethyl)phenyl)acetamide (**40**). General Procedure E: To a stirring solution of **85** (51 mg, 0.20 mmol) in MeCN (2 mL) was added EDCI-HCl (58 mg, 0.30 mmol) and 2-(trifluoromethyl)aniline (32 mg, 0.20 mmol). The mixture was stirred for 16 h before being diluted with EtOAc (10 mL) and H₂O (10 mL). The organics were separated, washed with brine (2 × 5 mL), dried over MgSO₄, filtered and concentrated. Column chromatography, eluting with 0–5% MeOH/DCM followed by reverse phase preparative HPLC eluting with a gradient of 5–75% MeCN/H₂O (including 0.1% formic acid) afforded **40** as a beige solid (18 mg, 26%). ¹H NMR (300 MHz, DMSO-*d*₆) δ 10.06 (s, 1H), 8.06 (s, 1H), 7.75 (dd, *J* = 8.3, 2.3 Hz, 2H), 7.72–7.63 (m, 2H), 7.63–7.51 (m, 2H), 7.46 (t, *J* = 7.6 Hz, 1H), 6.60 (d, *J* = 3.1 Hz, 1H), 5.25 (s, 2H), 2.58 (s, 3H). ¹³C NMR (75 MHz, DMSO-*d*₆) δ 167.3, 165.2, 163.2, 135.9, 134.7 (d, *J* = 2.1 Hz), 134.6, 133.1, 130.7, 129.7, 127.0, 126.4 (d, *J* = 5.0 Hz), 124.8, 124.4, 123.5 (d, *J* = 273.3 Hz), 121.3, 117.4, 116.4, 108.5, 101.6, 48.8, 10.6. LCMS *m/z* 401.2 [M + H]. HRMS *m/z*: [M + H] Calcd for C₂₀H₁₅F₃N₄O₂ 401.122; Found 401.1219.

2-(6-(5-Methyl-1,3,4-oxadiazol-2-yl)-1*H*-indol-1-yl)-*N*-(3-(trifluoromethyl)phenyl)acetamide (**41**). General Procedure D was followed using 3-(trifluoromethyl)aniline (27 μL, 0.22 mmol). Column chromatography eluting with 0–5% MeOH/DCM afforded **41** as a beige solid (22 mg, 28%). ¹H NMR (300 MHz, DMSO-*d*₆) δ 10.77 (s, 1H), 8.10 (d, *J* = 1.6 Hz, 2H), 7.84–7.71 (m, 2H), 7.67 (dd, *J* = 8.3, 1.4 Hz, 1H), 7.64–7.53 (m, 2H), 7.43 (d, *J* = 7.7 Hz, 1H), 6.61 (dd, *J* = 3.1, 0.9 Hz, 1H), 5.26 (s, 2H), 2.57 (s, 3H). ¹³C NMR (75 MHz, DMSO-*d*₆) δ 166.9, 165.2, 163.3, 139.5, 136.3, 133.2, 130.6, 130.2, 129.5 (d, *J* = 31.6 Hz), 128.9, 124.0 (d, *J* = 272.4 Hz), 122.7, 119.9 (d, *J* = 4.0 Hz), 117.3, 116.3, 115.1 (d, *J* = 4.0 Hz), 108.7, 101.7, 49.1, 10.7. LCMS *m/z* 401.2 [M + H]. HRMS *m/z*: [M + H] Calcd for C₂₀H₁₅F₃N₄O₂ 401.122; Found 401.1224.

2-(6-(5-Methyl-1,3,4-oxadiazol-2-yl)-1*H*-indol-1-yl)-*N*-(4-(trifluoromethyl)phenyl)acetamide (**42**). General Procedure E was followed using **85** (51 mg, 0.20 mmol) and 4-(trifluoromethyl)aniline hydrochloride (44 mg, 0.22 mmol). Column chromatography eluting with 0–5% MeOH/DCM afforded **42** as a beige solid (13 mg, 17%). ¹H NMR (300 MHz, DMSO-*d*₆) δ 10.81 (s, 1H), 8.10 (s, 1H), 7.82 (d, *J* = 8.6 Hz, 2H), 7.77–7.64 (m, 4H), 7.62 (d, *J* = 3.2 Hz, 1H), 6.61 (d, *J* = 3.2 Hz, 1H), 5.27 (s, 2H), 2.56 (s, 3H). ¹³C NMR (75 MHz, DMSO-*d*₆) δ 166.9, 165.2, 163.3, 142.3, 136.3, 133.2, 130.6, 126.5–126.1 (m), 123.5 (d, *J* = 31.8 Hz), 122.5, 121.3, 119.1, 117.3, 116.3, 108.7, 101.7, 49.2, 10.7. LCMS *m/z* 401.2 [M + H]. HRMS *m/z*: [M + H] Calcd for C₂₀H₁₅F₃N₄O₂ 401.122; Found 401.1218.

N-(2-Cyanophenyl)-2-(6-(5-methyl-1,3,4-oxadiazol-2-yl)-1*H*-indol-1-yl)acetamide (**46**). General Procedure E was followed using **85** (51 mg, 0.20 mmol) and 2-aminobenzonitrile (26 mg, 0.22 mmol). Column chromatography eluting with 0–5% MeOH/DCM afforded **46** as a brown solid (21 mg, 29%). ¹H NMR (300 MHz, DMSO-*d*₆) δ 10.64 (s, 1H), 8.10 (s, 1H), 7.83 (d, *J* = 8.2 Hz, 1H), 7.78–7.64 (m, 4H), 7.61 (d, *J* = 3.2 Hz, 1H), 7.35 (ddd, *J* = 8.1, 5.3, 3.3 Hz, 1H), 6.61 (d, *J* = 3.1 Hz, 1H), 5.31 (s, 2H), 2.57 (s, 3H). ¹³C NMR (75 MHz, DMSO-*d*₆) δ 167.1, 165.2, 163.3, 139.7, 136.1, 134.0, 133.4, 133.1, 130.7, 125.9, 125.1, 121.3, 117.4, 116.7, 116.4, 108.7, 106.7,

101.8, 48.9, 10.7. LCMS m/z 358.2 [M + H]. HRMS m/z : [M + H] Calcd for $C_{20}H_{15}N_5O_2$ 358.1298; Found 358.1303.

N-(4-(Cyanophenyl)-2-(6-(5-methyl-1,3,4-oxadiazol-2-yl)-1H-indol-1-yl)acetamide (48). General Procedure E was followed using **85** (51 mg, 0.20 mmol) and 4-aminobenzonitrile (26 mg, 0.22 mmol). Column chromatography eluting with 0–5% MeOH/DCM afforded **48** as a green solid (15 mg, 21%). 1H NMR (300 MHz, DMSO- d_6) δ 10.86 (s, 1H), 8.10 (s, 1H), 7.76 (d, J = 17.2 Hz, 5H), 7.66 (dd, J = 8.3, 1.4 Hz, 1H), 7.60 (d, J = 3.2 Hz, 1H), 6.60 (dd, J = 3.1, 0.8 Hz, 1H), 5.28 (s, 2H), 2.57 (s, 3H). ^{13}C NMR (75 MHz, DMSO- d_6) δ 167.1, 165.2, 163.3, 142.9, 136.3, 133.4, 133.1, 130.6, 121.3, 119.2, 118.9, 117.4, 116.4, 108.7, 105.3, 101.7, 49.2, 10.7. LCMS m/z 358.2 [M + H]. HRMS m/z : [M + H] Calcd for $C_{20}H_{15}N_5O_2$ 358.1298; Found 358.1297.

N-(2,5-Difluorophenyl)-2-(6-(5-methyl-1,3,4-oxadiazol-2-yl)-1H-indol-1-yl)acetamide (50). General Procedure E was followed using **85** (51 mg, 0.20 mmol) and 2,5-difluoroaniline (22 μ L, 0.22 mmol). Column chromatography eluting with 0–5% MeOH/DCM afforded **50** as a white solid (31 mg, 42%). 1H NMR (300 MHz, DMSO- d_6) δ 10.45 (s, 1H), 8.11 (s, 1H), 7.90 (ddd, J = 10.0, 6.1, 3.3 Hz, 1H), 7.80–7.54 (m, 3H), 7.36 (ddd, J = 10.7, 9.2, 5.1 Hz, 1H), 6.99 (tt, J = 7.6, 3.4 Hz, 1H), 6.60 (d, J = 3.2 Hz, 1H), 5.33 (s, 2H), 2.57 (s, 3H). ^{13}C NMR (75 MHz, DMSO- d_6) δ 167.2, 165.2, 163.3, 159.5–156.0 (m), 150.8–147.4 (m), 136.2, 133.1, 130.6, 127.1 (dd, J = 13.7, 11.9 Hz), 121.3, 117.3, 116.5 (dd, J = 22.0, 10.1 Hz), 116.4, 110.8 (dd, J = 24.4, 8.1 Hz), 109.8–108.9 (m), 108.6, 101.7, 49.0, 10.7. LCMS m/z 369.2 [M + H]. HRMS m/z : [M + H] Calcd for $C_{19}H_{14}F_2N_4O_2$ 369.1158; Found 369.1160.

N-(2,6-Difluorophenyl)-2-(6-(5-methyl-1,3,4-oxadiazol-2-yl)-1H-indol-1-yl)acetamide (51). General Procedure E was followed using **85** (51 mg, 0.20 mmol) and 2,6-difluoroaniline (24 μ L, 0.22 mmol). Column chromatography eluting with 0–5% MeOH/DCM afforded **51** as a white solid (38 mg, 52%). 1H NMR (300 MHz, DMSO- d_6) δ 10.12 (s, 1H), 8.13 (s, 1H), 7.81–7.58 (m, 4H), 7.36 (td, J = 8.3, 6.2 Hz, 1H), 7.24 (td, J = 8.7, 1.5 Hz, 1H), 6.64–6.57 (m, 1H), 2.58 (s, 3H). ^{13}C NMR (75 MHz, DMSO- d_6) δ 166.6, 165.2, 163.3, 157.7 (dd, J = 249.0, 5.2 Hz), 136.0, 133.1, 130.8, 128.3 (t, J = 9.7 Hz), 121.3, 117.4, 116.4, 113.9 (t, J = 16.9 Hz), 112.6–111.5 (m), 108.5, 101.7, 48.6, 10.7. LCMS m/z 369.2 [M + H]. HRMS m/z : [M + H] Calcd for $C_{19}H_{14}F_2N_4O_2$ 369.1158; Found 369.1159.

N-(3,5-Difluorophenyl)-2-(6-(5-methyl-1,3,4-oxadiazol-2-yl)-1H-indol-1-yl)acetamide (52). General Procedure E was followed using **85** (51 mg, 0.20 mmol) and 3,5-difluoroaniline (28 mg, 0.22 mmol). Column chromatography eluting with 0–5% MeOH/DCM afforded **52** as a white solid (35 mg, 47%). 1H NMR (300 MHz, DMSO- d_6) δ 10.81 (s, 1H), 8.09 (dd, J = 1.5, 0.8 Hz, 1H), 7.75 (d, J = 8.3 Hz, 1H), 7.66 (dd, J = 8.3, 1.4 Hz, 1H), 7.60 (d, J = 3.1 Hz, 1H), 7.41–7.24 (m, 2H), 6.94 (tt, J = 9.4, 2.4 Hz, 1H), 6.60 (dd, J = 3.1, 0.8 Hz, 1H), 5.25 (s, 2H), 2.57 (s, 3H). ^{13}C NMR (75 MHz, DMSO- d_6) δ 167.0, 165.2, 163.3, 162.5 (dd, J = 243.4, 15.1 Hz), 141.2 (t, J = 13.7 Hz), 136.3, 133.1, 130.6, 121.3, 117.3, 116.3, 108.7, 102.0 (d, J = 28.9 Hz), 101.7, 98.7 (t, J = 26.2 Hz), 49.1, 10.7. LCMS m/z 369.2 [M + H]. HRMS m/z : [M + H] Calcd for $C_{19}H_{14}F_2N_4O_2$ 369.1158; Found 369.1157.

N-(3,5-Dichlorophenyl)-2-(6-(5-methyl-1,3,4-oxadiazol-2-yl)-1H-indol-1-yl)acetamide (53). General Procedure E was followed using **85** (51 mg, 0.20 mmol) and 3,5-dichloroaniline (49 mg, 0.30 mmol). Column chromatography eluting with 0–5% MeOH/DCM afforded **53** as a white solid (34 mg, 42%). 1H NMR (300 MHz, DMSO- d_6) δ 10.77 (s, 1H), 8.09 (d, J = 1.4 Hz, 1H), 7.74 (d, J = 8.3 Hz, 1H), 7.67 (dd, J = 5.7, 1.7 Hz, 3H), 7.59 (d, J = 3.2 Hz, 1H), 7.30 (t, J = 1.9 Hz, 1H), 6.60 (dd, J = 3.1, 0.8 Hz, 1H), 5.25 (s, 2H), 2.57 (s, 3H). ^{13}C NMR (75 MHz, DMSO- d_6) δ 167.1, 165.2, 163.3, 141.0, 136.3, 134.2, 133.1, 130.7, 122.8, 121.3, 117.4, 117.3, 116.4, 108.7, 101.8, 49.1, 10.7. LCMS m/z 401.2 [M + H]. HRMS m/z : [M + H] Calcd for $C_{19}H_{14}Cl_2N_4O_2$ 401.0567; Found 401.0566.

N-(2,3-Dichlorophenyl)-2-(6-(5-methyl-1,3,4-oxadiazol-2-yl)-1H-indol-1-yl)acetamide (54). General Procedure E was followed using **85** (39 mg, 0.15 mmol) and 2,3-dichloroaniline (36 mg, 0.23 mmol). Column chromatography eluting with 0–5% MeOH/DCM afforded

54 as a white solid (11 mg, 18%). 1H NMR (300 MHz, DMSO- d_6) δ 10.77 (s, 1H), 8.09 (d, J = 1.4 Hz, 1H), 7.74 (d, J = 8.3 Hz, 1H), 7.67 (dd, J = 5.7, 1.7 Hz, 3H), 7.59 (d, J = 3.2 Hz, 1H), 7.30 (t, J = 1.9 Hz, 1H), 6.60 (dd, J = 3.1, 0.8 Hz, 1H), 5.25 (s, 2H), 2.57 (s, 3H). ^{13}C NMR (75 MHz, DMSO- d_6) δ 166.9, 165.2, 163.3, 136.4, 136.0, 133.2, 132.0, 130.8, 128.2, 127.0, 125.1, 124.4, 121.4, 117.4, 116.4, 108.6, 101.7, 49.0, 10.7. LCMS m/z 401.2 [M + H]. HRMS m/z : [M + H] Calcd for $C_{19}H_{14}Cl_2N_4O_2$ 401.0567; Found 401.0566.

N-(2-Chloro-3-fluorophenyl)-2-(6-(5-methyl-1,3,4-oxadiazol-2-yl)-1H-indol-1-yl)acetamide (55). General Procedure E was followed using **85** (39 mg, 0.15 mmol) and 2-chloro-3-fluoroaniline (33 μ L, 0.30 mmol). Column chromatography eluting with 0–5% MeOH/DCM afforded **55** as a white solid (25 mg, 32%). 1H NMR (300 MHz, DMSO- d_6) δ 10.12 (s, 1H), 8.13 (s, 1H), 7.81–7.58 (m, 4H), 7.36 (td, J = 8.3, 6.2 Hz, 1H), 7.24 (td, J = 8.7, 1.5 Hz, 1H), 6.65–6.56 (m, 1H), 5.33 (s, 2H), 2.58 (s, 3H). ^{13}C NMR (75 MHz, DMSO) δ 166.9, 165.2, 163.3, 157.7 (d, J = 245.4 Hz), 136.4 (d), 136.0, 133.2, 130.7, 128.1 (d, J = 9.0 Hz), 121.3, 121.0 (d), 117.4, 116.4, 108.6, 101.7, 49.0, 10.7. LCMS m/z 385.2 [M + H]. HRMS m/z : [M + H] Calcd for $C_{19}H_{14}ClFN_4O_2$ 385.0862; Found 385.0861.

N-(2-Chloro-5-fluorophenyl)-2-(6-(5-methyl-1,3,4-oxadiazol-2-yl)-1H-indol-1-yl)acetamide (56). A stirring mixture of **85** (115 mg, 0.447 mmol) and EDCI-HCl (135 mg, 0.704 mmol) in MeCN (4.5 mL) at 20 °C was treated with 2-chloro-5-fluoroaniline (100 mg, 0.687 mmol) and stirred for 16 h. The incomplete reaction was then heated to 80 °C for 1 h which yielded no additional product formation. The mixture was concentrated under reduced pressure and the resulting brown oil was diluted with MeOH (2–3 mL) and H₂O (2–3 mL). The resulting solution was sonicated to produce a precipitate which was collected and washed with cold 1:1 MeOH/H₂O followed by cold MeOH to afford **56** as a beige solid (23 mg, 13%). LCMS m/z 385.2 [M + H]. 1H NMR (300 MHz, DMSO- d_6) δ 10.00 (s, 1H), 8.13 (s, 1H), 7.84–7.71 (m, 2H), 7.67 (d, J = 8.3 Hz, 1H), 7.64–7.50 (m, 2H), 7.08 (td, J = 8.4, 3.1 Hz, 1H), 6.61 (d, J = 3.1 Hz, 1H), 5.35 (s, 2H), 2.58 (s, 3H). ^{13}C NMR (75 MHz, DMSO- d_6) δ 167.2, 165.2, 163.2, 160.4 (d, J = 243.2 Hz), 136.1, 135.8 (d, J = 11.5 Hz), 133.1, 130.8, 130.7, 130.7, 121.3, 117.4, 116.4, 112.9 (d, J = 23.0 Hz), 111.4 (d, J = 27.5 Hz), 108.6, 101.8, 49.0, 10.7. LCMS m/z 385.2 [M + H]. HRMS m/z : [M + H] Calcd for $C_{19}H_{14}ClFN_4O_2$ 385.0862; Found 385.0862.

N-(3,4-Dimethoxyphenyl)-2-(6-(5-methyl-1,3,4-oxadiazol-2-yl)-1H-indol-1-yl)acetamide (57). General Procedure F: A 10 mL microwave vial with stir bar was charged with **106** (49 mg, 0.17 mmol), 3,4-dimethoxyaniline (28 mg, 0.18 mmol), DABAL-CH₃ (39 mg, 0.15 mmol) and toluene (1 mL). The resultant mixture was heated at 130 °C for 30 min using microwave irradiation. Additional portions of DABAL-CH₃ (40 mg, 0.16 mmol) and 3,4-dimethoxyaniline (26 mg, 0.17 mmol) were added and the mixture was resubjected to the reaction conditions. The mixture was quenched by stirring in a mixture of EtOAc (3 mL) and aq. 1 M HCl (3 mL) before diluting with EtOAc (20 mL) and aq. 1 M HCl (20 mL). The isolated organic phase was washed using H₂O (20 mL) and brine (20 mL), dried over MgSO₄, filtered and concentrated under reduced pressure. Column chromatography eluting with 50–100% EtOAc/heptane afforded **57** as an off-white solid (24 mg, 36%). 1H NMR (300 MHz, DMSO- d_6) δ 10.31 (s, 1H), 8.08 (s, 1H), 7.74 (d, J = 8.3 Hz, 1H), 7.66 (dd, J = 8.3, 1.4 Hz, 1H), 7.60 (d, J = 3.1 Hz, 1H), 7.34 (d, J = 2.4 Hz, 1H), 7.08 (dd, J = 8.7, 2.4 Hz, 1H), 6.90 (d, J = 8.7 Hz, 1H), 6.59 (dd, J = 3.1, 0.9 Hz, 1H), 5.17 (s, 2H), 3.71 (s, 3H), 3.69 (s, 3H), 2.57 (s, 3H). ^{13}C NMR (75 MHz, DMSO- d_6) δ 165.6, 165.2, 163.2, 148.6, 145.0, 136.1, 133.2, 132.3, 130.6, 121.2, 117.2, 116.2, 112.1, 111.0, 108.6, 104.2, 101.5, 55.7, 55.3, 49.1, 10.7. LCMS m/z 393.2 [M + H]. HRMS m/z : [M + H] Calcd for $C_{21}H_{20}N_4O_4$ 393.1557; Found 393.1555.

N-(3,5-Dimethoxyphenyl)-2-(6-(5-methyl-1,3,4-oxadiazol-2-yl)-1H-indol-1-yl)acetamide (58). General Procedure E was followed using **85** (39 mg, 0.15 mmol) and 3,5-dimethoxyaniline (35 mg, 0.23 mmol). Column chromatography eluting with 0–5% MeOH/DCM afforded **58** as a white solid (15 mg, 25%). 1H NMR (300 MHz, DMSO- d_6) δ 10.77 (s, 1H), 8.09 (d, J = 1.4 Hz, 1H), 7.74 (d, J = 8.3

Hz, 1H), 7.67 (dd, $J = 5.7, 1.7$ Hz, 3H), 7.59 (d, $J = 3.2$ Hz, 1H), 7.30 (t, $J = 1.9$ Hz, 1H), 6.60 (dd, $J = 3.1, 0.8$ Hz, 1H), 5.25 (s, 2H), 2.57 (s, 3H). ^{13}C NMR (75 MHz, DMSO- d_6) δ 166.3, 165.2, 163.3, 160.6, 140.4, 136.2, 133.2, 130.7, 121.3, 117.3, 116.3, 108.6, 101.6, 97.4, 95.6, 55.1, 49.2, 10.7. LCMS m/z 393.2 [M + H]. HRMS m/z : [M + H] Calcd for $\text{C}_{21}\text{H}_{20}\text{N}_4\text{O}_4$ 393.1557; Found 393.1555.

2-(6-(5-Methyl-1,3,4-oxadiazol-2-yl)-1H-indol-1-yl)-N-(3,4,5-trimethoxyphenyl)acetamide (59). General Procedure E was followed using **85** (51 mg, 0.20 mmol) and 3,4,5-trimethoxyaniline (31 mg, 0.22 mmol). Column chromatography eluting with 0–5% MeOH/DCM afforded **59** as a white solid (37 mg, 44%). ^1H NMR (300 MHz, DMSO- d_6) δ 10.39 (s, 1H), 8.07 (d, $J = 1.4$ Hz, 1H), 7.77–7.63 (m, 2H), 7.60 (d, $J = 3.1$ Hz, 1H), 6.98 (s, 2H), 6.60 (d, $J = 3.1$ Hz, 1H), 5.18 (s, 2H), 3.72 (s, 6H), 3.61 (s, 3H), 2.57 (s, 3H). ^{13}C NMR (75 MHz, DMSO- d_6) δ 166.0, 165.2, 163.3, 152.8, 136.2, 134.8, 133.6, 133.2, 130.7, 121.3, 117.3, 116.3, 108.6, 101.6, 96.8, 60.1, 55.7, 49.2, 10.7. LCMS m/z 423.2 [M + H]. HRMS m/z : [M + H] Calcd for $\text{C}_{22}\text{H}_{22}\text{N}_4\text{O}_5$ 423.1663; Found 423.1666.

2-(6-(5-Methyl-1,3,4-oxadiazol-2-yl)-1H-indol-1-yl)-N-(pyridin-3-yl)acetamide (61). General Procedure E was followed using **85** (51 mg, 0.20 mmol) and 3-aminopyridine (21 mg, 0.22 mmol). Column chromatography eluting with 0–5% MeOH/DCM afforded **61** as a white solid (21 mg, 31%). ^1H NMR (300 MHz, DMSO- d_6) δ 10.66 (s, 1H), 8.77 (d, $J = 2.5$ Hz, 1H), 8.28 (dd, $J = 4.7, 1.5$ Hz, 1H), 8.10 (dd, $J = 1.6, 0.8$ Hz, 1H), 8.04 (ddd, $J = 8.4, 2.6, 1.5$ Hz, 1H), 7.82–7.58 (m, 3H), 7.36 (dd, $J = 8.3, 4.7$ Hz, 1H), 6.61 (dd, $J = 3.1, 0.9$ Hz, 1H), 5.26 (s, 2H), 2.57 (s, 3H). ^{13}C NMR (75 MHz, DMSO- d_6) δ 166.8, 165.2, 163.3, 144.5, 140.7, 136.2, 135.4, 133.1, 130.6, 126.1, 123.7, 121.2, 117.3, 116.3, 108.6, 101.7, 49.0, 10.7. LCMS m/z 334.2 [M + H]. HRMS m/z : [M + H] Calcd for $\text{C}_{18}\text{H}_{15}\text{N}_5\text{O}_2$ 334.1298; Found 334.1297.

2-(6-(5-Methyl-1,3,4-oxadiazol-2-yl)-1H-indol-1-yl)-N-(pyridin-4-yl)acetamide (62). General Procedure E was followed using **85** (51 mg, 0.20 mmol) and 3-aminopyridine (28 mg, 0.30 mmol). Column chromatography eluting with 0–5% MeOH/DCM afforded **62** as a white solid (26 mg, 38%). ^1H NMR (300 MHz, DMSO- d_6) δ 10.81 (s, 1H), 8.48–8.40 (m, 2H), 8.10 (dd, $J = 1.6, 0.8$ Hz, 1H), 7.75 (dd, $J = 8.3, 0.7$ Hz, 1H), 7.67 (dd, $J = 8.3, 1.4$ Hz, 1H), 7.63–7.53 (m, 3H), 6.61 (dd, $J = 3.1, 0.9$ Hz, 1H), 5.28 (s, 2H), 2.56 (s, 3H). ^{13}C NMR (75 MHz, DMSO- d_6) δ 167.5, 165.2, 163.3, 150.5, 145.3, 136.3, 133.2, 130.6, 121.3, 117.4, 116.4, 113.2, 108.7, 101.8, 49.2, 10.7. LCMS m/z 334.2 [M + H]. HRMS m/z : [M + H] Calcd for $\text{C}_{18}\text{H}_{15}\text{N}_5\text{O}_2$ 334.1298; Found 334.1296.

N-(2-Chloropyridin-3-yl)-2-(6-(5-methyl-1,3,4-oxadiazol-2-yl)-1H-indol-1-yl)acetamide (63). General Procedure G: Compound **85** (52 mg, 0.20 mmol) was dissolved in DMF (1.5 mL). 50% T3P in DMF (407 μL , 0.70 mmol) was added followed by 3-amino-2-chloropyridine (34 mg, 0.26 mmol) and pyridine (85 μL , 1.05 mmol). The mixture was stirred at 20 $^\circ\text{C}$ for 16 h and diluted with EtOAc (5 mL) and H_2O (5 mL). The organic fraction was separated and further washed with brine (2 \times 5 mL) before being dried over MgSO_4 , filtered and concentrated under reduced pressure. Column chromatography eluting with 0–5% MeOH/DCM afforded **63** as a white solid (25 mg, 37%). ^1H NMR (300 MHz, DMSO- d_6) δ 10.13 (s, 1H), 8.33–8.06 (m, 3H), 7.84–7.54 (m, 3H), 7.42 (dd, $J = 7.7, 5.0$ Hz, 1H), 6.61 (d, $J = 3.1$ Hz, 1H), 5.36 (s, 2H). ^{13}C NMR (75 MHz, DMSO- d_6) δ 167.4, 165.3, 163.4, 145.6, 142.9, 136.1, 133.7, 133.2, 131.6, 130.8, 123.6, 121.4, 117.5, 116.4, 108.7, 101.8, 49.1, 10.7. LCMS m/z 368.2 [M + H]. HRMS m/z : [M + H] Calcd for $\text{C}_{18}\text{H}_{14}\text{ClN}_5\text{O}_2$ 368.0909; Found 368.0908.

N-(3-Chloropyridin-4-yl)-2-(6-(5-methyl-1,3,4-oxadiazol-2-yl)-1H-indol-1-yl)acetamide (64). General Procedure G was followed using 4-amino-3-chloropyridine (34 mg, 0.26 mmol). Column chromatography eluting with 0–5% MeOH/DCM afforded **64** as a white solid (17 mg, 23%). ^1H NMR (300 MHz, DMSO- d_6) δ 10.13 (s, 1H), 8.63 (s, 1H), 8.40 (d, $J = 5.5$ Hz, 1H), 8.12 (s, 1H), 8.07 (d, $J = 5.5$ Hz, 1H), 7.75 (d, $J = 8.3$ Hz, 1H), 7.67 (dd, $J = 8.3, 1.4$ Hz, 1H), 7.61 (d, $J = 3.1$ Hz, 1H), 6.62 (dd, $J = 3.1, 0.8$ Hz, 1H), 5.43 (s, 2H), 2.57 (s, 3H). ^{13}C NMR (75 MHz, DMSO- d_6) δ 168.1, 165.2, 163.4, 149.7, 148.9, 141.7, 136.2, 133.2, 130.7, 121.4, 120.7, 117.5,

116.5, 116.4, 108.6, 101.9, 49.3, 10.7. LCMS m/z 368.2 [M + H]. HRMS m/z : [M + H] Calcd for $\text{C}_{18}\text{H}_{14}\text{ClN}_5\text{O}_2$ 368.0909; Found 368.0907.

N-Methyl-2-(6-(5-methyl-1,3,4-oxadiazol-2-yl)-1H-indol-1-yl)-N-phenylacetamide (65). General Procedure G was followed using N-methylaniline (28 μL , 0.26 mmol). Column chromatography eluting with 0–5% MeOH/DCM afforded **65** as a white solid (32 mg, 51%). ^1H NMR (300 MHz, DMSO- d_6) δ 7.91 (s, 1H), 7.76–7.29 (m, 9H), 6.52 (d, $J = 3.2$ Hz, 1H), 4.88 (s, 2H), 2.60 (s, 3H). ^{13}C NMR (75 MHz, DMSO- d_6) δ 166.6, 165.2, 163.2, 142.4, 136.2, 133.0, 130.5, 129.9, 128.1, 127.4, 121.1, 117.1, 116.1, 108.7, 101.4, 47.8, 37.2, 10.7. LCMS m/z 347.2 [M + H]. HRMS m/z : [M + H] Calcd for $\text{C}_{20}\text{H}_{18}\text{N}_4\text{O}_2$ 347.1502; Found 347.1501.

N-(2-Chlorophenyl)-2-(6-(1-methyl-1H-pyrazol-4-yl)-1H-indol-1-yl)propanamide (66). General Procedure C was followed using **96** (40 mg, 0.16 mmol) and **107** (50 mg, 0.19 mmol). Column chromatography eluting with 0–4% MeOH/DCM afforded **66** as a yellow solid (25 mg, 40%). ^1H NMR (300 MHz, CDCl_3) δ 8.13 (dd, $J = 8.2, 1.5$ Hz, 1H), 7.61 (s, 1H), 7.46 (q, $J = 7.7$ Hz, 3H), 7.18–7.10 (m, 2H), 7.10–6.99 (m, 2H), 6.80 (td, $J = 7.8, 1.6$ Hz, 1H), 6.53 (d, $J = 3.3$ Hz, 1H), 5.08 (q, $J = 7.3$ Hz, 1H), 3.75 (s, 3H), 1.82 (d, $J = 7.3$ Hz, 3H). LCMS m/z 379.2 [M + H]. HRMS m/z : [M + H] Calcd for $\text{C}_{21}\text{H}_{19}\text{ClN}_4\text{O}$ 379.132; Found 379.1320.

N-(2-Chlorophenyl)-2-(2-methyl-6-(1-methyl-1H-pyrazol-4-yl)-1H-indol-1-yl)acetamide (67). General Procedure B was followed using **97** (30 mg, 0.08 mmol) and 1-methyl-4-(4,4,5,5-tetramethyl-1,3,2-dioxaborolan-2-yl)-1H-pyrazole (25 mg, 0.12 mmol). Column chromatography eluting with 0–5% MeOH/DCM followed by reverse phase preparative HPLC eluting with a gradient of 5–75% MeCN/ H_2O (including 0.1% formic acid) afforded **67** as a beige solid (4 mg, 14%). ^1H NMR (300 MHz, DMSO- d_6) δ 9.80 (s, 1H), 8.03 (s, 1H), 7.82 (s, 1H), 7.77 (dd, $J = 8.1, 1.6$ Hz, 1H), 7.65 (s, 1H), 7.51 (dd, $J = 8.0, 1.5$ Hz, 1H), 7.40 (d, $J = 8.1$ Hz, 1H), 7.32 (td, $J = 7.7, 1.5$ Hz, 1H), 7.20 (ddd, $J = 8.4, 7.0, 1.5$ Hz, 2H), 6.22 (s, 1H), 5.12 (s, 2H), 3.86 (s, 3H), 2.39 (s, 3H). ^{13}C NMR (75 MHz, DMSO- d_6) δ 167.2, 137.9, 137.3, 135.7, 134.4, 129.5, 127.6, 127.0, 126.5, 126.2, 126.1, 125.7, 125.1, 123.4, 119.5, 117.3, 105.6, 100.1, 45.9, 38.6, 12.4. LCMS m/z 379.2 [M + H]. HRMS m/z : [M + H] Calcd for $\text{C}_{21}\text{H}_{19}\text{ClN}_4\text{O}$ 379.132; Found 379.1322.

N-(2-Chlorophenyl)-2-(2-methyl-6-(1-methyl-1H-pyrazol-4-yl)-1H-indol-1-yl)acetamide (68). General Procedure B was followed using **98** (30 mg, 0.08 mmol) and 1-methyl-4-(4,4,5,5-tetramethyl-1,3,2-dioxaborolan-2-yl)-1H-pyrazole (25 mg, 0.12 mmol). Column chromatography eluting with 0–5% MeOH/DCM followed by reverse phase preparative HPLC eluting with a gradient of 5–75% MeCN/ H_2O (including 0.1% formic acid) afforded **68** as a beige solid (6 mg, 20%). ^1H NMR (300 MHz, CDCl_3) δ 8.30 (dd, $J = 8.2, 1.5$ Hz, 1H), 7.79 (d, $J = 0.8$ Hz, 1H), 7.68–7.53 (m, 3H), 7.37 (dd, $J = 1.5, 0.7$ Hz, 1H), 7.32 (dd, $J = 8.2, 1.4$ Hz, 1H), 7.26–7.17 (m, 2H), 6.99 (ddd, $J = 8.2, 7.3, 1.6$ Hz, 1H), 6.91 (d, $J = 1.2$ Hz, 1H), 4.92 (s, 2H), 3.94 (s, 3H), 2.36 (s, 3H). ^{13}C NMR (75 MHz, DMSO- d_6) δ 167.2, 137.3, 135.7, 134.4, 129.5, 127.5, 127.2, 127.0, 126.3, 126.1, 125.8, 125.3, 123.3, 118.9, 116.8, 109.7, 105.8, 48.7, 38.6, 9.4. LCMS m/z 379.2 [M + H]. HRMS m/z : [M + H] Calcd for $\text{C}_{21}\text{H}_{19}\text{ClN}_4\text{O}$ 379.132; Found 379.1325.

N-(2-Chlorophenyl)-2-(3-fluoro-6-(1-methyl-1H-pyrazol-4-yl)-1H-indol-1-yl)acetamide (69). General Procedure B was followed using **99** (30 mg, 0.08 mmol) and 1-methyl-4-(4,4,5,5-tetramethyl-1,3,2-dioxaborolan-2-yl)-1H-pyrazole (25 mg, 0.12 mmol). Column chromatography eluting with 0–5% MeOH/DCM afforded **69** as a beige solid (20 mg, 66%). ^1H NMR (300 MHz, DMSO- d_6) δ 9.74 (s, 1H), 8.10 (s, 1H), 7.86 (s, 1H), 7.78 (dd, $J = 8.1, 1.6$ Hz, 1H), 7.71 (s, 1H), 7.56–7.46 (m, 2H), 7.37 (d, $J = 2.6$ Hz, 1H), 7.32 (ddd, $J = 7.6, 6.2, 1.4$ Hz, 2H), 7.19 (td, $J = 7.7, 1.6$ Hz, 1H), 5.10 (s, 2H), 3.87 (s, 3H). ^{13}C NMR (75 MHz, DMSO- d_6) δ 166.8, 145.3, 142.2, 135.9, 134.4, 133.9 (d, $J = 5.2$ Hz), 129.5, 127.5, 127.5, 127.4, 126.4, 125.9, 125.5, 122.7, 117.8, 114.8 (d, $J = 16.5$ Hz), 112.5 (d, $J = 26.9$ Hz), 106.2, 48.7, 38.6. LCMS m/z 383.0 [M + H]. HRMS m/z : [M + H] Calcd for $\text{C}_{20}\text{H}_{16}\text{ClFN}_4\text{O}$ 383.1069; Found 383.1068.

2-(3-Chloro-6-(1-methyl-1H-pyrazol-4-yl)-1H-indol-1-yl)-N-(2-chlorophenyl)acetamide (**70**). A stirring solution of **9** (24 mg, 0.066 mmol) in DMF (650 μ L) at 20 $^{\circ}$ C was treated with NCS (12 mg, 0.088 mmol). After 3 h H₂O (~3 mL) was added to the mixture which appeared to give a precipitate. This material was collected using vacuum filtration to give a black solid. Purification by reverse phase preparative HPLC eluting with a gradient of 5–75% MeCN/H₂O (including 0.1% formic acid) afforded **70** as a white solid (5 mg, 19%). ¹H NMR (300 MHz, DMSO-*d*₆) δ 9.85 (s, 1H), 8.12 (d, *J* = 2.0 Hz, 1H), 7.87 (t, *J* = 1.2 Hz, 1H), 7.76 (dd, *J* = 8.3, 1.7 Hz, 2H), 7.58–7.44 (m, 3H), 7.43–7.28 (m, 2H), 7.20 (td, *J* = 7.7, 1.7 Hz, 1H), 5.17 (s, 2H), 3.87 (d, *J* = 1.8 Hz, 3H). LCMS *m/z* 399.2 [M + H]. HRMS *m/z*: [M + H] Calcd for C₂₀H₁₆Cl₂N₄O 399.0774; Found 399.0772.

2-(3-Bromo-6-(1-methyl-1H-pyrazol-4-yl)-1H-indol-1-yl)-N-(2-chlorophenyl)acetamide (**71**). A stirring solution of **9** (195 mg, 0.534 mmol) in DMF (5 mL) at 20 $^{\circ}$ C was treated with NBS (98 mg, 0.55 mmol). After 3 h H₂O (~3 mL) was added to the mixture which appeared to give a precipitate. This material was collected using vacuum filtration to give a brown solid. Purification by reverse phase preparative HPLC eluting with a gradient of 5–75% MeCN/H₂O (including 0.1% formic acid) afforded **71** as a white solid (4 mg, 2%). ¹H NMR (300 MHz, DMSO-*d*₆) δ 9.86 (s, 1H), 8.11 (s, 1H), 7.87 (s, 1H), 7.81–7.71 (m, 2H), 7.58 (s, 1H), 7.51 (dd, *J* = 8.0, 1.5 Hz, 1H), 7.44–7.37 (m, 2H), 7.32 (td, *J* = 7.7, 1.6 Hz, 1H), 7.20 (td, *J* = 7.7, 1.6 Hz, 1H), 5.19 (s, 2H), 3.87 (s, 3H). LCMS *m/z* 443.0 [M + H]. HRMS *m/z*: [M + H] Calcd for C₂₀H₁₆BrClN₄O 443.0269; Found 443.0268.

N-(2-Chlorophenyl)-2-(3-cyano-6-(1-methyl-1H-pyrazol-4-yl)-1H-indol-1-yl)acetamide (**72**). General Procedure B was followed using **100** (60 mg, 0.15 mmol) and 1-methyl-4-(4,4,5,5-tetramethyl-1,3,2-dioxaborolan-2-yl)pyrazole (48 mg, 0.23 mmol). Column chromatography eluting with 0–5% MeOH/DCM followed by reverse phase preparative HPLC eluting with a gradient of 5–75% MeCN/H₂O (including 0.1% formic acid) afforded **72** as a white solid (5 mg, 8%). ¹H NMR (300 MHz, DMSO-*d*₆) δ 10.06 (s, 1H), 8.27 (s, 1H), 8.15 (s, 1H), 7.90 (s, 1H), 7.86 (s, 1H), 7.74 (dd, *J* = 8.1, 1.7 Hz, 1H), 7.63 (d, *J* = 8.3 Hz, 1H), 7.52 (ddd, *J* = 8.3, 3.4, 1.4 Hz, 2H), 7.33 (td, *J* = 7.7, 1.6 Hz, 1H), 7.21 (td, *J* = 7.7, 1.7 Hz, 1H), 5.30 (s, 2H), 3.87 (s, 3H). LCMS *m/z* 390.2 [M + H]. HRMS *m/z*: [M + H] Calcd for C₂₁H₁₆ClN₅O 390.1116; Found 390.1117.

N-(2-Chlorophenyl)-2-(6-(1-methyl-1H-pyrazol-4-yl)-1H-indazol-1-yl)acetamide (**73**). General Procedure B was followed using **101** (55 mg, 0.15 mmol) and 1-methyl-4-(4,4,5,5-tetramethyl-1,3,2-dioxaborolan-2-yl)pyrazole (48 mg, 0.23 mmol). Column chromatography eluting with 0–40% EtOAc/DCM afforded **73** as a white solid (15 mg, 27%). ¹H NMR (300 MHz, DMSO-*d*₆) δ 9.83 (s, 1H), 8.20 (s, 1H), 8.11–8.04 (m, 1H), 7.94 (s, 1H), 7.91 (s, 1H), 7.80 (dd, *J* = 8.1, 1.6 Hz, 1H), 7.74 (d, *J* = 8.4 Hz, 1H), 7.51 (dd, *J* = 8.0, 1.5 Hz, 1H), 7.39 (dd, *J* = 8.4, 1.3 Hz, 1H), 7.32 (td, *J* = 7.8, 1.5 Hz, 1H), 7.19 (td, *J* = 7.6, 1.6 Hz, 1H), 5.42 (s, 2H), 3.88 (s, 3H). ¹³C NMR (75 MHz, DMSO-*d*₆) δ 166.3, 141.3, 136.3, 134.4, 133.7, 130.9, 129.5, 128.2, 127.5, 126.3, 125.7, 125.3, 122.2, 122.1, 121.1, 119.1, 105.1, 51.3, 24.9. LCMS *m/z* 366.2 [M + H]. HRMS *m/z*: [M + H] Calcd for C₁₉H₁₆ClN₅O 366.1116; Found 366.1114.

N-(2-Chlorophenyl)-2-(6-(1-methyl-1H-pyrazol-4-yl)-1H-benzodilimidazol-1-yl)acetamide (**74**). General Procedure B was followed using **102** (40 mg, 0.11 mmol). Column chromatography eluting with 0–5% MeOH/DCM followed by reverse phase preparative HPLC eluting with a gradient of 5–75% MeCN/H₂O (including 0.1% formic acid) afforded **74** as a white solid (9 mg, 21%). ¹H NMR (300 MHz, DMSO-*d*₆) δ 10.11 (s, 1H), 8.20 (s, 1H), 8.10 (s, 1H), 7.85 (s, 1H), 7.75 (dd, *J* = 8.0, 1.7 Hz, 2H), 7.63 (d, *J* = 8.4 Hz, 1H), 7.52 (dd, *J* = 8.0, 1.5 Hz, 1H), 7.43 (dd, *J* = 8.4, 1.6 Hz, 1H), 7.33 (td, *J* = 7.7, 1.6 Hz, 1H), 7.21 (td, *J* = 7.7, 1.7 Hz, 1H), 5.27 (s, 2H), 3.87 (s, 3H). ¹³C NMR (75 MHz, DMSO-*d*₆) δ 166.2, 145.0, 141.8, 135.9, 135.0, 134.4, 129.6, 128.9, 127.5, 127.4, 126.6, 126.4, 126.0, 122.6, 119.6, 119.2, 106.3, 47.1, 38.6. LCMS *m/z* 366.2 [M + H]. HRMS *m/z*: [M + H] Calcd for C₁₉H₁₆ClN₅O 366.1116; Found 366.1116.

N-(2-Chlorophenyl)-2-(6-(1-methyl-1H-pyrazol-4-yl)-1H-pyrrolo[3,2-*b*]pyridin-1-yl)acetamide (**75**). General Procedure B was followed using **103** (40 mg, 0.11 mmol) and 1-methyl-4-(4,4,5,5-tetramethyl-1,3,2-dioxaborolan-2-yl)pyrazole (34 mg, 0.16 mmol). Column chromatography eluting with 0–5% MeOH/DCM followed by reverse phase preparative HPLC eluting with a gradient of 5–75% MeCN/H₂O (including 0.1% formic acid) afforded **75** as a white solid (22 mg, 55%). ¹H NMR (300 MHz, DMSO-*d*₆) δ 9.93 (s, 1H), 8.76 (d, *J* = 1.8 Hz, 1H), 8.42 (s, 1H), 8.26 (s, 1H), 7.99 (s, 1H), 7.87 (d, *J* = 3.3 Hz, 1H), 7.77 (dd, *J* = 8.1, 1.6 Hz, 1H), 7.51 (dd, *J* = 8.0, 1.5 Hz, 1H), 7.32 (td, *J* = 7.7, 1.6 Hz, 1H), 7.20 (td, *J* = 7.7, 1.7 Hz, 1H), 6.69 (d, *J* = 3.3 Hz, 1H), 5.30 (s, 2H), 3.90 (s, 3H). ¹³C NMR (75 MHz, DMSO-*d*₆) δ 166.4, 163.0, 140.9, 137.2, 136.2, 135.8, 134.4, 131.3, 129.6, 128.0, 127.5, 126.5, 126.2, 125.8, 122.1, 119.1, 116.6, 99.8, 49.2, 38.8. LCMS *m/z* 366.2 [M + H]. HRMS *m/z*: [M + H] Calcd for C₁₉H₁₆ClN₅O 366.1116; Found 366.1120.

N-(2-Chlorophenyl)-2-(6-(1-methyl-1H-pyrazol-4-yl)-1H-pyrrolo[3,2-*c*]pyridin-1-yl)acetamide (**76**). General Procedure B was followed using **104** (40 mg, 0.12 mmol) and 1-methyl-4-(4,4,5,5-tetramethyl-1,3,2-dioxaborolan-2-yl)pyrazole (39 mg, 0.19 mmol). Column chromatography eluting with 0–5% MeOH/DCM followed by reverse phase preparative HPLC eluting with a gradient of 5–75% MeCN/H₂O (including 0.1% formic acid) afforded **76** as a white solid (8 mg, 18%). ¹³C NMR (75 MHz, DMSO-*d*₆) δ 166.5, 143.3, 142.6, 141.2, 136.4, 134.4, 130.9, 129.5, 128.5, 127.5, 126.5, 126.1, 125.6, 124.2, 123.5, 100.7, 100.1, 48.6, 38.6. LCMS *m/z* 366.2 [M + H]. HRMS *m/z*: [M + H] Calcd for C₁₉H₁₆ClN₅O 366.1116; Found 366.1118.

N-(2-Chlorophenyl)-2-(6-(1-methyl-1H-pyrazol-4-yl)-1H-pyrrolo[2,3-*b*]pyridin-1-yl)acetamide (**77**). General Procedure B was followed using **105** (48 mg, 0.15 mmol) and 1-methyl-4-(4,4,5,5-tetramethyl-1,3,2-dioxaborolan-2-yl)pyrazole (47 mg, 0.23 mmol). Column chromatography eluting with 0–40% EtOAc/DCM afforded **77** as a white solid (25 mg, 46%). ¹H NMR (300 MHz, DMSO-*d*₆) δ 9.87 (s, 1H), 8.24 (s, 1H), 8.02 (s, 1H), 7.95 (d, *J* = 8.1 Hz, 1H), 7.78 (dd, *J* = 8.1, 1.6 Hz, 1H), 7.56–7.47 (m, 2H), 7.41 (d, *J* = 8.1 Hz, 1H), 7.33 (td, *J* = 7.7, 1.5 Hz, 1H), 7.20 (td, *J* = 7.7, 1.6 Hz, 1H), 5.23 (s, 2H), 3.89 (s, 3H). ¹³C NMR (75 MHz, DMSO-*d*₆) δ 167.1, 147.2, 145.1, 136.9, 134.5, 129.6, 129.5, 129.2, 128.8, 127.5, 126.3, 125.8, 125.5, 123.6, 117.9, 112.4, 99.6, 46.9, 38.7. LCMS *m/z* 366.2 [M + H]. HRMS *m/z*: [M + H] Calcd for C₁₉H₁₆ClN₅O 366.1116; Found 366.1115.

2-(6-(1-Methyl-1H-pyrazol-4-yl)-1H-indol-1-yl)-N-(3,4,5-trimethoxyphenyl)acetamide (**78**). General Procedure F was followed using **106** (54 mg, 0.19 mmol) and 3,4-dimethoxyaniline (63 mg, 0.34 mmol). Column chromatography eluting with 50–100% EtOAc/DCM afforded **78** as a tan solid (18 mg, 22%). ¹H NMR (300 MHz, DMSO-*d*₆) δ 10.32 (s, 1H), 8.06 (s, 1H), 7.83 (s, 1H), 7.63 (s, 1H), 7.51 (d, *J* = 8.2 Hz, 1H), 7.32 (d, *J* = 3.1 Hz, 1H), 7.25 (dd, *J* = 8.2, 1.4 Hz, 1H), 6.99 (s, 2H), 6.42 (d, *J* = 3.1 Hz, 1H), 5.04 (s, 2H), 3.85 (s, 3H), 3.72 (s, 6H), 3.60 (s, 3H). ¹³C NMR (75 MHz, DMSO-*d*₆) δ 166.2, 152.7, 137.1, 135.8, 134.9, 133.5, 129.9, 127.2, 126.6, 125.9, 123.2, 120.6, 117.3, 105.9, 100.9, 96.8, 60.1, 55.6, 49.0, 38.6. LCMS *m/z* 421.2 [M + H]. HRMS *m/z*: [M + H] Calcd for C₂₃H₂₄N₄O₄ 421.187; Found 421.1876.

2-(3-Chloro-6-(1-methyl-1H-pyrazol-4-yl)-1H-indol-1-yl)-N-(3,4,5-trimethoxyphenyl)acetamide (**79**). General Procedure B was followed using **108** (74 mg, 0.16 mmol) and 1-methyl-4-(4,4,5,5-tetramethyl-1,3,2-dioxaborolan-2-yl)pyrazole (55 mg, 0.26 mmol). Column chromatography eluting with 50–100% EtOAc/DCM afforded **79** as a pale-purple solid (20 mg, 27%). ¹H NMR (300 MHz, DMSO-*d*₆) δ 10.33 (s, 1H), 8.11 (s, 1H), 7.88 (s, 1H), 7.73 (s, 1H), 7.52 (s, 1H), 7.47 (d, *J* = 8.2 Hz, 1H), 7.38 (dd, *J* = 8.2, 1.3 Hz, 1H), 6.99 (s, 2H), 5.06 (s, 2H), 3.86 (s, 3H), 3.72 (s, 6H), 3.61 (s, 3H). ¹³C NMR (75 MHz, DMSO-*d*₆) δ 165.9, 152.8, 136.5, 136.0, 134.8, 133.5, 127.5, 127.4, 126.6, 123.4, 122.7, 118.2, 117.7, 106.5, 103.1, 96.8, 60.1, 55.6, 48.9, 38.6. LCMS *m/z* 455.2 [M + H]. HRMS *m/z*: [M + H] Calcd for C₂₃H₂₃ClN₄O₄ 455.1481; Found 455.1480.

2-(5-Fluoro-6-(1-methyl-1H-pyrazol-4-yl)-1H-indol-1-yl)-N-(3,4,5-trimethoxyphenyl)acetamide (**80**). General Procedure C was

followed using **111** (57 mg, 0.22 mmol) and **109** (43 mg, 0.20 mmol). Column chromatography eluting with 0–5% MeOH/DCM afforded **80** as a beige solid (17 mg, 22%). ¹H NMR (300 MHz, DMSO-*d*₆) δ 10.31 (s, 1H), 8.05 (d, *J* = 2.7 Hz, 1H), 7.88 (s, 1H), 7.74 (d, *J* = 6.4 Hz, 1H), 7.43–7.32 (m, 2H), 6.98 (s, 2H), 6.43 (d, *J* = 3.1 Hz, 1H), 5.06 (s, 2H), 3.88 (s, 3H), 3.71 (s, 6H), 3.60 (s, 3H). ¹³C NMR (75 MHz, DMSO-*d*₆) δ 166.4, 152.9, 137.1 (d, *J* = 3.8 Hz), 135.0, 133.9, 133.8, 131.9, 129.1 (d, *J* = 8.2 Hz), 126.7 (d, *J* = 10.7 Hz), 117.0, 114.6, 114.4, 107.9 (d, *J* = 5.5 Hz), 105.8 (d, *J* = 24.6 Hz), 101.1 (d, *J* = 4.4 Hz), 97.1, 60.3, 55.9, 49.4. LCMS *m/z* 439.2 [M + H]. HRMS *m/z*: [M + H] Calcd for C₂₃H₂₃FN₄O₄ 439.1776; Found 439.1774.

2-(6-(1,3-Dimethyl-1H-pyrazol-4-yl)-1H-indol-1-yl)-N-(3,4,5-trimethoxyphenyl)acetamide (81). General Procedure B was followed using **112** (38 mg, 0.090 mmol) and 1,3-dimethyl-4-(4,4,5,5-tetramethyl-1,3,2-dioxaborolan-2-yl)pyrazole (30 mg, 0.14 mmol). Column chromatography eluting with 0–5% MeOH/DCM followed by reverse phase preparative HPLC eluting with a gradient of 5–75% MeCN/H₂O (including 0.1% formic acid) afforded **81** as a white solid (11 mg, 28%). ¹H NMR (300 MHz, DMSO-*d*₆) δ 10.34 (s, 1H), 7.78 (s, 1H), 7.55 (d, *J* = 8.1 Hz, 1H), 7.39 (s, 1H), 7.35 (d, *J* = 3.2 Hz, 1H), 7.09 (dd, *J* = 8.1, 1.4 Hz, 1H), 6.97 (s, 2H), 6.44 (dd, *J* = 3.1, 0.8 Hz, 1H), 5.03 (s, 2H), 3.77 (s, 3H), 3.71 (s, 6H), 3.60 (s, 3H), 2.27 (s, 3H). ¹³C NMR (75 MHz, DMSO-*d*₆) δ 166.2, 152.7, 143.8, 136.8, 134.8, 133.5, 130.1, 129.2, 126.7, 126.4, 120.9, 120.4, 119.2, 107.9, 100.7, 96.8, 60.1, 55.6, 49.2, 38.1, 13.1. LCMS *m/z* 435.2 [M + H]. HRMS *m/z*: [M + H] Calcd for C₂₄H₂₆N₄O₄ 435.2027; Found 435.2017.

2-(3-Chloro-5-fluoro-6-(1-methyl-1H-pyrazol-4-yl)-1H-indol-1-yl)-N-(3,4,5-trimethoxyphenyl)acetamide (82). General Procedure B was followed using **113** (47 mg, 0.10 mmol) and 1,3-dimethyl-4-(4,4,5,5-tetramethyl-1,3,2-dioxaborolan-2-yl)pyrazole (31 mg, 0.15 mmol). Column chromatography eluting with 0–5% MeOH/DCM followed by reverse phase preparative HPLC eluting with a gradient of 5–75% MeCN/H₂O (including 0.1% formic acid) afforded **82** as a white solid (8 mg, 17%). ¹H NMR (300 MHz, DMSO-*d*₆) δ 10.32 (s, 1H), 8.09 (d, *J* = 2.7 Hz, 1H), 7.91 (s, 1H), 7.86 (d, *J* = 6.2 Hz, 1H), 7.61 (s, 1H), 7.30 (d, *J* = 11.3 Hz, 1H), 6.97 (s, 2H), 5.07 (s, 2H), 3.88 (s, 3H), 3.71 (s, 6H), 3.60 (s, 3H). ¹³C NMR (75 MHz, DMSO-*d*₆) δ 165.8, 154.6 (d, *J* = 237.5 Hz), 152.7, 137.1 (d, *J* = 4.0 Hz), 134.8, 133.5, 133.0, 129.2 (d, *J* = 8.7 Hz), 128.5, 123.3 (d, *J* = 11.0 Hz), 116.3, 116.1 (d, *J* = 18.2 Hz), 108.9 (d, *J* = 5.3 Hz), 102.8 (d, *J* = 30.5 Hz), 102.7, 96.8, 60.1, 55.6, 49.1, 38.6. LCMS *m/z* 473.2 [M + H]. HRMS *m/z*: [M + H] Calcd for C₂₃H₂₂ClFN₄O₄ 473.1386; Found 473.1376.

2-(3-Chloro-6-(1,3-dimethyl-1H-pyrazol-4-yl)-1H-indol-1-yl)-N-(3,4,5-trimethoxyphenyl)acetamide (83). General Procedure B was followed using **113** (45 mg, 0.099 mmol) and 1,3-dimethyl-4-(4,4,5,5-tetramethyl-1,3,2-dioxaborolan-2-yl)pyrazole (33 mg, 0.15 mmol). Column chromatography eluting with 0–5% MeOH/DCM followed by reverse phase preparative HPLC eluting with a gradient of 5–75% MeCN/H₂O (including 0.1% formic acid) afforded **83** as a white solid (2 mg, 5%). ¹H NMR (300 MHz, DMSO-*d*₆) δ 10.36 (s, 1H), 7.83 (s, 1H), 7.58–7.42 (m, 3H), 7.22 (dd, *J* = 8.2, 1.4 Hz, 1H), 6.96 (s, 2H), 5.04 (s, 2H), 3.77 (s, 3H), 3.70 (s, 6H), 3.60 (s, 3H), 2.28 (s, 3H). LCMS *m/z* 469.2 [M + H]. HRMS *m/z*: [M + H] Calcd for C₂₄H₂₅ClN₄O₄ 469.1637; Found 469.1636.

2-(3-Chloro-6-(1,3-dimethyl-1H-pyrazol-4-yl)-5-fluoro-1H-indol-1-yl)-N-(3,4,5-trimethoxyphenyl)acetamide (84). General Procedure C was followed using **114** (50 mg, 0.19 mmol) and **109** (54 mg, 0.21 mmol), except that when the reaction was complete H₂O (~5 mL) was added and the precipitate was collected by vacuum filtration. The filter cake was washed with H₂O, dried and purified by reverse phase preparative HPLC eluting with a gradient of 5–75% MeCN/H₂O (including 0.1% formic acid) to afford **84** as a white solid (31 mg, 34%). ¹H NMR (300 MHz, DMSO-*d*₆) δ 10.34 (s, 1H), 7.77 (d, *J* = 2.0 Hz, 1H), 7.64 (s, 1H), 7.46 (d, *J* = 6.1 Hz, 1H), 7.32 (d, *J* = 10.4 Hz, 1H), 6.95 (s, 2H), 5.05 (s, 2H), 3.79 (s, 3H), 3.70 (s, 6H), 3.60 (s, 3H), 2.17 (s, 3H). ¹³C NMR (75 MHz, DMSO-*d*₆) δ 165.8, 154.9 (d, *J* = 236.0 Hz), 152.8, 145.2, 134.8, 133.7, 132.4, 131.0 (d, *J* = 4.4

Hz), 128.6, 123.9 (d, *J* = 10.7 Hz), 116.7 (d, *J* = 19.8 Hz), 113.9, 111.8 (d, *J* = 4.4 Hz), 102.8 (d, *J* = 23.5 Hz), 102.7 (d, *J* = 7.6 Hz), 96.9, 60.2, 55.7, 49.4, 38.3, 12.6 (d, *J* = 2.7 Hz). LCMS *m/z* 487.2 [M + H]. HRMS *m/z*: [M + H] Calcd for C₂₄H₂₄ClFN₄O₄ 487.1543; Found 487.1543.

2-[6-(5-Methyl-1,3,4-oxadiazol-2-yl)indol-1-yl]acetic Acid (85). A stirred solution of **86** (150 mg, 0.75 mmol) in DMF (3 mL) was chilled on an ice bath and sodium hydride (60.2 mg, 1.51 mmol) was added as a 60% dispersion in mineral oil all in one portion. The solution was stirred for 30 min before a solution of ethyl 2-bromoacetate (0.100 mL, 0.904 mmol) in DMF (3 mL) was added in a dropwise manner. The solution was then removed from the ice bath and stirred for an additional 16 h. The mixture was then diluted with H₂O (30 mL) and extracted with EtOAc (2 × 10 mL). The organic fractions were combined and washed with brine (10 mL) before being dried over MgSO₄, filtered and concentrated. The crude material (220 mg, 0.75 mmol) was then dissolved in THF (3 mL) and a solution of lithium hydroxide monohydrate (158 mg, 3.77 mmol) in H₂O (3 mL) was added. The mixture was stirred at 20 °C until a complete conversion was observed on LCMS. One M HCl (aq) was then added slowly to the mixture until pH < 4 was reached. The mixture was then diluted with EtOAc and the aqueous portion was separated. The organic portion was washed with brine, dried over MgSO₄, filtered and concentrated to afford **85** as a solid (187 mg, 97%). ¹H NMR (300 MHz, DMSO-*d*₆) δ 12.89 (s, 1H), 8.03 (s, 1H), 7.80–7.61 (m, 2H), 7.55 (d, *J* = 3.1 Hz, 1H), 6.58 (d, *J* = 3.1 Hz, 1H), 5.17 (s, 2H), 2.58 (s, 3H). ¹³C NMR (75 MHz, DMSO-*d*₆) δ 170.4, 165.3, 163.3, 136.1, 132.9, 130.7, 121.3, 117.4, 116.4, 108.7, 101.7, 47.3, 10.7. LCMS *m/z* 256.2 [M-H].

2-(1H-Indol-6-yl)-5-methyl-1,3,4-oxadiazole (86). To a stirring, heterogeneous, mixture of **87** (1.1 g, 6.4 mmol) in EtOH (8 mL) at 20 °C was added 1,1,1-triethoxyethane (1.3 mL, 7.1 mmol). The mixture was heated to reflux and stirred for 3 h. Upon completion it was allowed to cool to 20 °C and H₂O (20 mL) was added. The mixture was allowed to sit overnight at 20 °C, then cooled on an ice bath briefly before precipitate was collected by vacuum filtration and washed with H₂O (10 mL) to afford **86** as a beige solid (1.05 g, 82%). ¹H NMR (300 MHz, DMSO-*d*₆) δ 11.50 (s, 1H), 8.01 (d, *J* = 1.4 Hz, 1H), 7.72 (d, *J* = 8.3 Hz, 1H), 7.65–7.52 (m, 2H), 6.55 (t, *J* = 2.3 Hz, 1H), 2.58 (s, 3H). LCMS *m/z* 200.2 [M + H].

1H-Indole-6-carbohydrazide (87). To a stirring, heterogeneous mixture of 1H-indole-6-carboxylic acid (2.90 g, 18.0 mmol) and TCFH (5.99 g, 21.3 mmol) in MeCN (60 mL) at 20 °C was added 1-methylimidazole (3.30 mL, 54.3 mmol) and stirred for 20 min. The yellow mixture was poured into a stirring solution of hydrazine hydrate (2.6 mL, 54 mmol) in MeCN (30 mL) to give a white opaque mixture which was stirred a further 20 min. When reaction is complete by LCMS the mixture was concentrated to ~10 mL volume and then diluted with H₂O (~80 mL) and the solid was collected using vacuum filtration to give **87** as a white powder (2.28 g, 73%). ¹H NMR (300 MHz, DMSO-*d*₆) δ 11.40 (s, 1H), 9.65 (s, 1H), 7.93 (s, 1H), 7.69–7.35 (m, 3H), 6.47 (s, 1H), 4.46 (s, 2H). ¹³C NMR (75 MHz, DMSO-*d*₆) δ 167.1, 135.2, 129.7, 127.8, 126.1, 119.4, 117.6, 111.0, 101.2. LCMS *m/z* 176.2 [M + H].

N-(2-Chlorophenyl)-2-[6-(N-hydroxycarbamimidoyl)indol-1-yl]acetamide (88). A mixture of **89** (96 mg, 0.29 mmol) and hydroxylamine (150 μL, 2.29 mmol) in EtOH (1.5 mL) was heated at 60 °C for 16 h. The mixture was then diluted with H₂O (2 mL) the precipitate collected by vacuum filtration. Washing with H₂O and drying afforded **88** as a white solid (82 mg, 81%). ¹H NMR (300 MHz, DMSO-*d*₆) δ 9.74 (s, 1H), 9.46 (s, 1H), 7.82 (dd, *J* = 8.1, 1.6 Hz, 2H), 7.60–7.39 (m, 6H), 7.33 (td, *J* = 7.7, 1.6 Hz, 1H), 7.20 (td, *J* = 7.7, 1.7 Hz, 1H), 6.57–6.46 (m, 1H), 5.19 (s, 2H). LCMS *m/z* 343.2 [M + H].

N-(2-Chlorophenyl)-2-(6-cyanoindol-1-yl)acetamide (89). A stirring solution containing 1H-indole-6-carbonitrile (350 mg, 2.46 mmol) and **90** (662 mg, 3.23 mmol) in DMF (5 mL) was treated with Cs₂CO₃ (977 mg, 3.00 mmol) at 20 °C and stirred for 1 h before heating to 60 °C for 16 h. The mixture was then diluted with EtOAc (50 mL), washed with H₂O (3 × 40 mL), brine (40 mL), dried over

MgSO₄, filtered and concentrated. The residue was dissolved in MeOH (5 mL), cooled to 0 °C and the precipitate collected by vacuum filtration to afford **89** as a white solid (323 mg, 40%). ¹H NMR (300 MHz, DMSO-*d*₆) δ 9.92 (s, 1H), 8.11 (p, *J* = 0.8 Hz, 1H), 7.84–7.65 (m, 3H), 7.52 (dd, *J* = 8.0, 1.5 Hz, 1H), 7.45–7.28 (m, 2H), 7.20 (td, *J* = 7.7, 1.7 Hz, 1H), 6.64 (dd, *J* = 3.1, 0.9 Hz, 1H), 5.27 (s, 2H). LCMS *m/z* 310.2 [M + H].

2-Chloro-N-(2-chlorophenyl)acetamide (90). To a stirring solution of 2-chloroacetyl chloride (2.6 mL, 33 mmol) in DCM (100 mL) under N₂ atmosphere at 0 °C was added 2-chloroaniline (3.0 mL, 29 mmol) in a dropwise manner followed by DIPEA (6.0 mL, 34 mmol) in a dropwise manner. The mixture was stirred overnight at 20 °C and then diluted with H₂O (40 mL). The organics were separated and further washed with sat. aq. NaHCO₃ (20 mL) and brine (10 mL). Organics were then dried over MgSO₄, filtered and concentrated to dryness. The resulting material (6.66 g) was triturated with 1:1 EtOH/H₂O (~40 mL). Sonication was used to break up chunks of the material and the solid was collected by vacuum filtration where it was further washed with 1:1 EtOH/H₂O (10 mL). The filtrate was then concentrated and the trituration process repeated. The solid material was pooled to afford **90** as a dark brown solid (5.3 g, 90%). ¹H NMR (300 MHz, CDCl₃) δ 8.93 (s, 1H), 8.36 (dd, *J* = 8.3, 1.6 Hz, 1H), 7.40 (dd, *J* = 8.0, 1.5 Hz, 1H), 7.30 (ddd, *J* = 8.9, 7.6, 1.5 Hz, 1H), 7.10 (td, *J* = 7.7, 1.6 Hz, 1H), 4.23 (s, 2H). LCMS *m/z* 204.0 [M + H].

1-[2-(2-Chloroanilino)-2-oxo-ethyl]indole-6-carboxylic Acid (91). An oven-dried flask equipped with stir bar was charged with N₂, methyl 1H-indole-6-carboxylate (353 mg, 2.01 mmol) and DMF (10 mL). The stirring mixture was cooled on to 0 °C before treatment with sodium hydride (317 mg, 7.93 mmol). After 1 h, **90** (476 mg, 2.33 mmol) was added in a single portion and the mixture stirred for 16 h at which time LCMS indicated the presence of the desired free acid as the major product. The mixture was diluted with H₂O (15 mL) and washed using EtOAc (3 × 25 mL). The aqueous fraction was acidified to pH 1 using 1 M HCl to give a precipitate that was collected using vacuum filtration to afford **91** as a tan solid (306 mg, 46%). ¹H NMR (300 MHz, DMSO-*d*₆) δ 12.57 (s, 1H), 9.93 (s, 1H), 8.15 (d, *J* = 1.2 Hz, 1H), 7.74 (dd, *J* = 8.1, 1.6 Hz, 1H), 7.70–7.57 (m, 3H), 7.51 (dd, *J* = 8.0, 1.5 Hz, 1H), 7.32 (td, *J* = 7.7, 1.6 Hz, 1H), 7.20 (td, *J* = 7.7, 1.7 Hz, 1H), 6.57 (dd, *J* = 3.1, 0.9 Hz, 1H), 5.27 (s, 2H). LCMS *m/z* 329.2 [M + H].

2-(6-Bromoindol-1-yl)-N-(2-chlorophenyl)acetamide (92). A solution of 6-bromoindole (1.20 g, 6.12 mmol) in anhydrous DMF (40 mL) was prepared in a dry flask. The solution was cooled to 0 °C on an ice bath under an N₂ atmosphere and sodium hydride (0.61 g, 15 mmol) was added portion-wise. The mixture was stirred at 0 °C for 30 min before a solution of **90** (1.44 g, 7.04 mmol) in DMF (20 mL) was added slowly over approximately 2 min. The mixture was then removed from the ice bath and stirred for 16 h at 20 °C. The mixture was then diluted slowly with H₂O (~100 mL) and the precipitate was collected by vacuum filtration. The precipitate was washed with H₂O (50 mL) and a 2:1 mixture of H₂O/MeOH (20 mL). The material was then dried to afford **92** as a beige solid which was of sufficient purity (1.77 g, 80%). ¹H NMR (300 MHz, DMSO-*d*₆) δ 9.84 (s, 1H), 7.75 (dd, *J* = 6.1, 1.8 Hz, 2H), 7.57–7.48 (m, 2H), 7.43 (d, *J* = 3.2 Hz, 1H), 7.33 (td, *J* = 7.7, 1.5 Hz, 1H), 7.19 (ddd, *J* = 14.5, 8.1, 1.7 Hz, 2H), 6.50 (dd, *J* = 3.3, 0.9 Hz, 1H), 5.17 (s, 2H). LCMS *m/z* 365.2 [M + H].

Ethyl 2-(6-(1,3,4-oxadiazol-2-yl)-1H-indol-1-yl)acetate (93). A stirring mixture of 2-(1H-indol-6-yl)-1,3,4-oxadiazole (330 mg, 1.78 mmol) and K₂CO₃ (490 mg, 3.55 mmol) in DMF (9 mL) at 20 °C was treated with ethyl 2-bromoacetate (240 μL, 2.17 mmol). After 16 h the mixture was diluted with EtOAc (50 mL), washed with H₂O (2 × 50 mL) and brine (50 mL), dried over MgSO₄, filtered and concentrated. Column chromatography, eluting with 20–50% EtOAc/heptane afforded **93** as a white solid (418 mg, 86%). ¹H NMR (300 MHz, CDCl₃) δ 8.45 (s, 1H), 8.07 (s, 1H), 7.82 (dd, *J* = 8.3, 1.4 Hz, 1H), 7.75 (d, *J* = 8.3 Hz, 1H), 7.27 (s, 1H), 6.64 (dd, *J* = 3.1, 0.9 Hz, 1H), 4.93 (s, 2H), 4.25 (q, *J* = 7.1 Hz, 2H), 1.29 (t, *J* = 7.1 Hz, 3H). ¹³C NMR (75 MHz, CDCl₃) δ 168.2, 166.1, 152.4,

136.4, 131.8, 131.8, 122.0, 118.8, 117.0, 108.8, 103.3, 62.1, 48.0, 14.3. LCMS *m/z* 272.2 [M + H].

N-(2-Chlorophenyl)-2-[6-(hydrazinecarbonyl)indol-1-yl]-acetamide (94). A stirring mixture containing **91** (150 mg, 0.456 mmol) and 1-methylimidazole (70 μL, 1.2 mmol) in MeCN (2 mL) at 20 °C was treated with TCFH (155 mg, 0.552 mmol). After 1 h the mixture was added to a stirred solution of hydrazine monohydrate (110 μL, 2.3 mmol) in MeCN (2 mL) at 20 °C. After 1 h the mixture was diluted with H₂O (5 mL) and left to stand overnight. The precipitate was collected by vacuum filtration, washed with H₂O (3 × 1 mL) and dried to afford **94** as a white solid (146 mg, 93%). ¹H NMR (300 MHz, DMSO-*d*₆) δ 9.82 (s, 1H), 9.63 (s, 1H), 8.04 (s, 1H), 7.79 (dd, *J* = 8.1, 1.6 Hz, 1H), 7.64–7.46 (m, 4H), 7.32 (td, *J* = 7.8, 1.5 Hz, 1H), 7.19 (td, *J* = 7.7, 1.6 Hz, 1H), 6.53 (d, *J* = 3.0 Hz, 1H), 5.22 (s, 2H), 4.47 (s, 2H). LCMS *m/z* 343.2 [M + H].

2-(1H-Indol-6-yl)-5-isopropyl-1,3,4-oxadiazole (95). A stirring mixture of **87** (176 mg, 1.00 mmol), 1,1,1-trimethoxy-2-methylpropane (320 μL, 2.01 mmol) and NH₄Cl (13 mg, 0.24 mmol) in EtOH (10 mL) was heated at 90 °C for 2 h at which point the mixture was cooled to 20 °C and concentrated under reduced pressure. The solid residue was then diluted with H₂O (~10–15 mL) and stirred at 20 °C before collection by vacuum filtration. Washing with H₂O and drying afforded **95** as a white solid (209 mg, 92%). ¹H NMR (300 MHz, DMSO-*d*₆) δ 11.47 (s, 1H), 8.03 (s, 1H), 7.72 (d, *J* = 8.3 Hz, 1H), 7.67–7.48 (m, 2H), 6.55 (s, 1H), 3.31–3.20 (m, 1H), 1.38 (d, *J* = 6.9 Hz, 6H). ¹³C NMR (75 MHz, DMSO-*d*₆) δ 169.9, 165.1, 135.4, 130.2, 128.6, 120.9, 117.0, 116.0, 110.0, 101.7, 25.7, 19.8. LCMS *m/z* 228.2 [M + H].

6-(1-Methyl-1H-pyrazol-4-yl)-1H-indole (96). A flask equipped with stir bar and fitted with reflux condenser was charged with 6-bromoindole (605 mg, 3.09 mmol), 1-methyl-4-(4,4,5,5-tetramethyl-1,3,2-dioxaborolan-2-yl)pyrazole (1.04 g, 4.98 mmol) and K₂CO₃ (4.66 g, 33.7 mmol). The solids were suspended in DMF (5.4 mL) and H₂O (0.6 mL) before sparging with N₂ for 15 min. The mixture was then treated with Pd(PPh₃)₄ (173 mg, 0.150 mmol) at 90 °C for 4 h before the mixture was cooled to 20 °C. The resultant mixture was diluted with H₂O (15 mL) and the solid was collected using vacuum filtration. Washing with H₂O gives **96** as a pale yellow solid which contains approximately 18% triphenylphosphine oxide by mass (720 mg, 96% yield). LCMS *m/z* 198.2 [M + H].

2-(6-Bromo-2-methyl-1H-indol-1-yl)-N-(2-chlorophenyl)-acetamide (97). General Procedure H: To a stirred solution of 6-bromo-2-methyl-1H-indole (50 mg, 0.24 mmol) in DMF (1 mL) and chilled on an ice bath was added sodium hydride (28.6 mg, 0.714 mmol) as a 60% dispersion in mineral oil all in one portion. The solution was stirred for 30 min before a solution of **90** (55.9 mg, 0.274 mmol) in DMF (1 mL) was added in a dropwise manner. The solution was then removed from the ice bath and stirred for an additional 16 h. H₂O (5 mL) was then added and the precipitate was collected by vacuum filtration. Washing with H₂O and drying afforded **97** as a beige solid (54 mg, 60%). LCMS *m/z* 377.2 [M + H].

2-(6-Bromo-3-methyl-1H-indol-1-yl)-Nm-(2-chlorophenyl)-acetamide (98). General Procedure H was followed using 6-bromo-3-methyl-1H-indole (50 mg, 0.24 mmol) to afford **98** as an off-white solid (62 mg, 69%). LCMS *m/z* 377.2 [M + H].

2-(6-Bromo-3-fluoro-1H-indol-1-yl)-N-(2-chlorophenyl)-acetamide (99). A solution of 6-bromo-3-fluoro-1H-indole (100 mg, 0.467 mmol) in anhydrous DMF (2 mL) was degassed, filled with N₂ and cooled to 0 °C. Sodium hydride (46.7 mg, 1.17 mmol) was added slowly and the mixture was stirred at 0 °C for 0.5 h. Then a solution of **90** (100 mg, 0.51 mmol) in DMF (1 mL) was added dropwise and left to react at 20 °C for 16 h. The mixture was slowly diluted with H₂O (15 mL), no precipitate was observed, and the aq. fraction was extracted with EtOAc (2 × 10 mL). The combined organic layers were washed with brine, dried over MgSO₄, and concentrated. Column chromatography, eluting with 0–40% EtOAc/heptane, afforded **99** as a light pink solid (60 mg, 32%). ¹H NMR (300 MHz, DMSO-*d*₆) δ 9.84 (s, 1H), 7.82 (s, 1H), 7.74 (dd, *J* = 8.1, 1.6 Hz, 1H), 7.54–7.46 (m, 3H), 7.37–7.30 (m, 1H), 7.26–7.16 (m, 2H), 5.11 (s, 2H). LCMS *m/z* 383.0 [M + H].

2-(6-Bromo-3-cyano-1H-indol-1-yl)-N-(2-chlorophenyl)-acetamide (**100**). To a stirred solution of 6-bromo-1H-indole-3-carbonitrile (120 mg, 0.54 mmol) in DMF (2 mL) chilled on an ice bath was added sodium hydride (65 mg, 1.6 mmol) as a 60% dispersion in mineral oil all in one portion. The solution was allowed to warm to 20 °C over 30 min before being heated to 70 °C. A solution of **90** (127 mg, 0.624 mmol) in DMF (2 mL) was then added in a dropwise manner and stirred at 70 °C for 3 h. The mixture was allowed to cool to 20 °C and diluted with H₂O (10 mL). The precipitate was collected by vacuum filtration, washed with H₂O and dried to afford **100** as a beige solid with sufficient purity to use directly in the next step (71 mg, 34%). LCMS *m/z* 388.0 [M + H].

2-(6-Bromo-1H-indazol-1-yl)-N-(2-chlorophenyl)acetamide (**101**). General Procedure H was followed using 6-bromo-1H-indazole (118 mg, 0.60 mmol). Column chromatography, eluting with 0–5% MeOH/DCM, afforded **101** as well as its regioisomer 2-(6-bromo-2H-indazol-2-yl)-N-(2-chlorophenyl)acetamide as a ~1:1 mixture which was carried on to the next step (154 mg, 73%). ¹H NMR (300 MHz, DMSO-*d*₆) δ 10.04 (s, 1H), 9.92 (s, 1H), 8.50 (d, *J* = 1.0 Hz, 1H), 8.22–8.11 (m, 1H), 8.05 (s, 1H), 7.92–7.84 (m, 1H), 7.81–7.70 (m, 4H), 7.52 (dt, *J* = 8.0, 1.6 Hz, 2H), 7.38–7.26 (m, 3H), 7.25–7.11 (m, 3H), 5.47 (s, 2H), 5.44 (s, 2H). LCMS *m/z* 366.0 [M + H].

2-(6-Bromo-1H-benzo[d]imidazol-1-yl)-N-(2-chlorophenyl)-acetamide (**102**). General Procedure H was followed using 6-bromo-1H-benzimidazole (50 mg, 0.25 mmol) to afford **102** as a beige solid. (57 mg, 62%). ¹H NMR (300 MHz, DMSO-*d*₆) δ 10.11 (s, 1H), 8.37 (s, 1H), 7.90 (dd, *J* = 8.1, 1.9 Hz, 1H), 7.73 (ddd, *J* = 8.1, 4.6, 1.7 Hz, 1H), 7.68–7.48 (m, 2H), 7.48–7.28 (m, 2H), 7.26–7.17 (m, 1H), 5.31 (s, 2H). LCMS *m/z* 366.0 [M + H].

2-(6-Bromo-1H-pyrrolo[3,2-*b*]pyridin-1-yl)-N-(2-chlorophenyl)-acetamide (**103**). General Procedure H was followed using 6-bromo-1H-pyrrolo[3,2-*b*]pyridine (50 mg, 0.25 mmol) to afford **103** as a beige solid. (46 mg, 50%). ¹H NMR (300 MHz, DMSO-*d*₆) δ 9.92 (s, 1H), 8.44 (d, *J* = 2.0 Hz, 1H), 8.31 (dd, *J* = 2.0, 0.9 Hz, 1H), 7.81–7.70 (m, 2H), 7.52 (dd, *J* = 8.0, 1.5 Hz, 1H), 7.32 (td, *J* = 7.7, 1.5 Hz, 1H), 7.20 (td, *J* = 7.7, 1.7 Hz, 1H), 6.65 (dd, *J* = 3.3, 0.9 Hz, 1H), 5.23 (s, 2H). LCMS *m/z* 366.0 [M + H].

2-(6-Chloro-1H-pyrrolo[3,2-*c*]pyridin-1-yl)-N-(2-chlorophenyl)-acetamide (**104**). General Procedure H was followed using 6-bromo-1H-pyrrolo[3,2-*b*]pyridine (50 mg, 0.25 mmol) to afford **104** as a brown solid. (49 mg, 60%). ¹H NMR (300 MHz, DMSO-*d*₆) δ 9.93 (s, 1H), 8.63 (s, 1H), 7.93–7.42 (m, 4H), 7.26 (dt, *J* = 36.4, 7.4 Hz, 2H), 6.67 (s, 1H), 5.22 (s, 2H). LCMS *m/z* 320.0 [M + H].

2-(6-Chloro-1H-pyrrolo[2,3-*b*]pyridin-1-yl)-N-(2-chlorophenyl)-acetamide (**105**). General Procedure H was followed using 6-bromo-1H-pyrrolo[3,2-*b*]pyridine (50 mg, 0.25 mmol). Column chromatography, eluting with 0–20% EtOAc/DCM afforded **105** as a beige solid of approximately 60% purity which was carried on to the next step (61 mg, 42%). ¹H NMR (300 MHz, DMSO-*d*₆) δ 9.94 (s, 1H), 8.05 (d, *J* = 8.2 Hz, 1H), 7.74 (dd, *J* = 8.1, 1.6 Hz, 1H), 7.60 (d, *J* = 3.5 Hz, 1H), 7.57–7.46 (m, 2H), 7.32 (td, *J* = 7.8, 1.5 Hz, 1H), 7.17 (d, *J* = 8.2 Hz, 1H), 6.56 (d, *J* = 3.5 Hz, 1H), 5.21 (s, 2H). LCMS *m/z* 320.2 [M + H].

Ethyl 2-[6-(5-methyl-1,3,4-oxadiazol-2-yl)indol-1-yl]acetate (**106**). To a stirred solution of **86** (359 mg, 1.80 mmol) in DMF (10 mL) was added ethyl 2-bromoacetate (0.24 mL, 2.2 mmol) and Cs₂CO₃ (704 mg, 2.2 mmol). The solution was stirred at 90 °C for 5 h before an extra portion of ethyl 2-bromoacetate (0.060 mL, 0.54 mmol) was added. The mixture was stirred an additional 16 h before being diluted with EtOAc (50 mL) and washed with H₂O (3 × 40 mL) and brine (40 mL), dried over MgSO₄, filtered and concentrated to afford **106** in sufficient purity to be used in the next step (451 mg, 88%). ¹H NMR (300 MHz, CDCl₃) δ 8.00 (q, *J* = 0.7 Hz, 1H), 7.74 (qd, *J* = 8.3, 1.1 Hz, 2H), 7.24 (d, *J* = 3.2 Hz, 1H), 6.62 (dd, *J* = 3.2, 0.9 Hz, 1H), 4.91 (s, 2H), 4.23 (q, *J* = 7.1 Hz, 2H), 2.62 (s, 3H), 1.28 (t, *J* = 7.1 Hz, 4H). LCMS *m/z* 286.2 [M + H].

2-Bromo-N-(2-chlorophenyl)propanamide (**107**). To a stirring solution of 2-bromopropanoyl bromide (0.34 mL, 3.3 mmol) in DCM (15 mL) under N₂ at 0 °C was added 2-chloroaniline (0.30 mL, 2.9

mmol) in a dropwise manner followed by DIPEA (0.60 mL, 3.4 mmol) in a dropwise manner. The mixture was stirred for 4 h at 20 °C and then diluted with H₂O (20 mL). The organics were separated and further washed with H₂O (20 mL) and brine (10 mL). Organics were then dried over MgSO₄, filtered and concentrated to afford **107** as a brown solid (590 mg, 79%). ¹H NMR (300 MHz, CDCl₃) δ 8.69 (s, 1H), 8.34 (dd, *J* = 8.3, 1.5 Hz, 1H), 7.40 (dd, *J* = 8.0, 1.5 Hz, 1H), 7.34–7.26 (m, 1H), 7.09 (td, *J* = 7.7, 1.6 Hz, 1H), 4.60 (q, *J* = 7.1 Hz, 1H), 1.99 (d, *J* = 7.0 Hz, 3H). LCMS *m/z* 264.2 [M + H].

2-(6-Bromo-3-chloro-1H-indol-1-yl)-N-(3,4,5-trimethoxyphenyl)-acetamide (**108**). General Procedure H was followed using **110** (75 mg, 0.33 mmol) and **109** (93 mg, 0.36 mmol) to afford **108** as a beige solid (108 mg, 73%). ¹H NMR (300 MHz, DMSO-*d*₆) δ 10.31 (s, 1H), 7.84 (d, *J* = 1.6 Hz, 1H), 7.62 (s, 1H), 7.45 (t, *J* = 8.4 Hz, 1H), 7.29 (dd, *J* = 8.5, 1.6 Hz, 1H), 6.97 (s, 2H), 5.07 (s, 2H), 3.72 (s, 6H), 3.61 (s, 3H). LCMS *m/z* 454.8 [M + H].

2-Chloro-N-(3,4,5-trimethoxyphenyl)acetamide (**109**). To a stirring solution of 2-chloroacetyl chloride (1.4 mL, 17 mmol) in DCM (100 mL) under N₂ at 0 °C was slowly added 3,4,5-trimethoxyaniline (2.3 mL, 15 mmol) followed by DIPEA (3.2 mL, 18 mmol) in a dropwise manner. The mixture was stirred overnight and diluted with H₂O (20 mL). The organics were separated and further washed with H₂O (20 mL) and brine (10 mL). Organics were then dried over MgSO₄, filtered and concentrated to afford **109** as a brown solid (3.76 g, 97%). ¹H NMR (300 MHz, CDCl₃) δ 8.19 (s, 1H), 6.84 (s, 2H), 4.18 (s, 2H), 3.85 (s, 6H), 3.82 (s, 3H). LCMS *m/z* 260.2 [M + H].

6-Bromo-3-chloro-1H-indole (**110**). To a stirred solution of 6-bromo-1H-indole (314 mg, 1.60 mmol) in anhydrous 1,4-dioxane (16 mL) at 20 °C was added 1,3-dichloro-5,5-dimethyl-imidazolidine-2,4-dione (173 mg, 0.880 mmol). The solution was stirred at 20 °C under an N₂ atmosphere for 4 h and then poured into sat. aq. NaHCO₃ (30 mL) and extracted with EtOAc (2 × 20 mL). The organic fractions were combined and washed with brine (10 mL) before being dried over MgSO₄, filtered and concentrated. Column chromatography eluting with 0–10% EtOAc/heptane afforded **110** as a yellow solid (282 mg, 76%). ¹H NMR (300 MHz, CDCl₃) δ 8.04 (s, 1H), 7.60–7.41 (m, 2H), 7.30 (dd, *J* = 8.5, 1.6 Hz, 1H), 7.15 (s, 1H). LCMS *m/z* 230.0 [M-H].

5-Fluoro-6-(1-methyl-1H-pyrazol-4-yl)-1H-indole (**111**). 6-Bromo-5-fluoro-1H-indole (130 mg, 0.60 mmol) and 1-methyl-4-(4,4,5,5-tetramethyl-1,3,2-dioxaborolan-2-yl)pyrazole (187 mg, 0.900 mmol) were dissolved in DMF (1.8 mL). H₂O (0.2 mL) and K₂CO₃ (249 mg, 1.80 mmol) were added and the mixture was sparged with a stream of N₂ for 5 min. Pd(PPh₃)₄ (35 mg, 0.030 mmol) was then added and the mixture sealed under N₂ atmosphere and stirred at 90 °C for 18 h. The mixture was allowed to cool to 20 °C and H₂O was added. The precipitate was collected by vacuum filtration and washed further with H₂O to afford **111** as an orange solid (78 mg, 60%). ¹H NMR (300 MHz, DMSO-*d*₆) δ 11.12 (s, 1H), 8.04 (d, *J* = 2.6 Hz, 1H), 7.83 (dd, *J* = 1.7, 0.8 Hz, 1H), 7.58 (d, *J* = 6.5 Hz, 1H), 7.41–7.29 (m, 2H), 6.39 (ddd, *J* = 3.0, 1.9, 0.9 Hz, 1H), 3.89 (s, 3H). LCMS *m/z* 216.2 [M + H].

2-(6-Bromo-1H-indol-1-yl)-N-(3,4,5-trimethoxyphenyl)-acetamide (**112**). General Procedure H was followed using 6-bromo-1H-indole (147 mg, 0.750 mmol) and **109** (214 mg, 0.825 mmol) to afford **112** as a beige solid (263 mg, 84%). ¹H NMR (300 MHz, DMSO-*d*₆) δ 10.36 (s, 1H), 7.71 (d, *J* = 1.7 Hz, 1H), 7.52 (d, *J* = 8.4 Hz, 1H), 7.40 (d, *J* = 3.3 Hz, 1H), 7.16 (dd, *J* = 8.4, 1.7 Hz, 1H), 6.98 (s, 2H), 6.49 (d, *J* = 3.1 Hz, 1H), 5.05 (s, 2H), 3.72 (s, 6H), 3.61 (s, 3H). LCMS *m/z* 419.0 [M + H].

2-(6-Bromo-3-chloro-5-fluoro-1H-indol-1-yl)-N-(3,4,5-trimethoxyphenyl)acetamide (**113**). General Procedure H was followed using **115** (345 mg, 1.33 mmol) and **109** (300 mg, 1.21 mmol) to afford **113** as a pink solid (250 mg, 44%). ¹H NMR (300 MHz, DMSO-*d*₆) δ 10.29 (s, 1H), 7.99 (d, *J* = 5.7 Hz, 1H), 7.71 (s, 1H), 7.46 (d, *J* = 9.0 Hz, 1H), 6.96 (s, 2H), 5.08 (s, 2H), 3.71 (s, 6H), 3.61 (s, 3H). LCMS *m/z* 473.0 [M + H].

3-Chloro-6-(1,3-dimethyl-1H-pyrazol-4-yl)-5-fluoro-1H-indole (**114**). General Procedure B was followed using **115** (100 mg, 0.402

mmol) and 1,3-dimethyl-4-(4,4,5,5-tetramethyl-1,3,2-dioxaborolan-2-yl)pyrazole (134 mg, 0.604 mmol). Column chromatography eluting with 0–20% EtOAc/DCM afforded **114** as a beige solid (65 mg, 61%). ¹H NMR (300 MHz, DMSO-*d*₆) δ 11.41 (s, 1H), 7.79 (d, *J* = 2.1 Hz, 1H), 7.58 (d, *J* = 2.6 Hz, 1H), 7.38 (d, *J* = 6.4 Hz, 1H), 7.27 (d, *J* = 10.7 Hz, 1H), 3.81 (s, 3H), 2.21 (s, 3H). LCMS *m/z* 264.2 [M + H].

6-Bromo-3-chloro-5-fluoro-1H-indole (115). To a stirred solution of 6-bromo-5-fluoro-1H-indole (1.00 g, 4.67 mmol) in anhydrous 1,4-dioxane (30 mL) at 20 °C was added 1,3-dichloro-5,5-dimethyl-imidazolidine-2,4-dione (506 mg, 2.57 mmol). The solution was stirred at 20 °C under an N₂ atmosphere for 4 h and then poured into sat. aq. NaHCO₃ (30 mL) and extracted with EtOAc (2 × 30 mL). The organic fractions were combined and washed with brine (20 mL) before being dried over MgSO₄, filtered and concentrated. Column chromatography eluting with 0–10% EtOAc/heptane) afforded **115** as a yellow solid (887 mg, 76%). ¹H NMR (300 MHz, DMSO-*d*₆) δ 11.57 (s, 1H), 7.73 (d, *J* = 5.8 Hz, 1H), 7.65 (s, 1H), 7.40 (d, *J* = 9.1 Hz, 1H). LCMS *m/z* 248.0 [M-H].

P. falciparum 3D7 Asexual Stage (72 h) LDH Assay. This is a platform assay conducted by the Screening Facility at the Walter and Eliza Hall Institute that precisely adheres to a previously described protocol.¹⁵

Human HepG2 Cell Viability Assay. This is a platform assay conducted by the Screening Facility at the Walter and Eliza Hall Institute that precisely adheres to a previously described protocol.¹⁵

In Vitro ADME Assays. Liver microsome stability, liver hepatocyte stability, aqueous solubility (PBS at pH 7.4), and eLogD were calculated using platform assays conducted at TCG Life Sciences adhering precisely to previously described protocols.¹¹

Parasite Culture and Staining. Unless otherwise stated, all *P. falciparum* parasite strains were cultured in human red blood cells (RBCs) (Australian Red Cross Life Blood, blood-group O+) at 4% hematocrit in RPMI-GlutaMAX medium supplemented with 10% AlbuMAX (herein as referred to as complete RPMI). Cultures were incubated at 37 °C in enclosed chambers following gassing with 1% O₂ and 5% CO₂ in 94% N₂. To monitor the parasitemia and parasite stages, thin blood smears were made, fixed in 100% methanol, and stained with Giemsa. Stained blood smears were then visualized under an Eclipse E600 microscope (Nikon) at 1000× objective. To prevent parasite overgrowth, cultures were diluted with complete RPMI to achieve a parasitemia of 0.2% to 0.5% every 2–3 days.

W454 Resistance Selection. *P. falciparum* 3D7 parasites were adjusted to 2% parasitemia and 4% hematocrit in three 10 mL dishes. All 3 dishes were treated with an increasing sublethal concentration of W454 (**5**) starting with 1.2 μM (~2 × EC₅₀). Complete RPMI media and W454 (**5**) were replaced daily, and parasites were observed by microscopy. Once parasites were observed to have died, W454 (**5**) was removed, and cultures were maintained in complete RPMI media without compound. When the population recovered, W454 (**5**) was added to the next increasing EC₅₀ concentration. Upon reaching 6 × EC₅₀, the EC₅₀ of W454-selected parasite lines was assessed using lactate dehydrogenase (LDH) growth assay (described below) to determine the shift in EC₅₀.

Asexual Stage *P. falciparum* LDH Growth Assay. This assay format was used to evaluate compounds against PfATP4 drug-resistant parasites. Ring-stage *P. falciparum* parasites were obtained via sorbitol synchronization one cycle of growth before assay setup. A nine-point serial dilution of desired compound was performed with a final hematocrit and parasitemia of 2% and 0.5%, respectively and plates were incubated at 37 °C for 72 h. To evaluate LDH activity, Malstat reagent mix (1 M Tris (pH 9.0), 1.24 g of sodium L-lactate, 500 μL of 20% Triton X, and 25 mg of APAD was dissolved in 50 mL of distilled water) was added to Nitroblue tetrazolium (2 mg/mL) and phenazine ethosulfate (0.1 mg/mL) at a ratio of 10:1:1. Parasite culture was resuspended and 30 μL was added to 75 μL of Malstat reagent and incubated for 30 to 40 min. Absorbance was measured using a ClarioStar Microplate reader at 650 nm. Values were plotted using a 4-parameter log dose, nonlinear regression analysis with a sigmoidal dose–response (variable slope) curve fit in GraphPad Prism

(version 10.1.0) to generate compound curve and half-maximal effective concentration (EC₅₀) values.

WEHI-454 Resistant Strain Genomic Library Preparation. This was performed as previously described.¹⁵

Whole Genome Sequencing. The pooled library was sequenced on a NextSeq 2000 instrument using the P2 300 cycle kit (Illumina) as per the manufacturer's instruction. Samples were aligned to the reference PlasmDB-54_Pfalciparum3D7 using BWA MEM with default settings. Sequences from the resistant genome were compared with 3D7 reference strains. Sequences were filtered using Picard Mark Duplicates and quality was confirmed using the fastQC program. Structural variant calling was done with the GRIDSS package. Small variant calling was done with bcftools. Calls were filtered by quality score GQ > 50. Indels of 6 or more nucleotides consisting of A and T only were removed, as were highly repetitive indels and events in hypervariable regions. Variants present in the comparison samples were removed, and the remaining variants were filtered to those in 2 or more of the 6 samples. Filtering to variants in gene regions excludes genes labeled as PfEMP1, Rifin, Stevor, and pseudogene. The data for this study have been deposited in the European Nucleotide Archive (ENA) at EMBL-EBI under accession number, PRJEB81781. (<https://www.ebi.ac.uk/ena/browser/view/PRJEB81781>).

PfATP4 Homology Model and Docking. The PfATP4 homology model was constructed from the rabbit sarcoendoplasmic reticulum calcium ATPase (SERCA) crystal structure (PDB 2C88),²⁷ as previously described.^{5,11} CLC Drug Discovery Workbench software (version 2.5.1) was used to dock WJM664 (**82**) to the homology model of PfATP4. The input ligand **82** was built using a ligand designer, and the ligand binding site was centralized to the intramembrane ligand binding site of PfATP4. The ligand **82** was docked using minimization of flexible ligand conformations while maintaining a rigid protein structure. The relative predicted binding location of **82** from the docking was observed using the CLC Drug Discovery visualization tool. The structural data were then exported and visualized using the PyMol Molecular Graphics System (version 2.0).

Minimum Inoculum of Resistance Assay. *P. falciparum* asexual blood stage (ABS) parasites were cultured at 3% hematocrit in human O⁺ RBCs in RPMI-1640 media, supplemented with 25 mM HEPES, 50 mg/L hypoxanthine, 2 mM L-glutamine, 0.21% sodium bicarbonate, 0.5% (wt/vol) AlbuMAXII (Invitrogen) and 10 μg/mL gentamycin, in modular incubator chambers (Billups-Rothenberg) at 5% O₂, 5% CO₂ and 90% N₂ at 37 °C. Dd2 parasites were obtained from T. Wellems (NIAID, NIH). Dd2-B2 is a genetically homogeneous line that was cloned from Dd2 by limiting dilution in the Fidock lab. Dd2-Polδ is a line edited in the Fidock Lab to have a hypermutable polymerase.⁴² To define the EC₅₀ of ABS parasites, we exposed Dd2-B2 and Dd2-Polδ ring-stage cultures at 0.3% parasitemia and 1% hematocrit for 72 h to a range of ten drug concentrations that were 2-fold serially diluted in duplicates along with drug-free controls. Parasite survival was assessed by flow cytometry on an iQue flow cytometer (Sartorius) using SYBR Green and MitoTracker Deep Red FM (Life Technologies) as nuclear stain and vital dyes, respectively. For the initial MIR, one single-step selection was set up using 3.3 × 10⁶ Dd2-B2 parasites in each well of a 24 well plate at a starting concentration of 3 × IC₉₀ (89 nM). We observed parasite clearance over the first 5 days. This selection had a consistent drug pressure of 3 × IC₉₀ over 42 days, and cultures were screened three times weekly by flow cytometry and smearing. Wells are considered positive for recrudescence when the overall parasitemia reaches 0.3% and parasites are seen on a blood smear. No recrudescence was observed over the course of this selection. Two higher inoculum selections were then set up to determine the MIR. This included two single-step selections, the first using 8 × 10⁷ Dd2-B2 parasites in three flasks at 3% hematocrit (HCT) each for a total of 2.4 × 10⁸ parasites at a starting concentration of 3 × IC₉₀ (89 nM). The second was set up in three flasks at 3.3 × 10⁸ parasitemia 5% HCT in each flask, for a total of 9.9 × 10⁸ parasites. We observed parasite clearance over the first 5 days. Both these selections had a consistent drug pressure of 3 × IC₉₀ over 40 days, and cultures were screened three times weekly by flow

cytometry and smearing. Wells and flasks are considered positive for recrudescence when the overall parasitemia reaches 0.3% and parasites are seen on a blood smear. No flasks recrudescenced for the lower inoculum ($8 \times 10^7 \times 3$) flask selection. For the higher inoculum flask selection ($3.3 \times 10^8 \times 3$), Flask F1 recrudescenced on day 13 and F2 recrudescenced on day 15. IC_{50} and IC_{90} values of the recrudescence parasites using the above methods.

Whole Genome Sequencing on MIR Recrudescence Parasites. Whole-genome sequencing was performed using an Illumina DNA prep kit with Nextera DNA CD Indexes (Illumina, San Diego, CA) and multiplexed on a MiSeq (MiSeq Reagent Kit V3 600, Illumina, San Diego, CA) to generate 300 bp paired-end reads. Sequences were aligned to the Pf 3D7 reference genome (PlasmoDB-48_Pfalciparum3D7; <https://plasmodb.org/plasmo/app/downloads/release-48/Pfalciparum3D7/fasta/>) using the Burrows-Wheeler Alignment (BWA version 0.7.17). PCR duplicates and unmapped reads were filtered using Samtools (version 1.13) and Picard MarkDuplicates (GATK version 4.2.2). Base quality scores were recalibrated using the GATK BaseRecalibrator (GATK version 4.2.2). The GATK HaplotypeCaller (GATK version 4.2.2) was used to identify all possible single-nucleotide variants (SNVs) in test parasite lines filtered based on quality scores (variant quality as a function of depth $QD > 1.5$, mapping quality >40 , min base quality score >18 , read depth >5) to obtain high-quality single-nucleotide polymorphisms (SNPs) that were annotated using SnpEff version 4.3t. BIC-Seq version 1.1.2 was used to discover copy number variants (CNVs) against the parental strain using the Bayesian statistical model. SNPs and CNVs were visually inspected and confirmed using the Integrative Genome Viewer (IGV). The data for this study have been deposited in the European Nucleotide Archive (ENA) at EMBL-EBI under accession number, PRJEB81672 (<https://www.ebi.ac.uk/ena/browser/view/PRJEB81672>).

Antimalarial Resistome Barcode Sequencing. The parasite pool consists of 47 barcoded lines covering both Dd2 and 3D7 strains, including wildtype lines for both (Table S10). Each line was CRISPR edited to insert a short 101 bp barcode cassette into the nonessential *pfp* locus.^{31,51} Throughout the assay, parasite growth was monitored by flow cytometry (Cytotflex, Beckman Coulter). Parasites were stained using $1 \times$ SYBR green/200 nM Mitotracker Deep Red for 25 min, 37 °C, and then diluted 5-fold with PBS. Adjustments to parasitemia during the assay were made to maintain the culture in a healthy range (0.3–5% parasitemia). On day 1 of the assay, the barcoded pool was adjusted to a starting parasitemia of 1% of predominantly ring stage parasites and dispensed into 24 well plates in duplicate 1 mL cultures. The pool was exposed to $3 \times IC_{50}$ of W452 over 14 days. On day 14, the cultures were harvested, and the RBCs were lysed by saponin (0.05%). Parasite pellets were collected by centrifugation (3000 rpm, 5 min) and washed twice with PBS, before resuspending in $\sim 30 \mu\text{L}$ of PBS and freezing at -20°C . Barcode amplification and indexing were performed essentially as described,³¹ with the barcode PCR performed directly on $5 \mu\text{L}$ of parasite pellet. PCR products were indexed via a second PCR and 25 ng of each sample was combined before diluting to 4 nM for Illumina sequencing. Barcode counts were further analyzed in R using DESeq2,⁵² an R package for RNAseq analysis to determine differentially represented barcodes, with significance testing performed using a Wald test. Differentially represented barcodes were determined as having a Log2 fold change (LFC) > 2.5 and $p < 0.001$.

Metabolomic Analysis. The metabolite extraction protocol was performed as described elsewhere,⁵³ with minor modifications. Briefly, *P. falciparum* 3D7 parasites synchronized to the mid trophozoite stage were magnet purified to achieve a parasitemia of $>90\%$ and hematocrit of 0.5%. After a period of recovery, infected RBCs were treated with $1.1 \mu\text{M}$ of analog **59** ($5 \times EC_{50}$), 5 nM ($5 \times EC_{50}$), or 20 nM ($20 \times EC_{50}$) of the known PfATP4 inhibitor KAE609 (**1**), or an equivalent volume of vehicle (DMSO), with at least three independent incubations per condition. Following incubation for 5 h, cultures were centrifuged, the cell pellets were washed with ice-cold PBS, and the metabolites from 5×10^7 cells were extracted using $90 \mu\text{L}$ of ice-cold methanol. Samples were vortexed for 1 h, centrifuged

and then supernatants were transferred into high-performance liquid chromatography (HPLC) vials for storage at -80°C until liquid chromatography–mass spectrometry (LC-MS) analysis. A $10 \mu\text{L}$ aliquot from each sample was pooled to serve as a quality control sample for monitoring instrument reproducibility and to aid downstream metabolite identification. LC-MS analysis and data processing were as previously described.²¹ Metabolite identification was performed based on accurate mass ($<2 \text{ ppm}$) and retention time (where authentic standards were analyzed on the same analytical system), or where standards were not available, metabolites were putatively annotated based on accurate mass and predicted retention time as previously described.³² Unless stated otherwise, LC-MS peak height (metabolite abundance) is expressed as the \log_2 fold-change of treated samples relative to the average of the untreated control ($n = 3\text{--}4$). Metabolites that were not detected in a sample are expressed relative to half the minimum detected intensity in the data set. Statistical significance was determined using Welch's *t* test ($\alpha = 0.05$). Principal component analysis and hierarchical clustering analysis were performed in MetaboAnalyst (version 6.0) on the log-transformed and autoscaled (mean-centered and divided by the standard deviation of each variable) metabolite peak intensity data. The metabolomics data for KAE609 and compound-free controls were reported previously.²¹ For mapping of putative peptides to hemoglobin, the sequences of human hemoglobin α , β , and δ chains were searched for any peptide with monoisotopic mass within 0.002 m/z of the identified peptide using custom Python scripts, as previously described.⁵⁴

Data availability: Raw metabolomic data is available at the NIH Common Fund's National Metabolomics Data Repository (NMDR) website, the Metabolomics Workbench, <https://www.metabolomicsworkbench.org>, where it has been assigned Study ID: ST003565. The data can be accessed directly via its Project DOI: 10.21228/M8CN7H

Stage of Asexual Arrest Assay. *P. falciparum* 3D7 parasites were synchronized using Percoll gradient purification followed by 5% D-sorbitol as described previously to obtain 0–4 h postinvasion rings. Ring-staged parasites were adjusted to 2% parasitemia and hematocrit. Compounds were added to a final concentration of $10 \times EC_{50}$ and replenished after 24 h. Plates were incubated at 37 °C for 48 h and every 12 h, and blood smears, and $50 \mu\text{L}$ aliquots (performed in triplicate) were obtained. These aliquots were fixed in 0.25% glutaraldehyde 20 min at room temperature followed by washing with DPBS and storing in 4 °C until the completion of the assay for flow cytometry analysis. To determine parasitemia, $2.5 \times$ SYBR Green was used to stain fixed blood pellets for 20 min before dilution with $230 \mu\text{L}$ of DPBS. Attune Flow Cytometer (ThermoFisher Scientific) was used to count 100,000 cells. Blood smears were fixed and stained with Giemsa and the morphology of parasites was observed using an Eclipse E600 microscope (Nikon).

Parasite Reduction Ratio Assay. This assay was conducted following a previously described protocol,¹⁵ which is an adaption of the original method by Sanz et al.⁵⁵

Red Blood Cell Lysis Assay. *P. falciparum* 3D7 parasites expressing the Hyp-1 Nluc fusion protein³⁷ were double synchronized with 5% D-sorbitol the day before the experiment to obtain synchronized trophozoite stage parasites for the assay. For the assay setup, Hyp1-Nluc parasites were first washed with complete RPMI media twice to remove background nanoluciferase. The following compounds were prepared at $2 \times$ concentration and $50 \mu\text{L}$ was added into each well of the 96-well plates in triplicates to achieve final concentrations of: $10 \times EC_{50}$ of W454 (**5**) ($5.7 \mu\text{M}$), **80** ($0.03 \mu\text{M}$), KAE609 (**1**) (6.7 nM), SJ733 (**2**) ($0.7 \mu\text{M}$), and chloroquine ($0.15 \mu\text{M}$). A 0.05% DMSO control was also included and triplicate $50 \mu\text{L}$ of DMSO was added to the same 96-well plate. Parasites were adjusted to 5% parasitemia in 2% hematocrit and $50 \mu\text{L}$ were added to all wells containing compounds or DMSO. A single 96-well U-bottom plate was used for each time point (0, 2, 4, 6, and 8 h) and incubated at 37 °C in 1% O_2 and 5% CO_2 , in 94% N_2 . At each time point, the culture was resuspended and $35 \mu\text{L}$ was aliquoted to a new well in the 96-well U-bottom plate. The remaining culture was spun down at

1200 rpm for 2 min and 35 μ L of supernatant was aliquoted to a new well in the 96-well U-bottom plate. Plates were stored at 4 °C until the end of the time course. Upon completion, 5 μ L of resuspended culture and 5 μ L of supernatant from each well were transferred to a 96-well white luminometer plate and 45 μ L of lysis buffer and 1:1000 NanoGlo substrate (Promega) was added. Luminescence was measured using a ClarioStar Microplate reader at 470 nm. Values were plotted using an XY graph in GraphPad Prism (version 10.1.0).

Measurements of *P. falciparum* Cytosolic Na⁺ Concentration, Cytosolic pH, and Membrane ATPase Activity. Parasites were cultured in RPMI 1640 containing 25 mM HEPES and GlutaMAX (Gibco) supplemented with 11 mM additional glucose, 0.2 mM hypoxanthine, 20 μ g/mL gentamicin sulfate and 3 g/L Albumax II. Cultures were maintained with continuous shaking at 37 °C in a low-O₂ atmosphere (1% O₂, 3% CO₂ and 96% N₂), at a hematocrit between 2 and 4%. Parasites were isolated from their host erythrocytes as outlined elsewhere.⁴¹ Measurements of the effects of compounds on [Na⁺]_{cyt} were performed using SBFI-loaded isolated trophozoites suspended in Physiological Saline (125 mM NaCl, 5 mM KCl, 1 mM MgCl₂, 20 mM glucose, 25 mM HEPES; pH 7.1) at 37 °C, as described elsewhere.^{7,41} Investigations of the effects of compounds on the pH in the cytosol of isolated trophozoite-stage parasites were carried out as described previously.¹¹ The procedure entailed loading parasites with BCECF then depleting them of ATP. The parasites were then suspended in a (glucose-containing) physiological saline containing the V-type H⁺ ATPase inhibitor concanamycin A (final concentration 100 nM) at 37 °C and fluorescence was monitored. ATPase assays were performed with membranes prepared from isolated trophozoite-stage parasites essentially as described previously³⁶ using a PiColorLock Gold Phosphate Detection System (Innova Biosciences). The final reaction mixtures had a pH of 7.2 and consisted of: 150 mM NaCl or choline chloride, 20 mM KCl, 2 mM MgCl₂, 50 mM Tris, 50 μ g/mL (total) protein, 1 mM Na₂ATP, 3H₂O (MP Biomedicals), and the compound(s) of interest or solvent (DMSO) alone. The final concentration of DMSO in the reactions did not exceed 0.2% v/v. The reactions were carried out at 37 °C for 10 min.

Multidrug-Resistant Asexual Stage Parasite Viability Assay. This assay was performed exactly as previously described.²²

***P. knowlesi* Asexual Stage Parasite Viability Assays.** This assay was performed exactly as previously described.²²

Dual Gamete Formation Assay. This is a platform assay conducted at the London School of Hygiene and Tropical Medicine (LSHTM).^{48,50} A protocol for this platform assay was adhered to as previously described.²²

Standard Membrane Feeding Assay. This model is conducted in the Wellcome Trust Human Malaria Transmission Facility at LSHTM following a previously described protocol.²¹ Briefly, *P. falciparum* NF54 gametocytes were prepared for blood-feeding to mosquitoes according to the method previously described.⁵⁰ Gametocyte aliquots from a single NF54 culture were mixed in the membrane feeder reservoir with WJM664 (82) at 500 nM or 100 nM, and methylene blue at 1 μ M (full-block control) or culture medium with DMSO (no-drug control). The concentration of DMSO during experimental mosquito feeds was at 1.0% v/v. Pots of 70–80 female *Anopheles stephensi* (SD500 strain) mosquitoes (two to 5 days old) were allowed to feed on 500 μ L of the respective culture-drug-DMSO mixture, presented to each pot of mosquitoes in a preheated water channel membrane feeder, until fully fed. Mosquitoes were placed in an incubator at standard conditions and midguts were dissected in 0.25% mercurochrome stain for oocyst counts by light microscopy 7–8 days postfeed. The statistical significance of observed differences was analyzed by *t* test.

Animal Ethics Statement. Experiments involving rodents were performed in strict accordance with the recommendations of the Australian Government and National Health and Medical Research Council Australian code of practice for the care and use of animals for scientific purposes. The protocols were approved by the Animal Welfare Committee at Deakin University (approval no. G11/2023).

Asexual *P. berghei* Mouse Model. A stock solution of WJM664 (82) was made by dissolving the compound in 70% (v/v) Tween 80 and 30% (v/v) ethanol in distilled sterile water. Each day, a fresh aliquot of the stock compound was diluted 1 in 10 in water for administration to mice. Biological assessment of the in vivo antimalarial efficacy of WJM664 (82) was assessed using the *P. berghei* rodent malaria 4-day suppressive test in 8 week old female mice from Ozgene. Mice at day 0 were infected with 2×10^7 *P. berghei* ANKA-infected erythrocytes. At 2 h and days 1, 2, and 3 postinfection, mice were orally gavaged with 50 mg/kg WJM664 (82) (6 mice) or vehicle control (6 mice). Two mice were also dosed with artesunate (Sigma) using the same regime at 30 mg/kg. The parasitemia levels in mice were assessed by visualizing Giemsa-stained thin blood smears by microscopy and a minimum of 1000 RBCs were counted. To calculate the percent antimalarial activity the following formula was used: $100 - (\text{mean parasitemia treated day 4 postinfection} / \text{mean parasitemia vehicle control day 4 postinfection}) \times 100$. Mice were culled the day following the last oral gavage.

Mouse Plasma Exposure. Ethical statement: The study was performed under protocol approved by the Institutional Animal Care Committee (IAEC) of TCG Lifesciences Pvt. Ltd. All animal procedures were conducted according to the guidelines of experimental animal care issued by the Committee for Control and Supervision of Experiments on Animals (CCSEA). The experiment was performed using 3 male CD1 mice (6–8 weeks) procured from Hylasco Bio-Technology (licensed breeder and supplier of Charles River Lab in India). Animals were housed under 12/12 h light dark cycle, 22 ± 3 °C temp, $50 \pm 20\%$ humidity in the AAALAC accredited facility. Animals were allowed free access to food and water ad libitum and were acclimatized to laboratory conditions for 5–7 days prior to enrollment in the study. The vehicle for WJM664 (82) was a homogeneous suspension of 5% DMSO, 95% HPBCD (20% in water). WJM664 (82) was administered by oral gavage at 20 mg/kg (dose volume 10 mL/kg). At 0.08, 0.25, 0.5, 1, 2, 4, 8, 24 h post dosing approximately 40 μ L of blood sample was collected manually through saphenous vein puncture from conscious animals using heparin sodium as an anticoagulant and subsequently transferred into centrifuge tubes. All blood samples were processed for plasma by centrifugation (1640 g, 10 min, +4 °C) within 30 min of collection. The plasma will be collected in precooled labeled 96-well polypropylene plate (glass coated). The sample plate will be stored immediately at –20 °C until analysis. LC/MS/MS analysis platform was used for plasma sample analysis. The plasma samples were subjected to protein-precipitation processing using cold acetonitrile/methanol/their mixture containing generic internal standard (ISTD). Area ratio (test item/ISTD) was used in quantitation. Primary stock solution was prepared in DMSO and used to prepare working stocks of controls in DMSO. The lower limit of quantitation (LLOQ) was 1–2 ng/mL or 2–4 nmol/L. Calibration standards (10–12 points, range covering 3 orders of magnitude) and QC (3–4 levels) were included in sample run. These controls were prepared in the same matrix as the test samples. At least 75% of all standards used to make up the standard line were back calculated to within $\pm 20\%$ of their nominal concentrations. At least eight nonzero concentrations that back-calculate to within $\pm 20\%$ of their nominal values were used for quantitation. The back-calculated values were determined typically by a weighted linear regression. All acceptable standards produced a regression such that $R^2 > 0.98$. At least 2/3 of all QC were back calculated to within $\pm 20\%$ of their nominal concentrations, and at least 50% of QC at a given concentration level were back calculated to within $\pm 20\%$ of their nominal values. Double blank, matrix blank and carryover blank samples were also analyzed along with test samples. For the sample run that contains diluted samples, dilution QCs were prepared (at least $n = 2$) at the greatest dilution factor within the run and analyzed in addition to the above QC. At least one of the dilution QCs was back calculated to within $\pm 20\%$ of their nominal values. Pharmacokinetic parameters were estimated following NCA model in WinNonlin. The active form of test item, nominal time and nominal dose was used in the calculation. The linear up/log down trapezoidal method was applied in the AUC calculation.

■ ASSOCIATED CONTENT

SI Supporting Information

The Supporting Information is available free of charge at <https://pubs.acs.org/doi/10.1021/acs.jmedchem.5c00614>.

The metabolomics data (XLSX)

File contains Caco-2 data, *P. falciparum* and *P. knowlesi* asexual (parental and drug-resistant lines) and gamete dose response data, MIR, AReBar, metabolomic, standard membrane feeding assay, mouse model and plasma exposure data, and compound spectra (PDF)

the Molecular Formula Strings (CSV)

Crystal structure (PDB)

■ AUTHOR INFORMATION

Corresponding Authors

Brad E. Sleebs – The Walter and Eliza Hall Institute of Medical Research, Parkville 3052, Australia; Department of Medical Biology, The University of Melbourne, Parkville 3010, Australia; orcid.org/0000-0001-9117-1048; Email: sleebs@wehi.edu.au

Madeline G. Dans – The Walter and Eliza Hall Institute of Medical Research, Parkville 3052, Australia; Department of Medical Biology, The University of Melbourne, Parkville 3010, Australia; Email: dans.m@wehi.edu.au

Authors

Jon Kyle Awalt – The Walter and Eliza Hall Institute of Medical Research, Parkville 3052, Australia; Department of Medical Biology, The University of Melbourne, Parkville 3010, Australia; orcid.org/0000-0003-4840-2757

Zi Kang Ooi – The Walter and Eliza Hall Institute of Medical Research, Parkville 3052, Australia; orcid.org/0009-0006-1790-207X

Trent D. Ashton – The Walter and Eliza Hall Institute of Medical Research, Parkville 3052, Australia; Department of Medical Biology, The University of Melbourne, Parkville 3010, Australia; orcid.org/0000-0002-6707-6064

Mahta Mansouri – The Walter and Eliza Hall Institute of Medical Research, Parkville 3052, Australia; Department of Medical Biology, The University of Melbourne, Parkville 3010, Australia; orcid.org/0000-0001-8428-5370

Petar P. S. Calic – Department of Medical Biology, The University of Melbourne, Parkville 3010, Australia; orcid.org/0000-0001-6538-2394

Qingmiao Zhou – The Walter and Eliza Hall Institute of Medical Research, Parkville 3052, Australia

Santhya Vasanthan – The Walter and Eliza Hall Institute of Medical Research, Parkville 3052, Australia

Serena Lee – The Walter and Eliza Hall Institute of Medical Research, Parkville 3052, Australia

Katie Loi – The Walter and Eliza Hall Institute of Medical Research, Parkville 3052, Australia

Kate E. Jarman – The Walter and Eliza Hall Institute of Medical Research, Parkville 3052, Australia; Department of Medical Biology, The University of Melbourne, Parkville 3010, Australia

Jocelyn S. Penington – The Walter and Eliza Hall Institute of Medical Research, Parkville 3052, Australia; orcid.org/0000-0003-1561-0074

Deyun Qiu – Research School of Biology, Australian National University, Canberra 2601, Australia

Xinxin Zhang – Research School of Biology, Australian National University, Canberra 2601, Australia

Adele M. Lehane – Research School of Biology, Australian National University, Canberra 2601, Australia; orcid.org/0000-0002-0050-9101

Emma Y. Mao – Research Centre for Infectious Diseases, School of Biological Sciences, University of Adelaide, Adelaide 5005, Australia

Maria R. Gancheva – Research Centre for Infectious Diseases, School of Biological Sciences, University of Adelaide, Adelaide 5005, Australia

Danny W. Wilson – Research Centre for Infectious Diseases, School of Biological Sciences, University of Adelaide, Adelaide 5005, Australia

Carlo Giannangelo – Monash Institute of Pharmaceutical Sciences, Monash University, Parkville 3052, Australia; orcid.org/0000-0002-6654-7266

Christopher A. MacRaid – Monash Institute of Pharmaceutical Sciences, Monash University, Parkville 3052, Australia; orcid.org/0000-0002-3694-3989

Darren J. Creek – Monash Institute of Pharmaceutical Sciences, Monash University, Parkville 3052, Australia; orcid.org/0000-0001-7497-7082

Tomas Yeo – Department of Microbiology & Immunology, Columbia University Irving Medical Center, New York, New York 10032, United States; Center for Malaria Therapeutics and Antimicrobial Resistance, Columbia University Irving Medical Center, New York, NY 10032, USA

Tanaya Sheth – Department of Microbiology & Immunology, Columbia University Irving Medical Center, New York, New York 10032, United States; Center for Malaria Therapeutics and Antimicrobial Resistance, Columbia University Irving Medical Center, New York, NY 10032, USA

David A. Fidock – Department of Microbiology & Immunology, Columbia University Irving Medical Center, New York, New York 10032, United States; Center for Malaria Therapeutics and Antimicrobial Resistance, Columbia University Irving Medical Center, New York, NY 10032, USA; Division of Infectious Diseases, Department of Medicine, Columbia University Irving Medical Center, New York, New York 10032, United States

Alisje Churchyard – Department of Life Sciences, Imperial College London, South Kensington SW7 2AZ, U.K.

Jake Baum – Department of Life Sciences, Imperial College London, South Kensington SW7 2AZ, U.K.; School of Biomedical Sciences, University of New South Wales, Sydney 2031, Australia

Mufuliat T. Famodimu – London School of Hygiene and Tropical Medicine, London WC1E 7HT, U.K.; orcid.org/0000-0002-8852-1040

Michael J. Delves – London School of Hygiene and Tropical Medicine, London WC1E 7HT, U.K.; orcid.org/0000-0001-8526-4782

Mojca Kristan – London School of Hygiene and Tropical Medicine, London WC1E 7HT, U.K.; orcid.org/0000-0002-0363-8558

Lindsay Stewart – London School of Hygiene and Tropical Medicine, London WC1E 7HT, U.K.

Colin J. Sutherland – London School of Hygiene and Tropical Medicine, London WC1E 7HT, U.K.

Rachael Coyle – London School of Hygiene and Tropical Medicine, London WC1E 7HT, U.K.; Wellcome Sanger Institute, Hinxton CB10 1SA, U.K.

Hannah Jagoe – London School of Hygiene and Tropical Medicine, London WC1E 7HT, U.K.

Marcus C. S. Lee – Wellcome Sanger Institute, Hinxton CB10 1SA, U.K.; Wellcome Centre for Anti-Infectives Research, Biological Chemistry and Drug Discovery, University of Dundee, Dundee DD1 5EH, U.K.

Mrittika Chowdury – School of Medicine, Deakin University, Waurin Ponds 3216, Australia; Institute for Mental and Physical Health and Clinical Translation, Deakin University, Geelong 3216, Australia

Tania F. de Koning-Ward – School of Medicine, Deakin University, Waurin Ponds 3216, Australia; Institute for Mental and Physical Health and Clinical Translation, Deakin University, Geelong 3216, Australia

Delphine Baud – Medicines for Malaria Venture, Geneva 1215, Switzerland; orcid.org/0009-0005-6745-233X

Stephen Brand – Medicines for Malaria Venture, Geneva 1215, Switzerland

Paul F. Jackson – Emerging Science & Innovation, Discovery Sciences, Janssen R&D LLC, La Jolla 92121, United States

Alan F. Cowman – The Walter and Eliza Hall Institute of Medical Research, Parkville 3052, Australia; Department of Medical Biology, The University of Melbourne, Parkville 3010, Australia

Complete contact information is available at:

<https://pubs.acs.org/10.1021/acs.jmedchem.5c00614>

Notes

The authors declare no competing financial interest.

ACKNOWLEDGMENTS

This work was funded by the National Health and Medical Research Council of Australia (Development Grants 20414427 and 2031542 to B.E.S. and A.F.C. and Synergy Grant 1185354 to T.F.d.K.-W.), the Victorian State Government Operational Infrastructure Support, and Australian Government NHMRC IRIISS. D.A.F., J.B., M.C.S.L., and B.E.S. acknowledge the support of Medicines for Malaria Venture (RD-08-0015, RD-08-2800, RD-18-0005, and RD-08-0003, respectively) for MIR, DGFA, AReBar, PRR, and in vitro ADME analyses. J.B. acknowledges support from Wellcome for an Investigator Award (100993/Z/13/Z). M.T.F. is supported by a grant awarded to M.J.D. by the Medicines for Malaria Venture (RD-21-1003). M.J.D. is supported by a UKRI Medical Research Council Career Development Award (MR/V010034/1). Mosquito infection studies at LSHTM are supported by Wellcome Trust Biomedical Resources Grant (221363/Z/20/Z) awarded to C.J.S. We thank the China Scholarship Council, the International Studies Abroad, and the International Student Program in Research Experience for supporting Q.Z., S.L., and S.V., respectively. Q.Z. and Z.-K.O. were WEHI Alan Harris Scholars. We thank Dr Keith Watson from the Walter and Eliza Hall Institute for helpful advice and Prof Paul Gilson from the Burnet Institute for the kind donation of the *P. falciparum* 3D7 Hyp-1 NLuc strain. We thank Australian Life Blood for the provision of fresh red blood cells. A.F.C. is a Howard Hughes International Scholar and an Australia Fellow of the NHMRC. B.E.S. is a Corin Centenary Fellow.

ABBREVIATIONS

ACT artemisinin combination therapy
AReBar Antimalarial Resistome Barcoding

CQ chloroquine
DGFA dual gamete formation assay
DHODH dihydroorotate dehydrogenase
DIPEA *N,N*-diisopropylethylamine
EDCI 1-ethyl-3-(3-(dimethylamino)propyl)carbodiimide hydrochloride
HT high throughput
LDH lactate dehydrogenase
MFQ mefloquine
MIR minimum inoculum of resistance
NLuc nano luciferase
Pb *Plasmodium berghei*
Pf *Plasmodium falciparum*
PfATP4 *P. falciparum* non-SERCA-type Ca²⁺ transporting P-ATPase
Pf *Plasmodium falciparum*
PRR parasite reduction ratio
RBC red blood cell
SAR structure activity relationship
TCP target candidate profile
WJM WEHI Janssen MMV.

REFERENCES

- (1) Ashley, E. A.; Dhorda, M.; Fairhurst, R. M.; Amaratunga, C.; Lim, P.; Suon, S.; Sreng, S.; Anderson, J. M.; Mao, S.; Sam, B.; Sopha, C.; Chuor, C. M.; Nguon, C.; Sovannaroeth, S.; Pukrittayakamee, S.; Jittamala, P.; Chotivanich, K.; Chutasmit, K.; Suchatsoonthorn, C.; Runchaoren, R.; Hien, T. T.; Thuy-Nhien, N. T.; Thanh, N. V.; Phu, N. H.; Htut, Y.; Han, K. T.; Aye, K. H.; Mokuolu, O. A.; Olaosebikan, R. R.; Folaranmi, O. O.; Mayxay, M.; Khantavong, M.; Hongvanthong, B.; Newton, P. N.; Onyamboko, M. A.; Fanello, C. I.; Tshefu, A. K.; Mishra, N.; Valecha, N.; Phyto, A. P.; Nosten, F.; Yi, P.; Tripura, R.; Borrmann, S.; Bashraheil, M.; Peshu, J.; Faiz, M. A.; Ghose, A.; Hossain, M. A.; Samad, R.; Rahman, M. R.; Hasan, M. M.; Islam, A.; Miotto, O.; Amato, R.; MacInnis, B.; Stalker, J.; Kwiatkowski, D. P.; Bozdech, Z.; Jeeyapant, A.; Cheah, P. Y.; Sakulthaew, T.; Chalk, J.; Intharabut, B.; Silamut, K.; Lee, S. J.; Vihokhern, B.; Kunsol, C.; Imwong, M.; Tarning, J.; Taylor, W. J.; Yeung, S.; Woodrow, C. J.; Flegg, J. A.; Das, D.; Smith, J.; Venkatesan, M.; Plowe, C. V.; Stepniewska, K.; Guerin, P. J.; Dondorp, A. M.; Day, N. P.; White, N. J. Spread of Artemisinin resistance in *Plasmodium falciparum* Malaria. *N. Engl. J. Med.* **2014**, *371* (5), 411–423.
- (2) Uwimana, A.; Legrand, E.; Stokes, B. H.; Ndikumana, J.-L. M.; Warsame, M.; Umulisa, N.; Ngamije, D.; Munyaneza, T.; Mazarati, J.-B.; Munguti, K.; Campagne, P.; Criscuolo, A.; Arie, F.; Murindahabi, M.; Ringwald, P.; Fidock, D. A.; Mbituyumuremyi, A.; Menard, D. Emergence and clonal expansion of in vitro artemisinin-resistant *Plasmodium falciparum* kelch13 R561H mutant parasites in Rwanda. *Nat. Med.* **2020**, *26*, 1602–1608.
- (3) Burrows, J. N.; Duparc, S.; Gutteridge, W. E.; Hooft van Huijsduijnen, R.; Kaszubska, W.; Macintyre, F.; Mazzuri, S.; Mohrle, J. J.; Wells, T. N. C. New developments in anti-malarial target candidate and product profiles. *Malar. J.* **2017**, *16* (1), 26.
- (4) Ashton, T. D.; Devine, S. M.; Möhrle, J. J.; Laleu, B.; Burrows, J. N.; Charman, S. A.; Creek, D. J.; Sleebs, B. E. The development process for discovery and clinical advancement of modern antimalarials. *J. Med. Chem.* **2019**, *62* (23), 10526–10562.
- (5) Jiménez-Díaz, M. B.; Ebert, D.; Salinas, Y.; Pradhan, A.; Lehane, A. M.; Myrand-Lapierre, M.-E.; O'Loughlin, K. G.; Shackleford, D. M.; Justino de Almeida, M.; Carrillo, A. K.; et al. (+)-SJ733, a clinical candidate for malaria that acts through ATP4 to induce rapid host-mediated clearance of *Plasmodium*. *Proc. Natl. Acad. Sci. U. S. A.* **2014**, *111* (50), No. E5455.
- (6) Rottmann, M.; McNamara, C.; Yeung, B. K. S.; Lee, M. C. S.; Zou, B.; Russell, B.; Seitz, P.; Plouffe, D. M.; Dharia, N. V.; Tan, J.; et al. Spiroindolones, a potent compound class for the treatment of malaria. *Science* **2010**, *329* (5996), 1175–1180.

- (7) Spillman, N. J.; Allen, R. J.; McNamara, C. W.; Yeung, B. K.; Winzeler, E. A.; Diagona, T. T.; Kirk, K. Na⁺ regulation in the malaria parasite *Plasmodium falciparum* involves the cation ATPase PfATP4 and is a target of the spiroindolone antimalarials. *Cell Host Microbe* **2013**, *13* (2), 227–237.
- (8) Spillman, N. J.; Kirk, K. The malaria parasite cation ATPase PfATP4 and its role in the mechanism of action of a new arsenal of antimalarial drugs. *Int. J. Parasitol. Drugs Drug Resist.* **2015**, *5* (3), 149–162.
- (9) Spillman, N. J.; Allen, R. J.; Kirk, K. Na⁺ extrusion imposes an acid load on the intraerythrocytic malaria parasite. *Mol. Biochem. Parasitol.* **2013**, *189* (1–2), 1–4.
- (10) Hameed, P. S.; Solapure, S.; Patil, V.; Henrich, P. P.; Magistrado, P. A.; Bharath, S.; Murugan, K.; Viswanath, P.; Puttur, J.; Srivastava, A.; et al. Triaminopyrimidine is a fast-killing and long-acting antimalarial clinical candidate. *Nat. Commun.* **2015**, *6*, 6715.
- (11) Ashton, T. D.; Dans, M. G.; Favuzza, P.; Ngo, A.; Lehane, A. M.; Zhang, X.; Qiu, D.; Maity, B. C.; Nirupam, D.; Schindler, K. A.; et al. Optimization of 2,3-dihydroquinazolinone-3-carboxamides as antimalarials targeting PfATP4. *J. Med. Chem.* **2023**, *66* (5), 3540–3565.
- (12) White, N. J.; Pukrittayakamee, S.; Phyo, A. P.; Rueangweerayut, R.; Nosten, F.; Jittamala, P.; Jeeyapant, A.; Jain, J. P.; Lefevre, G.; Li, R.; Magnusson, B.; Diagona, T. T.; Leong, F. J. Spiroindolone KAE609 for falciparum and vivax malaria. *N. Engl. J. Med.* **2014**, *371* (5), 403–410.
- (13) Gaur, A. H.; McCarthy, J. S.; Panetta, J. C.; Dallas, R. H.; Woodford, J.; Tang, L.; Smith, A. M.; Stewart, T. B.; Branum, K. C.; Freeman, B. B., III; Patel, N. D.; John, E.; Chalon, S.; Ost, S.; Heine, R. N.; Richardson, J. L.; Christensen, R.; Flynn, P. M.; Van Gessel, Y.; Mitasev, B.; Möhrle, J. J.; Gusovsky, F.; Bebrevska, L.; Guy, R. K. Safety, tolerability, pharmacokinetics, and antimalarial efficacy of a novel *Plasmodium falciparum* ATP4 inhibitor SJ733: a first-in-human and induced blood-stage malaria phase 1a/b trial. *Lancet Infect. Dis.* **2020**, *20* (8), 964–975.
- (14) Schmitt, E. K.; Ndayisaba, G.; Yeka, A.; Asante, K. P.; Grobusch, M. P.; Karita, E.; Mugerwa, H.; Asiimwe, S.; Oduro, A.; Fofana, B.; Doumbia, S.; Su, G.; Csermak Renner, K.; Venishetty, V. K.; Sayyed, S.; Straimer, J.; Demin, I.; Barsainya, S.; Boulton, C.; Gandhi, P. Efficacy of cipragamin (KAE609) in a randomized, phase II dose-escalation study in adults in sub-Saharan Africa with uncomplicated *Plasmodium falciparum* malaria. *Clin. Infect. Dis.* **2022**, *74* (10), 1831–1839.
- (15) Nguyen, W.; Dans, M. G.; Currie, I.; Awalt, J. K.; Bailey, B. L.; Lumb, C.; Ngo, A.; Favuzza, P.; Palandri, J.; Ramesh, S.; et al. 7-N-Substituted-3-oxadiazole quinolones with potent antimalarial activity target the cytochrome bc1 complex. *ACS Infect. Dis.* **2023**, *9* (3), 668–691.
- (16) Awalt, J. K.; Su, W.; Nguyen, W.; Loi, K.; Jarman, K. E.; Penington, J. S.; Ramesh, S.; Fairhurst, K. J.; Yeo, T.; Park, H.; Uhlemann, A. C.; Chandra Maity, B.; De, N.; Mukherjee, P.; Chakraborty, A.; Churchyard, A.; Famodimu, M. T.; Delves, M. J.; Baum, J.; Mittal, N.; Winzeler, E. A.; Papenfuss, A. T.; Chowdury, M.; de Koning-Ward, T. F.; Maier, A. G.; van Dooren, G. G.; Baud, D.; Brand, S.; Fidock, D. A.; Jackson, P. F.; Cowman, A. F.; Dans, M. G.; Sleebs, B. E. Exploration and characterization of the antimalarial activity of cyclopropyl carboxamides that target the mitochondrial protein, cytochrome b. *Eur. J. Med. Chem.* **2024**, *280*, 116921.
- (17) Bailey, B. L.; Nguyen, W.; Ngo, A.; Goodman, C. D.; Gancheva, M. R.; Favuzza, P.; Sanz, L. M.; Gamo, F.-J.; Lowes, K. N.; McFadden, G. I.; Wilson, D. W.; Laleu, B.; Brand, S.; Jackson, P. F.; Cowman, A. F.; Sleebs, B. E. Optimisation of 2-(N-phenyl carboxamide) triazolopyrimidine antimalarials with moderate to slow acting erythrocytic stage activity. *Bioorg. Chem.* **2021**, *115*, 105244.
- (18) Calic, P. P. S.; Ashton, T. D.; Mansouri, M.; Loi, K.; Jarman, K. E.; Qiu, D.; Lehane, A. M.; Roy, S.; Rao, G. P.; Maity, B.; Wittlin, S.; Crespo, B.; Gamo, F. J.; Deni, I.; Fidock, D. A.; Chowdury, M.; de Koning-Ward, T. F.; Cowman, A. F.; Jackson, P. F.; Baud, D.; Brand, S.; Laleu, B.; Sleebs, B. E. Optimization of pyrazolopyridine 4-carboxamides with potent antimalarial activity for which resistance is associated with the P. falciparum transporter ABCI3. *Eur. J. Med. Chem.* **2024**, *276*, 116677.
- (19) Dans, M. G.; Boulet, C.; Watson, G. M.; Nguyen, W.; Dziekan, J. M.; Evelyn, C.; Reaksudsan, K.; Mehra, S.; Razook, Z.; Geoghegan, N. D.; et al. Aryl amino acetamides prevent *Plasmodium falciparum* ring development via targeting the lipid-transfer protein PfSTART1. *Nat. Commun.* **2024**, *15* (1), 5219.
- (20) Nguyen, W.; Boulet, C.; Dans, M. G.; Loi, K.; Jarman, K. E.; Watson, G. M.; Tham, W. H.; Fairhurst, K. J.; Yeo, T.; Fidock, D. A.; Wittlin, S.; Chowdury, M.; de Koning-Ward, T. F.; Chen, G.; Yan, D.; Charman, S. A.; Baud, D.; Brand, S.; Jackson, P. F.; Cowman, A. F.; Gilson, P. R.; Sleebs, B. E. Activity refinement of aryl amino acetamides that target the P. falciparum STAR-related lipid transfer 1 protein. *Eur. J. Med. Chem.* **2024**, *270*, 116354.
- (21) Ashton, T. D.; Calic, P. P. S.; Dans, M. G.; Ooi, Z.-K.; Zhou, Q.; Palandri, J.; Loi, K.; Jarman, K. E.; Qiu, D.; Lehane, A. M.; et al. Property and activity refinement of dihydroquinazolinone-3-carboxamides as orally efficacious antimalarials that target PfATP4. *J. Med. Chem.* **2024**, *67* (16), 14493–14523.
- (22) Ashton, T. D.; Calic, P. P. S.; Dans, M. G.; Ooi, Z. K.; Zhou, Q.; Loi, K.; Jarman, K. E.; Palandri, J.; Qiu, D.; Lehane, A. M.; et al. Lactam truncation yields a dihydroquinazolinone scaffold with potent antimalarial activity that targets PfATP4. *ChemMedChem* **2024**, *19*, No. e202400549.
- (23) Boström, J.; Hogner, A.; Llinàs, A.; Wellner, E.; Plowright, A. T. Oxadiazoles in medicinal chemistry. *J. Med. Chem.* **2012**, *55* (5), 1817–1830.
- (24) Hutzler, J. M.; Melton, R. J.; Rumsey, J. M.; Thompson, D. C.; Rock, D. A.; Wienkers, L. C. Assessment of the metabolism and intrinsic reactivity of a novel catechol metabolite. *Chem. Res. Toxicol.* **2008**, *21* (5), 1125–1133.
- (25) Stepan, A. F.; Kauffman, G. W.; Keefer, C. E.; Verhoest, P. R.; Edwards, M. Evaluating the differences in cycloalkyl ether metabolism using the design parameter “lipophilic metabolism efficiency” (LipMetE) and a matched molecular pairs analysis. *J. Med. Chem.* **2013**, *56* (17), 6985–6990.
- (26) Dalvie, D. K.; Kalgutkar, A. S.; Khojasteh-Bakht, S. C.; Obach, R. S.; O'Donnell, J. P. Biotransformation reactions of five-membered aromatic heterocyclic rings. *Chem. Res. Toxicol.* **2002**, *15* (3), 269–299.
- (27) Jensen, A. M.; Sørensen, T. L.; Olesen, C.; Møller, J. V.; Nissen, P. Modulatory and catalytic modes of ATP binding by the calcium pump. *Embo J.* **2006**, *25* (11), 2305–2314.
- (28) Marchesini, M.; Gherli, A.; Montanaro, A.; Patrizi, L.; Sorrentino, C.; Pagliaro, L.; Rompietti, C.; Kitara, S.; Heit, S.; Olesen, C. E.; et al. Blockade of oncogenic NOTCH1 with the SERCA inhibitor CAD204520 in T cell acute lymphoblastic leukemia. *Cell Chem. Biol.* **2020**, *27* (6), 678–697.e13.
- (29) Zhang, M.; Wang, C.; Otto, T. D.; Oberstaller, J.; Liao, X.; Adapa, S. R.; Udenze, K.; Bronner, I. F.; Casandra, D.; Mayho, M.; Brown, J.; Li, S.; Swanson, J.; Rayner, J. C.; Jiang, R. H. Y.; Adams, J. H. Uncovering the essential genes of the human malaria parasite *Plasmodium falciparum* by saturation mutagenesis. *Science* **2018**, *360* (6388), No. eaap7847.
- (30) Vaidya, A. B.; Morrissey, J. M.; Zhang, Z.; Das, S.; Daly, T. M.; Otto, T. D.; Spillman, N. J.; Wyvratt, M.; Siegl, P.; Marfurt, J.; Wirjanata, G.; Sebayang, B. F.; Price, R. N.; Chatterjee, A.; Nagle, A.; Stasiak, M.; Charman, S. A.; Angulo-Barturen, I.; Ferrer, S.; Belén Jiménez-Díaz, M.; Martínez, M. S.; Gamo, F. J.; Avery, V. M.; Ruecker, A.; Delves, M.; Kirk, K.; Berriman, M.; Kortagere, S.; Burrows, J.; Fan, E.; Bergman, L. W. Pyrazoleamide compounds are potent antimalarials that target Na⁺ homeostasis in intraerythrocytic *Plasmodium falciparum*. *Nat. Commun.* **2014**, *5* (1), 5521.
- (31) Carrasquilla, M.; Drammeh, N. F.; Rawat, M.; Sanderson, T.; Zenonos, Z.; Rayner, J. C.; Lee, M. C. S. Barcoding genetically distinct *Plasmodium falciparum* strains for comparative assessment of fitness and antimalarial drug resistance. *mBio* **2022**, *13* (5), No. e0093722.

- (32) Creek, D. J.; Chua, H. H.; Cobbold, S. A.; Nijagal, B.; MacRae, J. I.; Dickerman, B. K.; Gilson, P. R.; Ralph, S. A.; McConville, M. J. Metabolomics-based screening of the Malaria Box reveals both novel and established mechanisms of action. *Antimicrob. Agents Chemother.* **2016**, *60* (11), 6650–6663.
- (33) Allman, E.; Painter, J.; Samra, J.; Carrasquilla, M.; Llinás, M. Metabolomic profiling of the Malaria Box reveals antimalarial target pathways. *Antimicrob. Agents Chemother.* **2016**, *60* (11), 6635–6649.
- (34) Murithi, J. M.; Owen, E. S.; Istvan, E. S.; Lee, M. C. S.; Otilie, S.; Chibale, K.; Goldberg, D. E.; Winzeler, E. A.; Llinás, M.; Fidock, D. A.; Vanaerschot, M. Combining stage specificity and metabolomic profiling to advance antimalarial drug discovery. *Cell Chem. Biol.* **2020**, *27* (2), 158–171.
- (35) Simwela, N. V.; Guiguemde, W. A.; Straimer, J.; Regnault, C.; Stokes, B. H.; Tavernelli, L. E.; Yokokawa, F.; Taft, B.; Diagana, T. T.; Barrett, M. P.; Waters, A. P. A conserved metabolic signature associated with response to fast-acting anti-malarial agents. *Microbiol. Spectrum*. **2023**, *11* (6), No. e03976–22.
- (36) Dennis, A. S. M.; Lehane, A. M.; Ridgway, M. C.; Holleran, J. P.; Kirk, K. Cell swelling induced by the antimalarial KAE609 (Cipargamin) and other PfATP4-associated antimalarials. *Antimicrob. Agents Chemother.* **2018**, *62* (6), No. e00087–18.
- (37) Gilson, P. R.; Kumarasingha, R.; Thompson, J.; Zhang, X.; Penington, J. S.; Kalhor, R.; Bullen, H. E.; Lehane, A. M.; Dans, M. G.; De Koning-Ward, T. F.; et al. A 4-cyano-3-methylisoquinoline inhibitor of *Plasmodium falciparum* growth targets the sodium efflux pump PfATP4. *Sci. Rep.* **2019**, *9* (1), 10292.
- (38) Lindblom, J. C. R.; Zhang, X.; Lehane, A. M. A pH fingerprint assay to identify inhibitors of multiple validated and potential antimalarial drug targets. *ACS Infect. Dis.* **2024**, *10* (4), 1185–1200.
- (39) Saliba, K. J.; Kirk, K. pH regulation in the intracellular malaria parasite, *Plasmodium falciparum*. H(+) extrusion via a V-type H(+)-ATPase. *J. Biol. Chem.* **1999**, *274* (47), 33213.
- (40) van Schalkwyk, D. A.; Chan, X. W. A.; Misiano, P.; Gagliardi, S.; Farina, C.; Saliba, K. J. Inhibition of *Plasmodium falciparum* pH regulation by small molecule indole derivatives results in rapid parasite death. *Biochem. Pharmacol.* **2010**, *79* (9), 1291–1299.
- (41) Qiu, D.; Pei, J. V.; Rosling, J. E. O.; Thathy, V.; Li, D.; Xue, Y.; Tanner, J. D.; Penington, J. S.; Aw, Y. T. V.; Aw, J. Y. H.; et al. A G358S mutation in the *Plasmodium falciparum* Na⁺ pump PfATP4 confers clinically-relevant resistance to cipargamin. *Nat. Commun.* **2022**, *13* (1), 5746.
- (42) Kumpornsin, K.; Kochakarn, T.; Yeo, T.; Okombo, J.; Luth, M. R.; Hoshizaki, J.; Rawat, M.; Pearson, R. D.; Schindler, K. A.; Mok, S.; Park, H.; et al. Generation of a putator parasite to drive resistance discovery in *Plasmodium falciparum*. *Nat. Commun.* **2023**, *14* (1), 3059.
- (43) Cowman, A. F.; Galatis, D.; Thompson, J. K. Selection for mefloquine resistance in *Plasmodium falciparum* is linked to amplification of the pfmdr1 gene and cross-resistance to halofantrine and quinine. *Proc. Natl. Acad. Sci. U. S. A.* **1994**, *91* (3), 1143–1147.
- (44) Sidhu, A. B.; Verdier-Pinard, D.; Fidock, D. A. Chloroquine resistance in *Plasmodium falciparum* malaria parasites conferred by pfcr1 mutations. *Science* **2002**, *298* (5591), 210–213.
- (45) Straimer, J.; Gnädig, N. F.; Witkowski, B.; Amaratunga, C.; Duru, V.; Ramadani, A. P.; Dacheux, M.; Khim, N.; Zhang, L.; Lam, S.; Gregory, P. D.; Urnov, F. D.; Mercereau-Puijalon, O.; Benoit-Vical, F.; Fairhurst, R. M.; Ménard, D.; Fidock, D. A. K13-propeller mutations confer artemisinin resistance in *Plasmodium falciparum* clinical isolates. *Science* **2015**, *347* (6220), 428–431.
- (46) Mohring, F.; Van Schalkwyk, D. A.; Henrici, R. C.; Blasco, B.; Leroy, D.; Sutherland, C. J.; Moon, R. W. Cation ATPase (ATP4) orthologue replacement in the Malaria parasite *Plasmodium knowlesi* reveals species-specific responses to ATP4-targeting drugs. *mBio* **2022**, *13* (5), No. e0117822.
- (47) van Pelt-Koops, J. C.; Pett, H. E.; Graumans, W.; van der Vegte-Bolmer, M.; van Gemert, G. J.; Rottmann, M.; Yeung, B. K. S.; Diagana, T. T.; Sauerwein, R. W. The spiroindolone drug candidate NITD609 potentially inhibits gametocytogenesis and blocks *Plasmodium falciparum* transmission to Anopheles mosquito vector. *Antimicrob. Agents Chemother.* **2012**, *56* (7), 3544.
- (48) Delves, M. J.; Miguel-Blanco, C.; Matthews, H.; Molina, I.; Ruecker, A.; Yahya, S.; Straschil, U.; Abraham, M.; León, M. L.; Fischer, O. J.; et al. A high throughput screen for next-generation leads targeting malaria parasite transmission. *Nat. Commun.* **2018**, *9* (1), 3805.
- (49) Miura, K.; Deng, B.; Tullo, G.; Diouf, A.; Moretz, S. E.; Locke, E.; Morin, M.; Fay, M. P.; Long, C. A. Qualification of standard membrane-feeding assay with *Plasmodium falciparum* malaria and potential improvements for future assays. *PLoS One* **2013**, *8* (3), No. e57909.
- (50) Delves, M. J.; Straschil, U.; Ruecker, A.; Miguel-Blanco, C.; Marques, S.; Dufour, A. C.; Baum, J.; Sinden, R. E. Routine in vitro culture of *P. falciparum* gametocytes to evaluate novel transmission-blocking interventions. *Nat. Protoc.* **2016**, *11* (9), 1668–1680.
- (51) Istvan, E. S.; Mallari, J. P.; Corey, V. C.; Dharia, N. V.; Marshall, G. R.; Winzeler, E. A.; Goldberg, D. E. Esterase mutation is a mechanism of resistance to antimalarial compounds. *Nat. Commun.* **2017**, *8*, 14240.
- (52) Love, M. I.; Huber, W.; Anders, S. Moderated estimation of fold change and dispersion for RNA-seq data with DESeq2. *Genome Biol.* **2014**, *15* (12), 550.
- (53) Giannangelo, C.; Siddiqui, G.; De Paoli, A.; Anderson, B. M.; Edgington-Mitchell, L. E.; Charman, S. A.; Creek, D. J. System-wide biochemical analysis reveals ozonide antimalarials initially act by disrupting *Plasmodium falciparum* haemoglobin digestion. *PLoS Pathog.* **2020**, *16* (6), No. e1008485.
- (54) Giannangelo, C.; Challis, M. P.; Siddiqui, G.; Edgar, R.; Malcolm, T. R.; Webb, C. T.; Drinkwater, N.; Vinh, N.; Macraill, C.; Counihan, N.; Duffy, S. Chemoproteomics validates selective targeting of *Plasmodium* M1 alanyl aminopeptidase as an antimalarial strategy. *eLife* **2024**, *13*, RP92990.
- (55) Sanz, L. M.; Crespo, B.; De-Cózar, C.; Ding, X. C.; Llergo, J. L.; Burrows, J. N.; García-Bustos, J. F.; Gamo, F.-J. *P. falciparum* in vitro killing rates allow to discriminate between different antimalarial mode-of-action. *PLoS One* **2012**, *7* (2), No. e30949.
- (56) Rosling, J. E. O.; Ridgway, M. C.; Summers, R. L.; Kirk, K.; Lehane, A. M. Biochemical characterization and chemical inhibition of PfATP4-associated Na(+)-ATPase activity in *Plasmodium falciparum* membranes. *J. Biol. Chem.* **2018**, *293* (34), 13327–13337.